The effect of deregulated JAK/STAT signaling on the structure of the fruit fly's respiratory epithelium

Christine Fink [1,*], Kimberly Kallsen [2], Ruben Prange [1], Marcus Thiedmann[1], Holger Heine[2] and Thomas Roeder[1]

[1]Molecular Physiology, Zoological Institute, Kiel University (Germany)
[2]Innate Immunity, Asthma & Allergy Research Center Borstel (Germany)

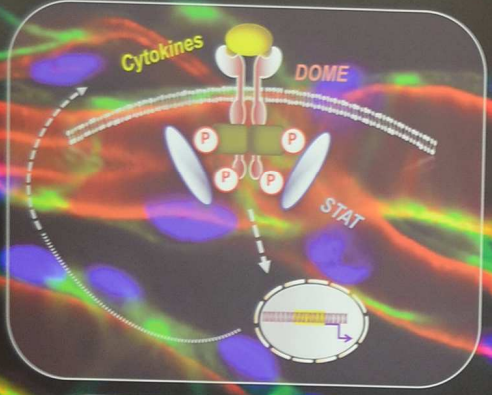

Abstract

The JAK/STAT signaling pathway is an evolutionary highly conserved pathway that is involved in developmental processes like cell proliferation, differentiation, cell migration and apoptosis. Moreover, it plays an important role in the development of the innate immune system.

The canonical pathway is activated by mainly two groups of ligands, chemokines and growth factors. After the activation of the receptor the intracellular Janus Kinase (JAK) leads to tyrosine phosphorylation and to STAT activation.

We are interested in the role of JAK/STAT signaling in the fly's airway epithelium under different stress conditions like oxidative stress, cigarette smoke and hypoxia. Furthermore, we wanted to know if the secretion of the ligands of the unpaired family (*upds*) is regional specific in the tracheal compartments and if a constitutive overexpression of *upds* leads to a structurally change of the airways epithelial cells.

With our results, we were able to show that there is a time dependent expression of two of the three unpaired ligands, upd2 and upd3 in oxygen undersupplied wildtype flies. By enhancing expression of different components of the JAK/STAT pathway we could observe structural changes in the dorsal trunks of the fly's airway mirrored by epithelial thickening and meta- as well as hyperplasia or even lethal effects by constitutive activation of the Dome-receptor in late larval stages.

Gene expression analysis

Cytokine expression

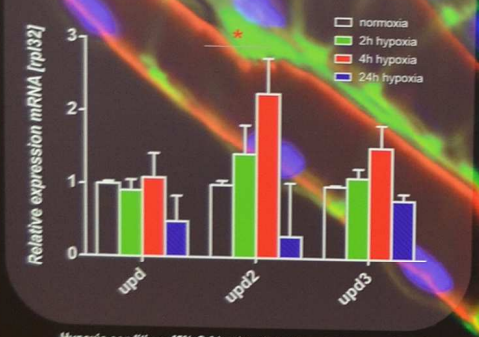

Hypoxic conditions [5% O_2] lead to time dependent expression of JAK/STAT activating genes.

JAK/STAT target genes

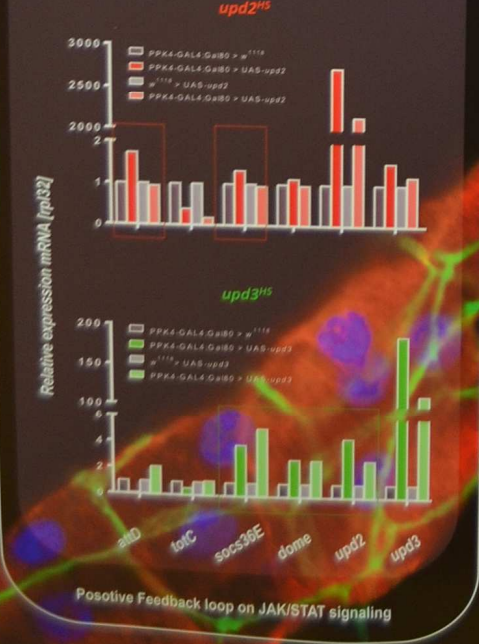

Posotive Feedback loop on JAK/STAT signaling

Changes in epithelial structure

Metaplasia

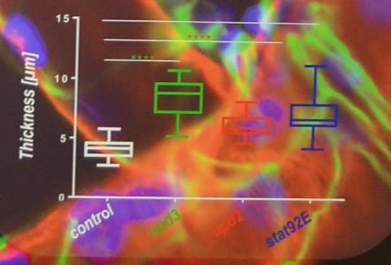

Ectopic activation of many JAK/STAT components lead to a compact increase of the epithalial thickness.

Hyperplasia

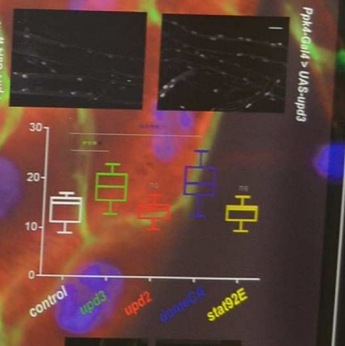

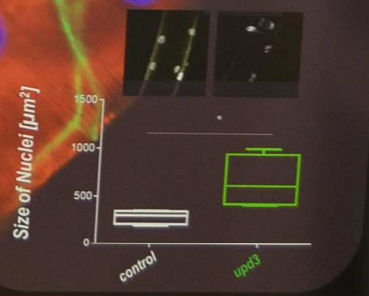

Ectopic activation of many JAK/STAT components lead to a compact increase of nuclei number & nuclei size.

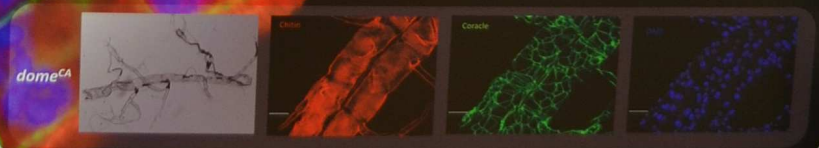

Constitutive dome-expression leads to intensive malformation of the dorsal trunks, including Hyperlasia and followed by early death (L2 larvae) .

Crosstalk with other Pathways

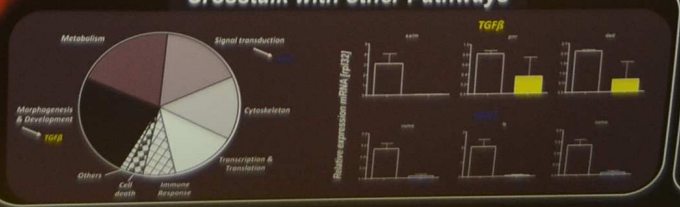

Special thanks to Britta Laubenstein & Christiane Sandberg

Drosophila melanogaster is a model for the study of *Bacillus cereus* pathogenicity

Zaynoun Attieh[1, 2], Agnès Rejasse[2], Christina Nielsen-Leroux[2], Mireille Kallassy[1], Vincent Sanchis[2], Laure El Chamy[1]

1- Unité de recherche Environnement, Génomique et Protéomique, Laboratoire de Génétique de la drosophile et virulence microbienne, Université Saint-Joseph, Beirut Lebanon

2- Micalis Institute, INRA, AgroParisTech, Université Paris-Saclay, 78350 Jouy-en-Josas, France

Introduction

Bacillus cereus sensu lato

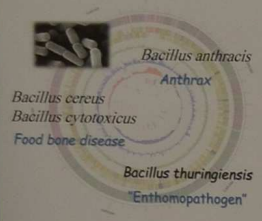

Pathogenic bacteria manipulate the host immune responses through the activity of virulence genes. The identification of these genes is of particular interest since it is essential for the onset of new therapeutic strategies for infectious diseases. The *Bacillus cereus* group includes eight species of Gram-positive sporulating bacteria. These bacilli share a highly similar genetic background with particular virulence genes enabling them to colonize different hosts. Taking advantage of *Drosophila*'s powerful genetic tools and its long studied immune system, we use it as a model organism for the study of *B. cereus* pathogenicity. Using a septic injury infection model, we showed that *B. cereus* is highly lethal to the flies. We then screened a *B. cereus* mutants library to isolate and characterize non-virulent mutant bacterial clones. In a complementary approach, we set up a *Drosophila* oral infection model to investigate the infectious process of food-borne *B. cereus* toxi-infections.

Drosophila immune response

Systemic Humoral response

Production of antimicrobial peptides (AMPs)

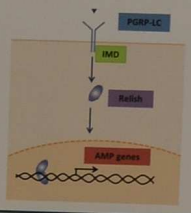

Cellular response

Phagocytosis

Epithelial defenses

AMPs and Reactive Oxygen Species (ROS)

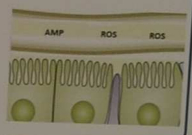

Research interests and work strategy

Identification of bacterial virulence genes

Screening of a *B. cereus* mutants library in a *Drosophila* septic injury infection model

Characterization of foodborne *B. cereus* infections

Screening of natural *B. cereus* strains in a *Drosophila* oral infection model

1. Screening by survival assay

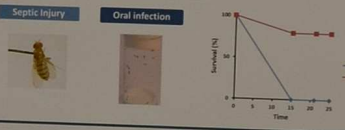

2. Selection of non-virulent bacterial clones
3. Phenotypic characterization of the non virulent mutants
4. Characterization of inducible immune response

Results

I- Characterization of *B. cereus* pathogenicity in a septic injury infection model

Set-up of the infection model and screening strategy

B. cereus* is highly lethal to *Drosophila

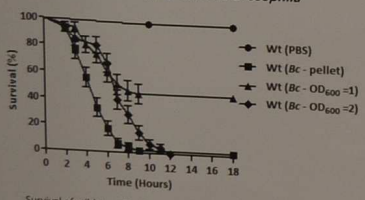

Survival of wild-type flies (Wt) to an infection with wild-type *B. cereus* (*Bc*) at different concentrations

***B. cereus* is resistant to the *Drosophila* systemic humoral response**

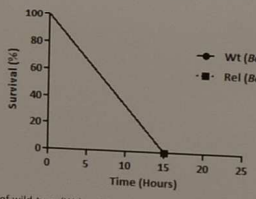

Survival of wild-type (Wt) and Relish (Rel) flies mutants to an infection with wild-type *B. cereus* (*Bc*)

Selection of bacterial mutant clones with attenuated virulence

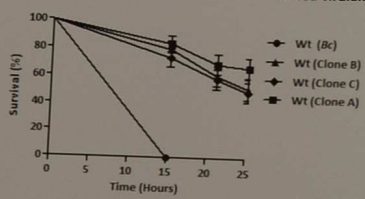

Survival of wild-type flies (Wt) to an infection with wild-type *B. cereus* (*Bc*) and mutants clones of *B. cereus*

Phenotypic characterization of bacterial mutant clones

All selected mutant clones have a reduced biofilm forming capacity, motility and growth and are sensitive to *Drosophila* systemic humoral response

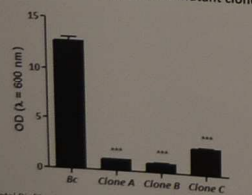

Total Biofilm Biomass at the air-liquid interface in glass tubes
Statistical test : Student's t test (***p < 0.001).

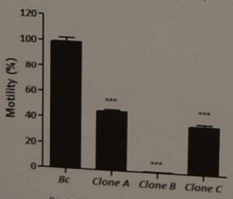

Bacterial motility on LB medium
Statistical test : Student's t test (***p < 0.001)

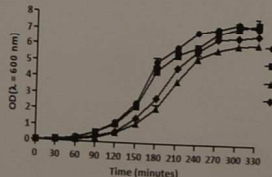

Bacterial growth on LB medium

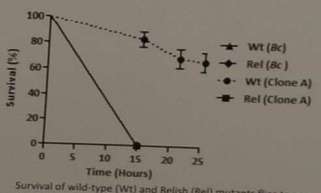

Survival of wild-type (Wt) and Relish (Rel) mutants flies to an infection with wild-type *B. cereus* (*Bc*) and the mutants clones

II- Isolation of a virulent *B. cereus* strain for the study of foodborne toxi-infections in *Drosophila*

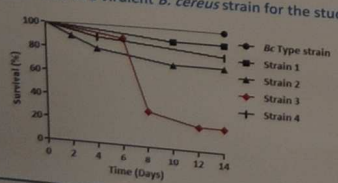

Survival of adult flies to an oral infection by different food poisoning and clinical *B. cereus* strains. While the type strain is not pathogenic, strain 3 is lethal to flies when ingested via contaminated food resources

Conclusions

Using a septic injury infection model in *Drosophila*, we isolated three non-virulent mutant of *B. cereus*, each affected in a different gene. The phenotypic characterization of the mutants indicate that the three selected clones are affected in their biofilm formation capacity and motility. Our results also put forward the resistance to the systemic humoral AMP-dependent response as a prominant aspect of *B. cereus* virulence mechanisms in *Drosophila*. Moreover, in an oral infection model, we isolated a virulent *B. cereus* strain that is lethal to the flies. This model will be used for the investigation of the infectious process of food-borne *B. cereus* toxi-infections in *Drosophila*.

Contact

Zaynoun ATTIEH (zaynoun.attieh@net.usj.edu.lb)
Laure El CHAMY, Dr (laure.chamy@usj.edu.lb)
Vincent SANCHIS BORJA, Dr (vincent.sanchis-borja@inra.fr)

Acknowledgment

P049

Using *Drosophila* to understand the genetic basis of obesity

Neha Agrawal[1], I. Sadaf Farooqi[2] and Andrea H. Brand[1]

[1]Wellcome Trust/Cancer Research UK Gurdon Institute, University of Cambridge, Tennis Court Road, Cambridge, United Kingdom.

[2]Institute of Metabolic Science, University of Cambridge, Addenbrooke's Hospital, Cambridge, United Kingdom.

Obesity is one of the greatest public health challenges facing the world today with the numbers of those affected continuing to rise at an alarming rate. Obesity ultimately represents an imbalance in the body's capacity to maintain energy homeostasis and is influenced by complex interactions between genetic and environmental factors. The Genetics of Obesity Study at the Institute of Metabolic Science, University of Cambridge has done pioneering work in identifying genetic factors underlying human obesity. We are now developing *Drosophila* models to identify and examine obesity causing genes and generate patient-specific obesity models, in collaboration with this study. This research will thus help identify novel genes and underlying cellular and molecular mechanisms involved in modulating energy homeostasis which will ultimately contribute to strategies for the prevention and treatment of obesity.

Human obesity is influenced by complex interactions between genetic and environmental influences

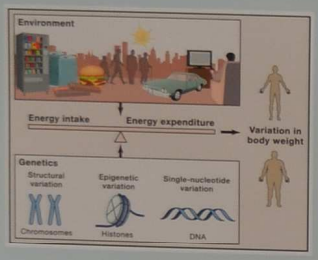

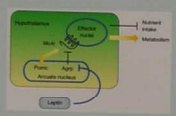

Montague et al., 1997; Farooqi et al., 1999, 2002, 2007; Licinio et al., 2004 ; van der Klaauw, A. A., & Farooqi, I. S. 2015; van der Voet, M., et al. 2014

Drosophila melanogaster will be used as a model system to examine novel obesity genes and generate patient-specific obesity models

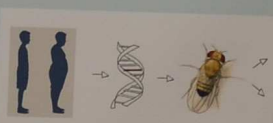

Fundamental Knowledge
- Gene identification and function
- Genetic modifiers
- Molecular targets and networks

Translational Benefits
- New diagnostic information for patients
- Insights into disease pathology
- Highlight targets for drug discovery

Phenotypic screen for obesity related genes - Buoyancy-based fat assay

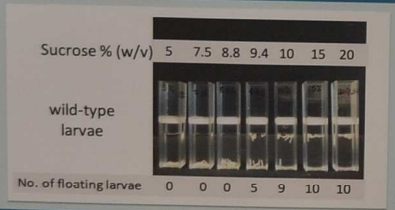

Reis, T., Van Gilst, M. R., & Hariharan, I. K. 2010

Knock-down of *Drosophila* orthologs of candidate genes causing obesity in human patients recapitulates the obesity phenotype as assessed by the buoyancy-based assay

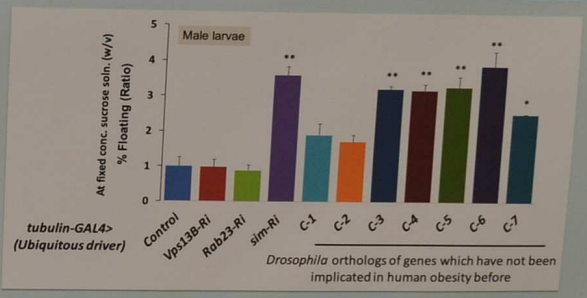

The obesity phenotype was confirmed with alternative RNAi lines. For the indicated genotypes, mean flotation scores (% floating larvae; y-axis) were calculated from multiple biological replicates of 10 larvae. ***p<0.001, **p<0.01

Fly Ortholog	Function
Vps13B	Vacuolar protein sorting 13B, post Golgi membrane trafficing
Rab23	Rab protein signal transduction
sim	single-minded, central nervous system development
C-1	G protein-coupled receptor
C-2	brain homeobox protein, neuron fate commitment
C-3	DNA binding, Circadian rhythm
C-4	DNA replication and repair endonuclease
C-5	Leucine-rich repeat-containing G protein-coupled receptor
C-6	5-hydroxytryptamine (serotonin) receptor
C-7	NAD-dependent histone deacetylase activity

Knock-down of the *Drosophila* glucagon ortholog (*akh*) or its receptor (*akhR*) by RNA-interference(*Ri*) increases fat levels while knockdown of *Drosophila* perilipin ortholog (*lsd-2*) decreases fat levels

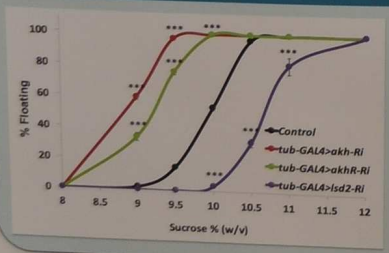

Many novel human variants from the Genetics of Obesity Study map to identical/conserved amino acid residues in *Drosophila*

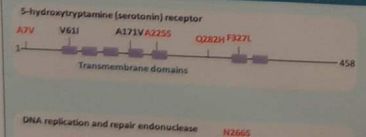

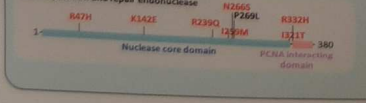

Incorporating patient-specific genetic mutations using CRISPR/Cas9

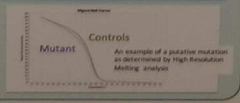

Future Perspectives

- Further validation of adiposity phenotype with other methods such as Triacylglycerol (TAG) estimation.
- Assess obesity phenotype in adult flies by ubiquitous knock-down of candidate genes.
- Incorporate patient-specific genetic mutations using CRISPR/Cas9 and assess adiposity.
- Elucidate the role of the selected candidate genes in the physiological regulation of energy homeostasis.

Identify expression and functional domains for the candidate genes

Parallel experiments in mammalian cell lines

Rescue experiments with the human or *Drosophila* gene

Identifying molecular targets of candidate genes

UNIVERSITY OF CAMBRIDGE

wellcome

CANCER RESEARCH UK

Gurdon INSTITUTE

Impacts of Innate Immunity against Tumors in *Drosophila*

Roychowdhury Arghyashree[1], Prakash Pragya[1], Goto Akira[1,2], Hoffmann Jules[1,3]

[1] Université de Strasbourg, CNRS, RIDI UPR 9022, 67000 Strasbourg, France
[2] INSERM (Institut National de la Santé et de la Recherche Médicale)
[3] University of Strasbourg Institute for Advanced Studies, Université de Strasbourg, France

Abstract

Flies have been well known in recognizing and responding to microbial invasions. These reactions include innate immune responses against various pathogens such as bacteria, fungi and viruses. Apart from this well known classical phenomena, there also have been recent reports of antitumor defense in *Drosophila* larvae . Despite considerable advances cancer treatment remains suboptimal, underlining the need for new models with which to tackle the multifaceted disease. The data although still fragmentary, a point to potential involvement of signaling pathways that mediate the interactions between tumor cells and innate immune system namely JNK pathway, the JAK-STAT pathway, the TNF pathway, the Toll and IMD pathways.

My aim is to elucidate the innate immune responses induced against oncogenic cells using adult fly as a model. A *Drosophila Ras[V12]-GFP* oncogenic cell line was used. I established an *in vivo* system by transplanting these oncogenic cells into the adult fly. Further, to have a better understanding of the response, I used flies deficient for the Toll and IMD pathway and examined its proliferation. Disappearance of the oncogenic *Ras[V12]-GFP* cells was observed in wild type and IMD mutants, but not in Toll mutant flies. The data pointed out that the Toll pathway seems to be involved in clearing off the transplanted cells in *Drosophila*.

To get further molecular insights, I examined the role of the Toll pathway in an *in vitro* cell culture system. Consistent with the *in vivo* data, the Toll pathway activation significantly hinders the proliferation of oncogenic *Ras[V12]-GFP* cells but not of *Drosophila* S2 cells in culture. Cell competition showed suppressed proliferation of *Ras[V12]-GFP* after co-culturing Toll over-expressed S2 cells.. The effect is cell non-autonomous.

Taken together , these results suggest a potential anti-proliferative role of the Toll pathway to oncogenic *Ras[V12]-GFP* in adult flies.

Ras[V12] cell : Background

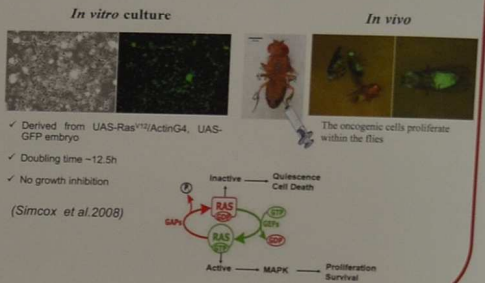

The Toll pathway is required for clearance of oncogenic *Ras[V12]* cells in adult flies

In vivo

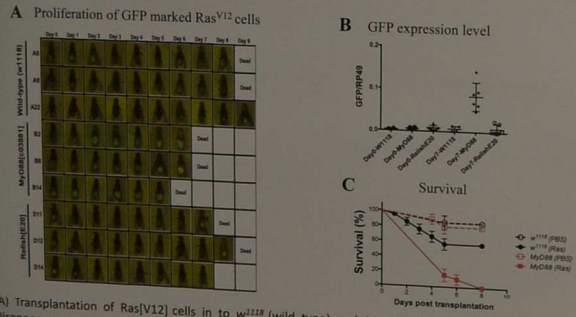

(A) Transplantation of Ras[V12] cells in to *w^{1118}* (wild type) and *MyD88^{c03881}* (Toll pathway mutant) Disappearance and re-appearance of the oncogenic cells in *wt* unlike of the Toll mutant. (B) q-PCR read out to quantify the level of GFP at Day 0 and Day 7 post transplantation. (C) Survival test of transplanted flies maintained at 22 °C.

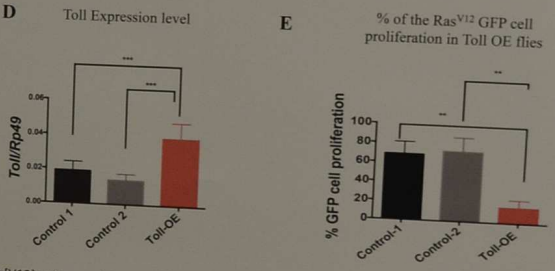

(D) Ras[V12] cells were injected in flies Act5cGal4TubG80^{ts}/UASToll10b(Toll-OE flies) +/Act5cGal4TubG80^{ts} +/UASToll10b(both used as controls). Post injection flies were maintained at 22°C. Toll over-expression in the flies. Tumor developed flies along with the control. Toll over-expression in the flies. Tumor developed flies along with the controls were collected for q-PCR validations.
(E) Tumor development rate in Toll OE and control flies. Flies injected with cells were monitored after 5-7 days under GFP fluorescence to see the oncogenic cell proliferation rate.

The Toll pathway activation hinders *Ras[V12]* cell proliferation

In vitro

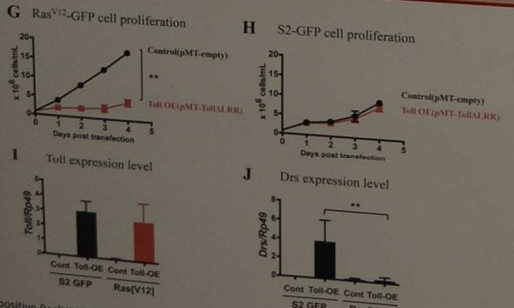

(G) GFP positive Ras[V12]cells shows decreased proliferation after Toll OE .Construct Toll OE (pMT-TollDLRR) and control vector (pMT-empty) were used for this Ca-phosphate transfection method. The cells were counted up to 96 hours post transfection . (H) Proliferation count of the S2GFP cells upon Toll OE. Unlike the Ras[V12]. Toll OE has no effect on the proliferation of the S2-GFP cells. (I) and (J) Level of Toll and Drosomycin was also monitored using q-PCR upon over-expression of Toll in Ras[V12] cell and S2-GFP cells.

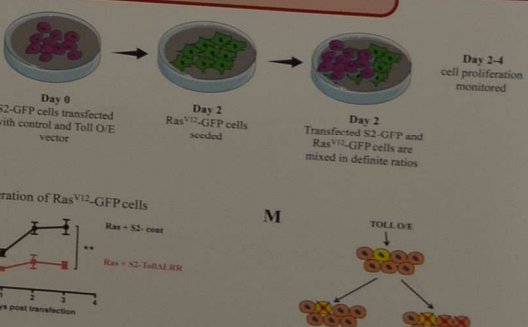

(J) The competition assay protocol. Toll transfected S2 cells (magenta) mixed with normal Ras[V12] (green) and monitored for 4 days. (L) GFP positive Ras[V12] shows decreased proliferation after co-culturing with Toll OE S2-GFP cells .Construct Toll OE (pMT-TollDLRR) and control vector (pMT-empty) were used for this Ca-phosphate transfection method. The cells were counted up to 96 hours post transfection . (K) The effect is non cell autonomous.

Conclusion and Perspectives

Highlights of the results

- Disappearance of GFP fluorescence was observed in wild type (*w^{1118}*) flies nearly 3 days after Ras[V12]-GFP cell injection, while no such phenotype was found in *MyD88^{c03881}* mutant flies.
- Activation of the Toll pathway significantly inhibits the proliferation of Ras[V12]-GFP cells but not of S2-GFP cells in cell culture system.
- Suppression of Ras[V12]-GFP cell proliferation after co-culturing with Toll over-expressed S2-GFP cells in a cell non-autonomous manner.
- RNA sequencing data identified the induction of many genes upon Toll over-expression in Ras[V12]-GFP and S2-GFP cell lines, some of which overlap.

Future Goals

- Identification of effectors involved in anti-proliferation factors by long RNA sequencing both *in vivo* and *in vitro*.
- Verification of phenotype by using different mutants of the Toll pathway *in vivo*.

Photosensitized Methylene Blue Inhibits Self-Assembly of β-Amyloid Peptides *in vitro* and *Drosophila* Model Systems

Yoon Seok Suh[1,2], Manivannan Subramanian[1,2], Byung Il Lee[3], You Jung Chung[3], Chan Beum Park[3], and Kweon Yu[1,2]

[1]Korea Research Institute of Bioscience and Biotechnology, Daejeon, Republic of Korea
[2]Korea Institute of Science and Technology, Seoul, Republic of Korea
[3]Korea Advanced Institute of Science and Technology, Daejeon, Republic of Korea

Abstract

Abnormal aggregation of β-amyloid (Aβ) peptides is a major hallmark of Alzheimer's disease (AD). In spite of numerous attempts to prevent the β-amyloidosis, no effective drugs for treating AD have been developed to date. Among many candidate chemicals, methylene blue (MB) has proved its therapeutic potential for AD in a number of *in vitro* and *in vivo* studies; but the result of recent clinical trials performed with MB and its derivative was negative. Here, with the aid of multiple photochemical analyses, we first report that photo-excited MB molecules can block Aβ aggregation *in vitro*. Furthermore, our *in vivo* study using *Drosophila* AD model demonstrates that photo-excited MB is highly effective in suppressing synaptic toxicity, resulting in a reduced damage to the neuromuscular junction (NMJ), an enhanced locomotion, and decreased vacuole in the brain. Our work suggests that light illumination can provide an opportunity to boost the efficacies of MB toward photodynamic therapy of AD in future.

Summary

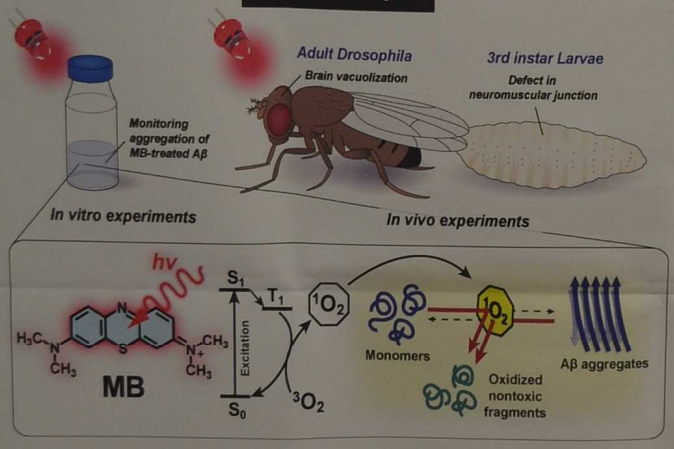

Schematic representation showing inhibition of Aβ aggregation by photo-excited MB. The *in vitro* and *in vivo* experiments performed with the *Drosophila* AD model were conducted under the illumination of red LED light. The binding interaction of MB to Aβ aggregates and the photo-oxidation of the peptides induce disruption in the structural conformation, thereby blocking (or reversing) the progress of aggregation.

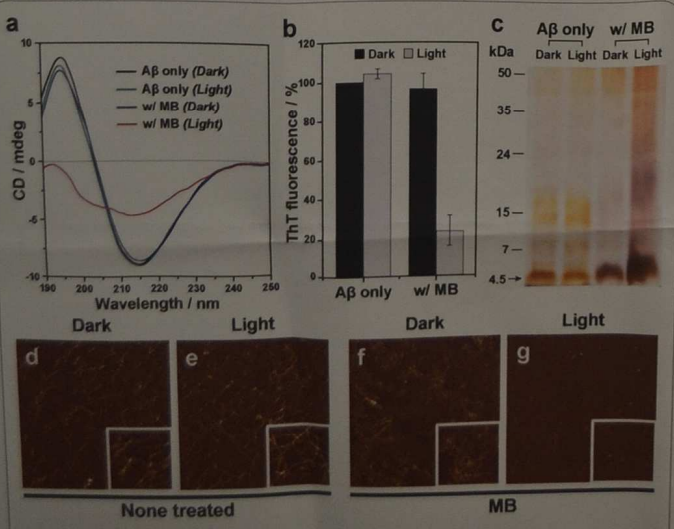

Figure 1. Light-induced suppression of Aβ self-assembly by MB. (a) CD spectra of Aβ aggregates incubated under various conditions. (b) ThT fluorescence assay to measure the formation of amyloid fibrils. (c) Silver-stained native gel electrophoresis showing that the monomeric contents was highly increased in MB treated Aβ under light illumination. The arrow indicates a 4.5 kDa molecular mass that corresponds to the monomers of Aβ. (d-g) Representative AFM images of Aβ incubated with or without MB under dark and light conditions

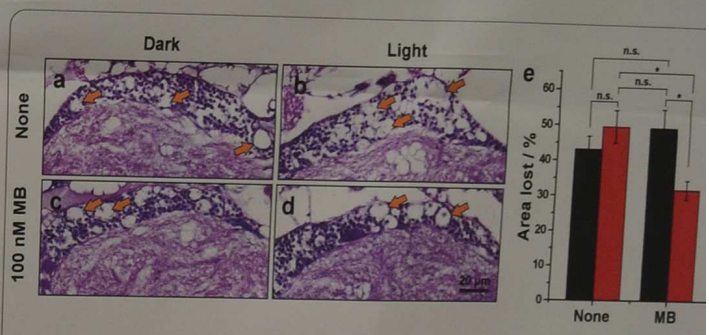

Figure 2. Photo-excited MB reduces the brain vacuolization in adult *Drosophila*. (a, d) Representative haematoxylin and eosin staining of adult head sections in AD model flies (*elav>Aβ42*) with or without 100 nM MB treatment under dark and red LED light conditions. Arrows indicate vacuole phenotypes in aged fly head. Scale bar: 20 μm. (e) Quantification of the vacuole size in adult head sections in AD model flies (*elav>Aβ42*) with or without MB treatment under dark and red LED light conditions.

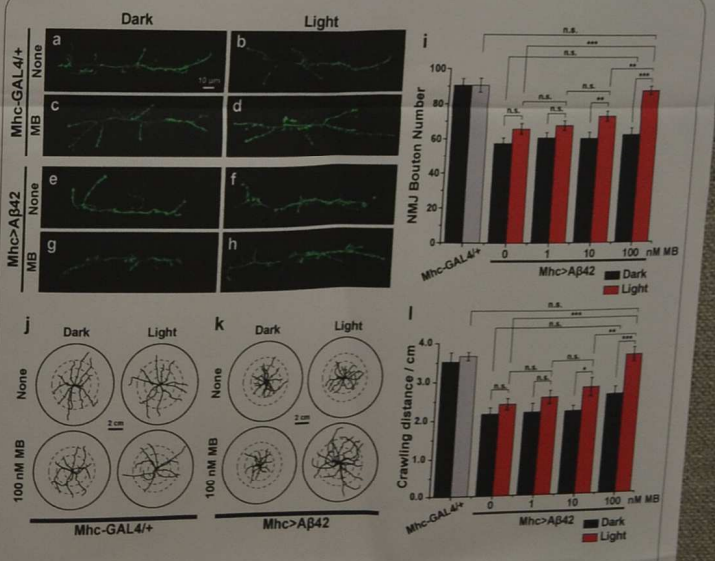

Figure 3. Photo-excited MB restores the phenotypes of Aβ toxicity in *Drosophila*. (a-h) The images of the NMJ boutons on muscle 6/7 of A3. Indicated genotype flies were incubated with or without 100 nM MB treatment under dark and red LED light. (a, c) NMJ of the *Mhc-GAL4/+* control and (e, g) NMJ of the *Mhc>Aβ42* under dark condition; (b, d) NMJ of the *Mhc-GAL4/+* control and (f, h) NMJ of the *Mhc>Aβ42* treated with or without 100 nM MB under red LED light. (h) NMJ morphology phenotype caused by Aβ42 overexpression is rescued by photo-excited MB. Scale bar: 10 μm. (i) Effect of various concentration of MB on the total number of NMJ boutons on muscle 6/7 of A3. (j, k) The diagram of the crawling path of the larvae on the plate. Diameter of inner-circles are 1.0 cm, 2.0 cm and 3.0 cm, respectively. (j) The crawling path of the *Mhc-GAL4/+* control and (k) *Mhc>Aβ42* with or without 100 nM MB treatment under dark and red LED light. Scale bar: 2 cm (l) Quantification of crawled distance of larvae within 90 seconds.

Conclusions

1. Photo-excited MB molecules exhibit a high degree of inhibition against β-amyloidosis *in vitro* and *in vivo*.

2. Photo-excited MB almost fully rescued the AD phenotypes in *in vivo* experiments performed with the *Drosophila* AD model.

3. This study hints at a new opportunity of inhibiting β-amyloidosis based on the photosensitizing property of MB, a therapeutic chemical that has been used for more than a century.

P117

Differential reactions against tumors
An insect model

Dilan Khalili, Robert Krautz*, Iris Söll, Giselbert Hauptmann and Ulrich Theopold

Department of Molecular Biosciences, The Wenner-Gren Institute, Stockholm University, SE- 106 91 Stockholm, Sweden
**Gurdon Institute and Department of Physiology, Development and Neuroscience, University of Cambridge, United Kingdom*

Introduction

We are interested in exploring how the immune system reacts against aberrant cells, including tissues at early stages of tumor progression. In our model for early stages of tumorigenesis, we induce a tumorigenic state in a non-immune tissue, namely the salivary glands (SG) in fly larvae. This induction leads to the activation of both the cellular and humoral immune response[1]. In addition, we observe differential regulation of genes in different parts of the tumor. Focusing on the JNK- and JAK/STAT-pathways, we find JNK is expressed in the distal part of the gland, whereas the JAK/STAT is upregulated in the proximal part. In the distal part of the salivary gland, tumors fall under stress due to a production of reactive oxygen species, induction of apoptosis, and invasion by hemocytes; the proximal part was stress-free. Our findings suggest that separate areas of a tissue may respond differently towards induction of aberrant cells.

Summary

- **Differential regulation of JNK and JAK/STAT pathways in tumorous SG**
- **JNK activated predominantly in the distal region**
- **JAK/STAT pathway is activated in the proximal region**
- **JNK is involved in basal membrane degradation, apoptotic induction and activation of ROS production**

At 120 h AED (after egg deposition), JNK-pathway is predominantly activated in the distal part, whereas JAK/STAT-pathway is restricted to the proximal part of the Ras^{V12} salivary glands

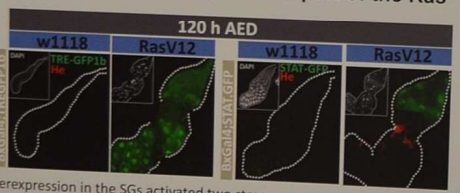

RasV12 overexpression in the SGs activated two stress response pathways, JNK and JAK/STAT. JNK (Left panel: green) is predominantly induced in the distal part and JAK/STAT (Right panel: green) in the proximal, assessed by the expression of their respective reporter constructs. In the distal part, hemocytes (red) are recruited to the region where the JNK pathway is also induced.

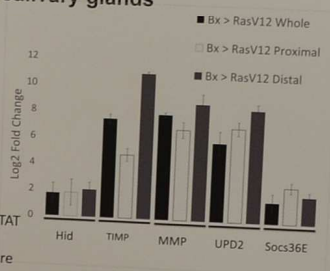

To verify the readout from the JNK and JAK/STAT reporter constructs, whole, distal and proximal 120 h AED SG were dissected. qPCR was performed for known JNK (hid, TIMP, MMP1 and UPD2) and JAK/STAT (Socs36E) target genes. In line with reporter constructs, JNK target genes (TIMP, MMP1, and UPD2) were expressed higher in the distal part of the SG in comparison to the proximal region. Moreover, JAK/STAT target genes (Socs36E) had a higher expression pattern in the proximal region whereas in the distal, the expression was lower. These results confirm that there is a differential regulation of the two stress response pathways.

RasV12 mediates action of Dronc (caspase), a down-stream component of JNK pathway

Drosophila JNK-pathway is known to mediate apoptosis, ROS production, and recruitment of hemocytes. Therefore, we asked whether JNK caused induction of apoptosis in the distal part of the RasV12 salivary gland and whether JNK is the apoptotic inducer in our model.

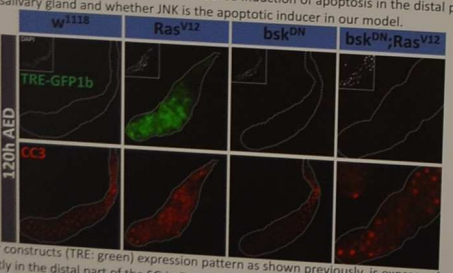

JNK-reporter constructs (TRE: green) expression pattern as shown previously, is expressed predominantly in the distal part of the SG in RasV12 SG. Knocking-down Bsk reduces expression of the JNK-reporter construct. Overexpression of RasV12 caused an increase of Dronc activity (CC3: red) in the distal part of SG. However, Dronc activity was also detected in the proximal region. Thus, further experiments are needed to conclude apoptotic distribution. Nevertheless, dronc activity is dependent on bsk (JNK ortholog), as demonstrated by the genetic knock-down of bsk (BskDN;;RasV12) reducing CC3 staining.

RasV12 mediates activation of ROS, a down-stream stress response via JNK

Next, we asked whether ROS was produced in RasV12 tumor model and whether it was also dependent of JNK.

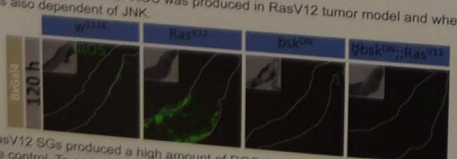

RasV12 SGs produced a high amount of ROS (green) in the distal part in comparison to the control. To answer whether ROS production was mediated via JNK-pathway we knocked-down Bsk. As a result, none or little ROS levels were detectable in bskDN;;RasV12 SGs. The evidence suggests that JNK mediates ROS induction in RasV12 SGs. However, whether activations of ROS occur via Dronc remains to be answered.

Activation of the JNK-pathway causes recruitment of hemocytes in RasV12 SG

From previous studies (Hauling et al., 2014), we could show that hemocytes (Hemese AB:Red) are recruited to the RasV12 tumors. Therefore, we investigated whether we could prevent hemocyte recruitment by knocking-down JNK

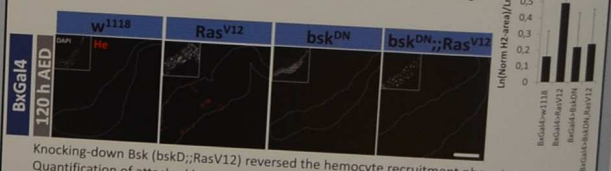

Knocking-down Bsk (bskD;;RasV12) reversed the hemocyte recruitment phenotype. Quantification of attached hemocytes to the SGs verified this observation (right figure), where bskDN;;RasV12 SG had the same amount of hemocytes as the control w1118. Hence, hemocyte recruitment is JNK dependent in RasV12 SG. Preliminary data suggests ROS is an important factor for recruitment of the blood cells (not shown here).

Tumor model

In the RasV12 SG tumor model, we found stronger JNK expression in the distal part of the SG. In parallel, in the proximal SG, the JAK/STAT-pathway was upregulated. Moreover, overexpression of RasV12 in SGs caused an increase in Dronc activity, ROS production and hemocyte recruitment. Blocking JNK reverted all the previously mentioned phenotypes;less dronc activity, greatly reduced levels of ROS and very few hemocytes were seen to be attached to the tumor. From previous studies (Hauling et al., 2014), we showed that RasV12 SG expressed MMPs which lead to basal membrane degradation and created possibility for hemocytes to infiltrate. These results indicate that blocking JNK restores the basal membrane (not shown here) and reduces ROS levels which thus hinders hemocyte ability to be recruited or infiltrate the RasV12 SGs.

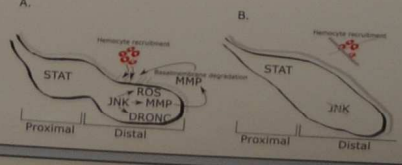

Reference
1. Hauling, T. *et al. Biol Open* 3, (2014)

P163

FlyBase & Community

Silvie Fexova, Jose M. Urbano, Alix Rey, Giulia Antonazzo, Gary Grumbling, Aoife Larkin, Jim Thurmond, Nicholas H. Brown and the ***FlyBase Consortium***

FlyBase Community Advisory Group

The **FlyBase Community Advisory Group (FCAG)** was launched in 2014 and currently has 542 members recruiting from among the FlyBase users around the world. The group provides essential feedback on new features and changes to FlyBase through regular surveys.

Members of the group are sent up to 6 surveys a year on a variety of different subjects, e.g. curation priorities or report page layout.

The FCAG currently has members in 41 countries. Our aim is to have at least one representative from every *Drosophila* research group.

Countries with representation in FCAG

FCAG survey pipeline

① FlyBase user becomes member of FCAG → ② FlyBase sends email to FCAG members with a link to a survey → ③ FlyBase evaluates the survey results and implements changes as appropriate

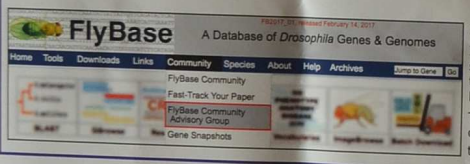

Join the FCAG

If you use FlyBase in your research we encourage you to join the FCAG and have your say on how it works!

The link to the FCAG wiki is located under the Community button menu.

Fast-Track Your Paper

Fast-Track Your Paper (FTYP) is an online tool which enables community curation of scientific papers.

FlyBase sends out an email the corresponding authors of all newly published *Drosophila* papers to encourage them to fill out the FTYP form. By using the FTYP tool, the authors ensure that their paper is quickly linked on the FlyBase website to the primary genes studied, help FlyBase by highlighting data types requiring in-depth manual curation and make sure their publication is prioritized for further curation by FlyBase. Papers lacking an FTYP entry made by the authors are screened by automated text-mining programmes to discover whether they contain data requiring manual curation but are ranked below the papers with an FTYP record in the queue for in-depth curation by FlyBase curators.

Fast-Track Your Paper pipeline

① FlyBase sends an email to corresponding authors of newly published papers every week. This email contains a link to a customized FTYP form pre-populated with citation data.

FTYP filled in → ② Data are entered into FlyBase (visible to users in the next public release)

FTYP NOT filled in → ③ Reminder email is sent to the authors two weeks after the original one

Access the FTYP tool

You can access the Fast-Track Your Paper tool from the Community button menu located at the top banner of every FlyBase page

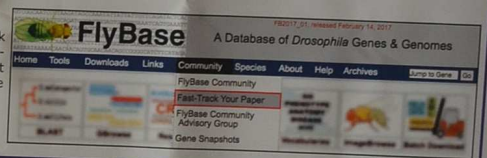

Video Tutorials

FlyBase regularly posts short video tutorials on a dedicated YouTube channel - the **FlyBase TV** - to help users navigate FlyBase and make the best use of the various tools it offers.

Access the Videos

You can access the FlyBase TV YouTube channel from our Help menu or from the YouTube button at the bottom of every FlyBase page. Links to videos are also present on tool pages where applicable.

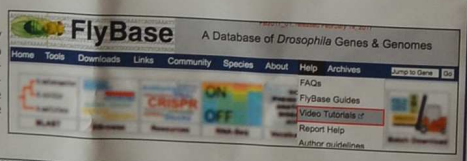

Be Alerted to Newly Released Video Tutorials

You can subscribe to FlyBase TV and be alerted directly by email to any new video releases. Simply go to the FlyBase TV channel, and click on the red Subscribe button.

Suggest a Topic for a Video

Please contact FlyBase if you have an idea for a new video. The 'Contact FlyBase' form can be found at the bottom of every FlyBase page.

Existing Video Tutorials

Basic Navigation & Tools

- How to find all data related to a gene
- How to generate an excel file of all alleles of a gene
- Finding related genes in FlyBase: Gene Groups
- Finding related genes/alleles in FlyBase: Vocabularies
- Finding related genes in FlyBase: The Gene Ontology
- Using the Orthology search tool

RNA Seq Series

- Part I: Using GBrowse
- Part II: Using RNA-Seq Profile Search
- Part III: Searching for Similarly Expressed Genes

FlyBase Guidelines

- How to cite FlyBase
- Authors Guidelines

Gene Snapshots

Gene Snapshots are short summaries solicited from an expert researcher, curated and standardized by FlyBase, that provide a quick overview of the function of a gene product. For now these are limited to protein-coding genes and appear at the top of each *D. melanogaster* gene report. Gene Snapshots are also downloadable via the Batch Download tool and our precomputed files page to aid in genome-wide analyses and screens.

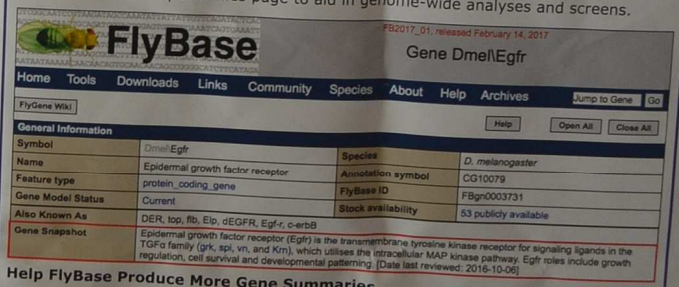

Help FlyBase Produce More Gene Summaries

- Thanks to the great response from the community, as of the FB2017_01 FlyBase release, there are 1901 gene summaries available in the database.
- However, many genes are still lacking their Snapshot and we very much welcome user contributions!
- If there currently is no Snapshot available for your subject gene, please send us your suggested summary via a standardized form accessible either directly from the gene page (via the 'Contributions welcome' hyperlink in the Gene Snapshot field) or from the Gene Snapshot wiki page via the Community button menu at the top banner of every FlyBase page.

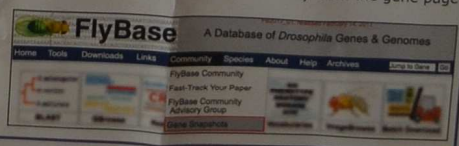

*The **FlyBase Consortium** include: Nicholas H. Brown, Steven J. Marygold, Gillian Millburn, Giulia Antonazzo, Helen Attrill, Silvie Fexova, Phani Garapati, Alex Holmes, Tamsin Jones, Aoife Larkin, Alix Rey, Vitor Trovisco, Jose M. Urbano (FlyBase-Cambridge), Nobert Perrimon, Cassandra Extavour, Julie Agapite, Kris Broll, Lynn Crosby, Gil dos Santos, David Emmert, L. Sian Gramates, Kathleen Falls, Beverley Matthews, Susan Russo, Christopher Tabone, Pinglei Zhou, Mark Zytkovicz (FlyBase-Harvard), Thomas Kaufman, Bryon Czoch, Josh Goodman, Gary Grumbling, Victor Strelets, Jim Thurmond (FlyBase-Indiana), Richard Cripps, Maggie Werner-Washburne, Phillip Baker (FlyBase-NewMexico)*

FlyBase is supported by a grant from the National Human Genome Research Institute at the **U.S. National Institutes of Health** (U41HG000739). Support is also provided by the **British Medical Research Council** (G1000968) , the Indiana Genomics Initiative, and the **National Science Foundation** through XSEDE resources provided by Indiana University.

Finding the right tool for the job: new ways to find particular types of transgenic construct in FlyBase

Gillian Millburn (gm119@cam.ac.uk) and the FlyBase Consortium

Introduction

The long history of fly research plus the sophisticated range of applicable genetic engineering techniques mean that a large number of increasingly complex transgenic fly lines have been generated and described in the literature. While this rich genetic tool-kit helps to make *Drosophila melanogaster* an ideal model organism to answer a wide range of biological questions, it also creates a potential problem - how to find the most appropriate fly line for a particular experiment from the large set that is available. To help overcome this issue, FlyBase will start to capture and display information about **Experimental Tools**, which will allow you to easily identify transgenic constructs and their insertions with particular characteristics. We are defining an experimental tool as "any sequence ***whose own biological function isn't really being studied*** in an experiment, but is instead being ***exploited*** to study the biological function of some other gene product or product somewhere specific within a cell (*e.g.* nuclear localisation signal, signal sequence), driving expression (*e.g.* GAL4, lexA), enabling clonal/conditional expression (*e.g.* FLP, FRT), being used as a sensor for changes in Ca^{2+}, pH, voltage *etc., etc.*

Experimental Tool Report

** MOCKUP **

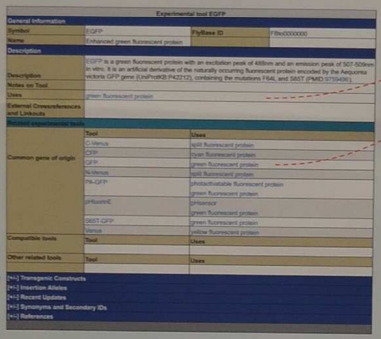

Uses term(s) describe what the tool is *used for*.
- Click on the term to go the **Uses Term Report**

Related experimental tools section will make it easy to jump to reports for related tools at a finer level of detail than the "Uses" section.
- Click on the **Tool** name to go to its **Tool Report**
- Click on the **Uses** to go to the corresponding **Term Report**

Columns list the components that make up the transgenic construct

Link to relevant **Gene** (*e.g. Rh4*) or **Tool** (*e.g. UAS*) report

Where the main gene product is a tool, columns list **Tool** (*EGFP*) and its **Uses** (*green fluorescent protein*)

Additional **Tool(s)** (*e.g. FRT*) in the construct that do not form part of the encoded product

** MOCKUP **

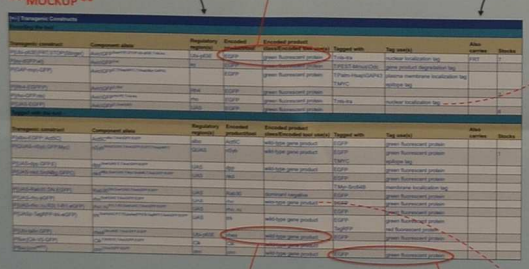

Click on any column heading to reorder the tables

Where the function of the encoded product is being studied, columns list the encoded **Gene** (*rheo*) and its **Product Class** (*wild-type gene product*)

List of **Tools** (*EGFP*) that are fused to the main gene product, plus their **Uses** (*green fluorescent protein*)

** MOCKUP **

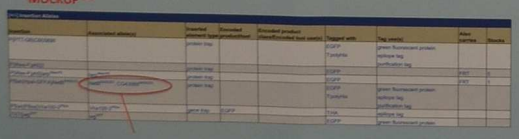

Insertion into overlapping genes

'Experimental Tool Uses' Term Report

** MOCKUP **

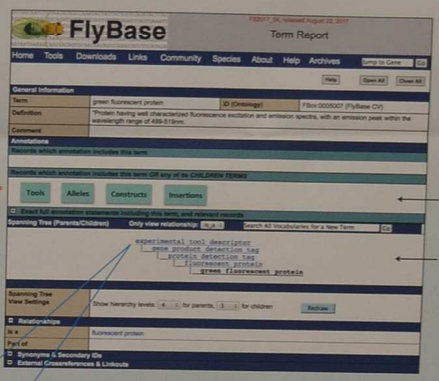

Click for a list of all objects associated with this term

Uses Tree
- Explore the hierarchy to find related uses and associated tools

Main branches of **Uses** tree and examples of **Tools**

- experimental tool descriptor
  - binary expression system component
  - gene product activity regulation tag
  - gene product cleavage tag
  - gene product degradation tag T:miGFPi, T:PEST-Mmus\Odc
  - gene product detection tag
    - RNA detection tag
    - protein detection tag
      - epitope tag T:MYC, T:FLAG, T:polyHis
      - fluorescent protein
      - reporter enzyme lacZ, pLUC
  - gene product localization tag T:Myr-Src64B, T:nla-tra
  - genetically encoded sensor
    - mechanical force sensor
    - pH sensor pHluorinF
    - redox state sensor
    - small molecule sensor
    - voltage sensor
  - purification tag T:polyHis
  - site-specific recombinase FLP, FLPm5, cre
  - site-specific recombination target region FRT, mFRT71, loxP
  - split system component

- binary expression system component
  - binary expression system - driver GAL4, GAL4::VP16, QF
  - binary expression system - regulatory region UAS, QUAS
  - binary expression system - repressor GAL80, QS

- fluorescent protein
  - blue fluorescent protein EBFP
  - cyan fluorescent protein Cerulean, CFP
  - far-red fluorescent protein mKate
  - green fluorescent protein EGFP, GFP, PA-GFP
  - infra-red fluorescent protein
  - modulatable fluorescent protein
    - fluorescent timer protein slowFT
    - photomodulatable fluorescent protein
      - photoactivatable fluorescent protein PA-GFP
      - photoconvertible fluorescent protein Dendra2
      - photoswitchable fluorescent protein Dronpa
  - orange fluorescent protein mKO
  - red fluorescent protein mCherry, tdTomato
  - yellow fluorescent protein EYFP, Venus

- split system component
  - split driver - DNA-binding fragment GAL4DBD-Zip-
  - split driver - transcription activation fragment VP16AD-Zip+
  - split fluorescent protein C-Venus, N-Venus
  - split reporter enzyme lacZ-$\Delta\alpha$, lacZ-$\Delta\omega$

New terms can be added to describe other kinds of tool as new techniques and tools are developed.

Current ideas to expand the list of terms include:
- 'genome engineering' tools *e.g.* Cas9
- neuron activation/inhibition tools *e.g. channel rhodopsins*
- ***Anything else ?***

feedback wanted !

'Transgenic Product Class' Term Report

The **Transgenic Product Class** is intended to give an *overview* of the nature of the gene product encoded by a transgenic construct, similar to **Allele Class** used for classical and insertional alleles.
- It will be used for constructs where the function of the encoded gene product is being studied or where the construct encodes a sequence that affects an endogenous gene product (*e.g.* RNAi)
- It will allow constructs to be grouped into broad categories for browsing and searching, for example in the **Transgenic Constructs** tables on the **Tool Report** and in similar tables on the **Gene Report** (see below).

** MOCKUP ** part of **rho** gene report

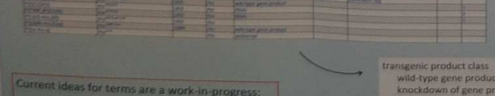

Click on any column heading to reorder the table

transgenic product class
- wild-type gene product
- knockdown of gene product
  - RNAi
  - antisense
- dominant negative
- constitutively active
- phosphomimetic mutation
- non-phosphorylatable mutation
- catalytic site mutation

Current ideas for terms are a work-in-progress:
- Are the terms shown useful ?
- Are there any terms missing that you'd like to see ?

feedback wanted !

Searching

We have recently introduced a '**GAL4 etc.**' search, but it is currently limited to searching for a small number of common drivers (*GAL4, QF, lexA*) and reporters (*lacZ, GFP*).

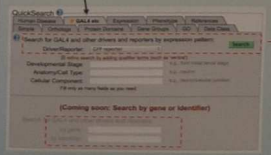

2. You will be able to use the **regulatory region** information to search for tools whose expression pattern reflects that of a particular gene.

Once we have introduced the **Tool Reports** and **Tool Uses** terms we will be able to expand this search as illustrated below.

1. The search can be expanded to include any type of tool.

Typing in the **Tool Uses** box will bring up all the matching Uses terms. *e.g. typing 'fluor'*

** MOCKUP **

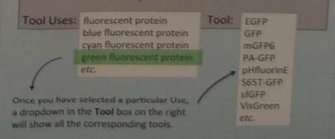

Once you have selected a particular Use, a dropdown in the **Tool** box on the right will show all the corresponding tools.

Alternatively, if you know which **Tool** you want to search for, you will be able to type it directly into the **Tool** box.

The FlyBase Consortium comprises: Nick Brown, Giulia Antonazzo, Helen Attrill, Silvie Fexova, Phani Garapati, Tamsin Jones, Alex Holmes, Aoife Larkin, Steven Marygold, Gillian Millburn, Alix Rey, Vitor Trovisco, Jose-Maria Urbano (FlyBase-Cambridge), Norbert Perrimon, Julie Agapite, Kris Broll, Lynn Crosbie, Gil dos Santos, David Emmert, Kathleen Falls, Susan Russo Gelbart, L. Sian Gramates, Beverley Matthews, Christopher Tabone, Pinglei Zhou, Mark Zytkovics (FlyBase-Harvard), Thomas Kaufman, Bryon Couch, Josh Goodman, Gary Grumbling, Victor Strelets, Jim Thurmond (FlyBase-Indiana), Richard Cripps, Maggie Werner-Washburne, Phillip Baker (FlyBase-NewMexico)

FlyBase is supported by a grant from the National Human Genome Research Institute at the U.S. National Institutes of Health (U41HG000739).
Support is also provided by the British Medical Research Council (AG83674) , the Indiana Genomics Initiative, and the National Science Foundation through XSEDE resources provided by Indiana University.

MRC Laboratory of Molecular Biology

UNIVERSITY OF CAMBRIDGE

Formation and function of supracellular actomyosin cables

Dina Julia Ashour, Yara Sanchéz-Corrales, Katja Röper

MRC Laboratory of Molecular Biology, Francis Crick Avenue, Cambridge Biomedical Campus, Cambridge CB2 0QH

INTRODUCTION

Our lab is interested in mechanisms guiding morphogenetic events. We use the fruit fly as our main model organism to investigate changes in tissue morphology during the invagination and tubulogenesis of the salivary gland during embryo development.

In our model system a supracellular actomyosin cable is formed during invagination of the epidermal cells to form the tubules of the salivary gland. This cable has shown to be under tension during invagination, pointing to a possible role of the cable in either driving invagination or possibly maintaining tissue integrity during this morphogenetic process.

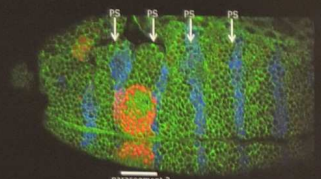

Figure 1: Localisation of the salivary gland placode in the developing embryo. The placode is located in the 2nd parasegment bordering the ventral midline. Myosin labelled with sqhGFP (green). Salivary gland placode labelled with anti-eyegone (red) and parasegmental boundaries highlighted with anti-engrailed (blue)

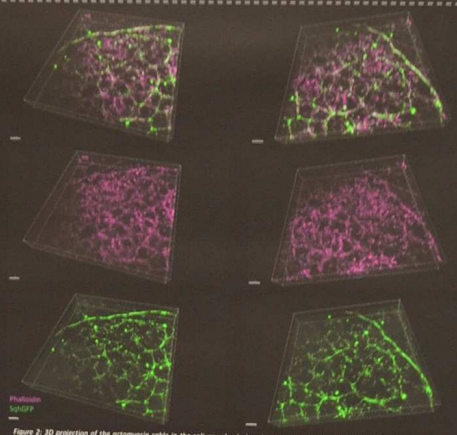

Figure 2: 3D projection of the actomyosin cable in the salivary gland placode. Myosin regulatory light chain (SqhGFP) in green and actin (Rhodamin phalloidin) in purple. Images were obtained using Structured Illumination Microscope OMX.

GLAND DEVELOPMENT

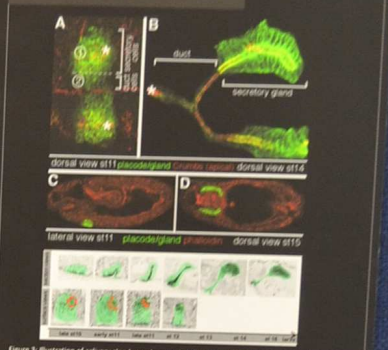

Figure 3: Illustration of salivary gland morphogenesis (A) Ventral view of the two salivary gland placodes at stage 11. Brackets: position of the cells fated to form the secretory part of (1) the gland and (2) the duct; asterisks: focal points through which the cells invaginate. (B) Fully formed gland at stage 14. Brackets: formed secretory and ductal parts; asterisk: opening of the duct on the surface of the embryo. green: UAS-membrane- GFP specifically expressed in the salivary glands using fkh-Gal4. Red: Crumbs outlining apical cortices in A and B; (C and D) Position of glands in whole embryos (C) lateral view; (D) dorsal view. phalloidin labeling F-actin (C and D); (E) section and surface views of the salivary gland placode and gland during development. Labelled for Crumbs (black), placodal cells highlighted in green.

Zasp52 – a new component of the cable

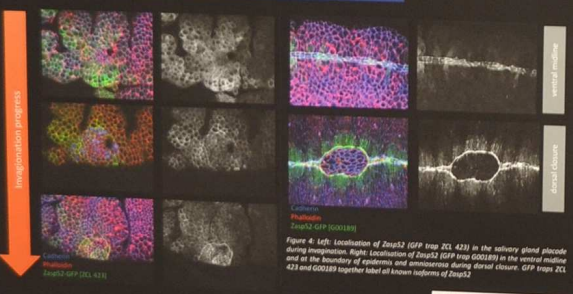

Figure 4: Left: Localisation of Zasp52 (GFP trap ZCL 423) in the salivary gland placode during invagination. Right: Localisation of Zasp52 (GFP trap G00189) in the ventral midline and at the boundary of epidermis and amnioserosa during dorsal closure. GFP traps ZCL 423 and G00189 together label all known isoforms of Zasp52

- Zasp52 is a Enigma/Alp family protein, it associates to α-actinin in muscle Z-lines via its PDZ domain
- Zasp is the only member of the Alp/Enigma family of PDZ-LIM domain proteins in *D. melanogaster*, while this family encompasses seven members in vertebrates
- Several isoforms of Zasp52 have been reported in flies that differ in the number of LIM domains present

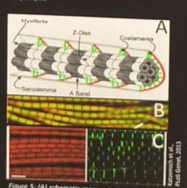

Figure 5: (A) schematic representation of a sarco-mere including its substructures (B) Image of fixed indirect flight muscles in D. melanogaster. Actin is shown in red, Myosin in green; Alayari et al., J Cell Sci. 2005 (C) Antibody staining of IFM in adult fly. Red = actin, green = Zasp52 in Z-lines

Other cable components

- The cable consists of actomyosin and other proteins have been shown to locate to the site of the cable itself or to be enriched inside the placode

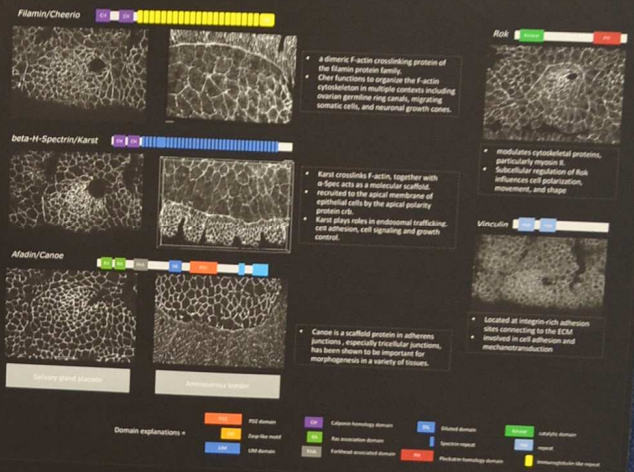

Assembly of cable myosin

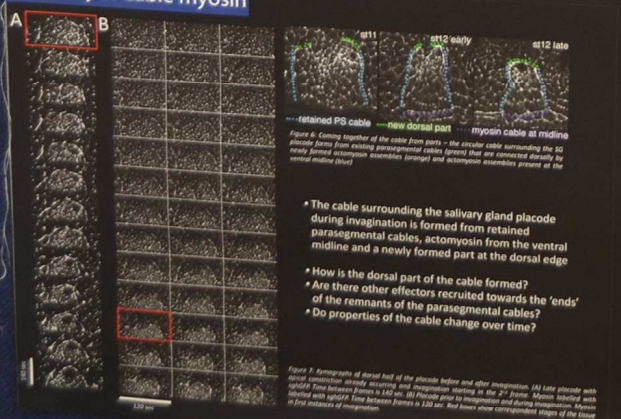

Figure 6: Coming together of the cable from parts – the circular cable surrounding the SG placode forms from existing parasegmental cables (green) that are connected dorsally by newly formed actomyosin assemblies (orange) and actomyosin assemblies present at the ventral midline (blue)

- The cable surrounding the salivary gland placode during invagination is formed from retained parasegmental cables, actomyosin from the ventral midline and a newly formed part at the dorsal edge
- How is the dorsal part of the cable formed?
- Are there other effectors recruited towards the 'ends' of the remnants of the parasegmental cables?
- Do properties of the cable change over time?

Figure 7: Kymographs of dorsal half of the placode before and after invagination. (A) Late placode with apical constriction already occurring and invagination starting in the 2nd frame. Myosin labelled with sqhGFP. Time between frames is 140 sec. (B) Placode prior to invagination and during invagination. Myosin labelled with sqhGFP. Time between frames is 120 sec. Red boxes show correspondent stages of the tissue in first instances of invagination.

Hypothesis and Outlook

- Zasp52 has been shown to be essential to formation of the supracellular actomyosin cable during dorsal closure (Ducuing et al., Nat Cell Biol, 2016)
- Zasp52 is also an integral part of sarcomere z-discs where it maintains structure necessary for muscles to contract
- The actomyosin cable is a contractile structure with unknown molecular organisation of its components
- Sarcomeric organisation of non-muscle myosin at apical junctions of epithelial cells has been observed in mouse tissues (Ebrahim et al.,Curr Biol, 2013)
- **The presence of Zasp52 in the cable opens up the possibility that the cable is structured similarly to a sarcomere**

Next steps:

- Confirm whether the cable of the salivary gland placode is absent in the Zasp52Δ mutant
- Assess presence of sarcomere-associated proteins in the cable
- Assess molecular organisation of actomyosin in the cable

Generation of non-centrosomal microtubules promotes apical-medial actomyosin accumulation during tube morphogenesis in *Drosophila*

Ghislain Gillard, Gemma C. Girdler, Alexander J.R. Booth, & Katja Röper

MRC Laboratory of Molecular Biology, Cambridge Biomedical Campus, Francis Crick Ave, Cambridge CB2 0QH, UK.

MRC Laboratory of Molecular Biology

INTRODUCTION

Most of our organs, including all the respiratory, secretory and circulatory organs, are composed of tubes. Using *Drosophila* embryos, we are investigating tube formation during salivary gland morphogenesis. SG formation begins at embryonic stage 11 with invagination of two sets of ectodermal cells, this invagination being due to apical constriction that change the cell morphology into a wedge-like shape. Proper apical constriction relies on the accumulation of actomyosin at the apical-medial domain. Surprisingly, whereas the role of the actomyosin cytoskeleton in morphogenesis has been extensively studied, little is known about the role of MTs in morphogenesis. However, recent work in the lab has highlighted a role for non-centrosomal MTs (ncMTs) in apical-constriction by promoting apical-medial recruitment of actomyosin [1]. I will present here a project and preliminary results aiming to identify first how these ncMTs are formed then how they promote apical constriction.

Salivary gland (SG) morphogenesis

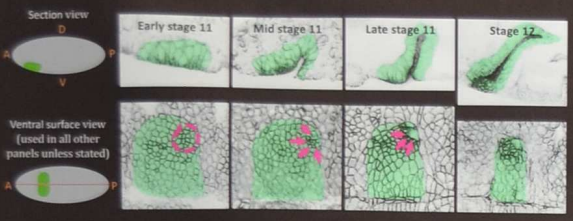

Apical constriction

Apical-medial recruitment of actomyosin

Formation of ncMTs during SG morphogenesis

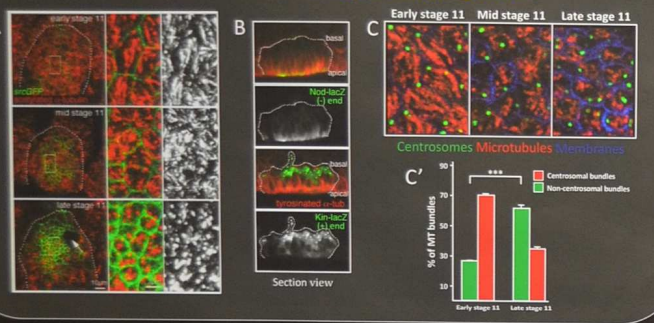

ncMTS are required for medial actomyosin accumulation

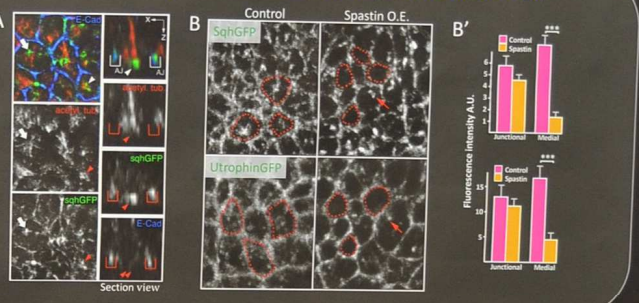

1. Formation of ncMTs through centrosomal release?

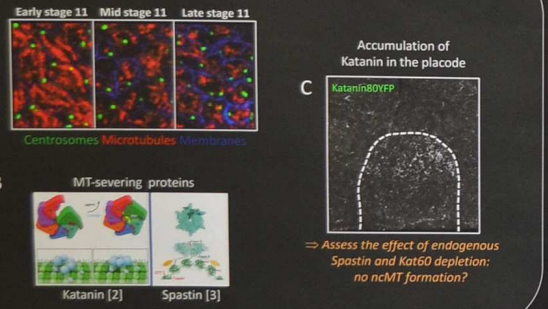

⇒ *Assess the effect of endogenous Spastin and Kat60 depletion: no ncMT formation?*

2. ncMTs recruit the actomyosin meshwork through the formation of a medial hub

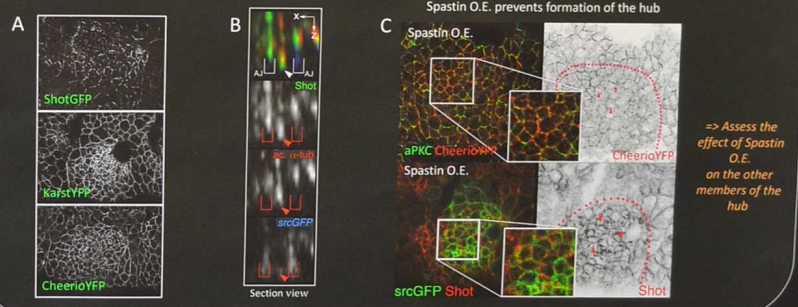

⇒ *Assess the effect of Spastin O.E. on the other members of the hub*

3. How are ncMTs relocated to the apical-medial site?

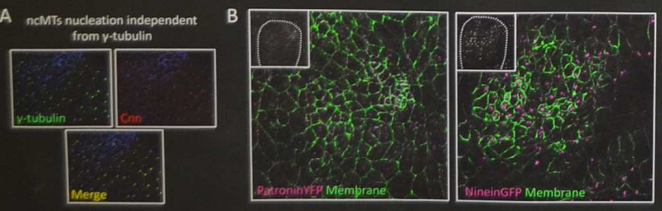

⇒ *Assess the effect of Patronin and Ninein depletion: no ncMT stabilisation at medial site?*

Who comes first? Protein degradation in the placode

Proof of concept of the efficiency of degradFP-mediated protein depletion [4] in *Drosophila* SG placode. Karst is degraded in SG placode as well as in the surrounding epidermis under enGal4-driven degradFP expression (brackets).

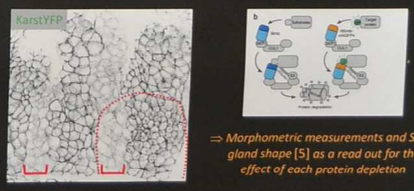

⇒ *Morphometric measurements and SG gland shape [5] as a read out for the effect of each protein depletion*

Who comes first? Live imaging of individual components of the hub

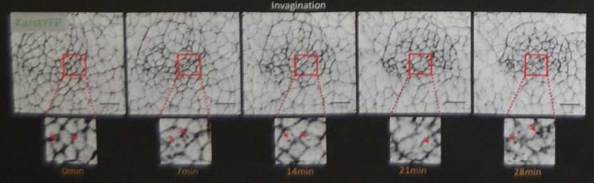

Karst accumulates medially in the placode (red arrows) before invagination, suggesting an early requirement in this process

WORKING MODEL

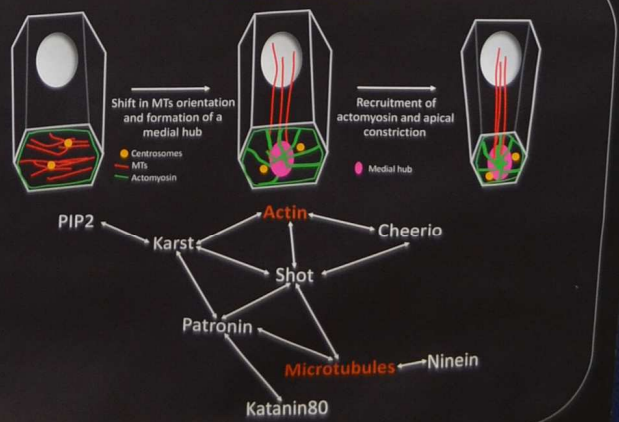

References

1. Booth et al. (2014) *Dev. Cell* 29:562-576
2. Zehr et al. (2017) *Nat. Struct. Mol. Biol.* 24:717-725
3. Caussinus et al. (2011) *Nat. Struct. Mol. Biol.* 19:117-122
4. Sharp & Ross (2012) *J. Cell Sci.* 125:2561-2569
5. Maybeck & Röper (2008) *Genetics* 181:543-56

Role of Collagen IV in cell intercalation

Vincent Loreau, Audrey Placenti, Delphine Cérézo, Marilyne Malbouyres, Florence Ruggiero, Stéphane Noselli and Véronique Van De Bor

Introduction

Basement membranes (BMs) form an essential extracellular protein meshwork, holding cells together. BMs are quite diverse and their composition defines organ biomechanical properties. They have essential role in different cellular behaviors like migration, polarity, cell survival and differentiation. However, the molecular mechanisms underlying these functions as well as the signalling pathways involved are poorly characterized. To tackle these questions we study how BM controls the cell intercalation process leading to the inter-follicular stalks' formation in *Drosophila*'s ovaries.

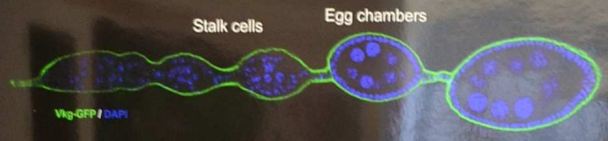

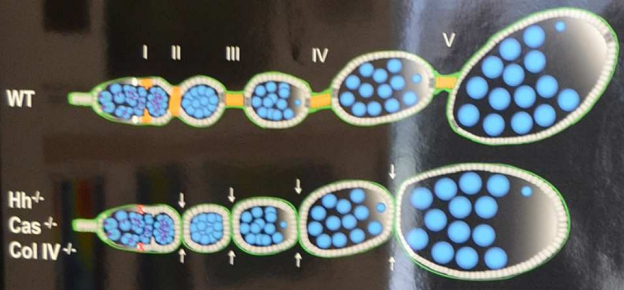

1 – Stalks' BM is thickening during intercalation

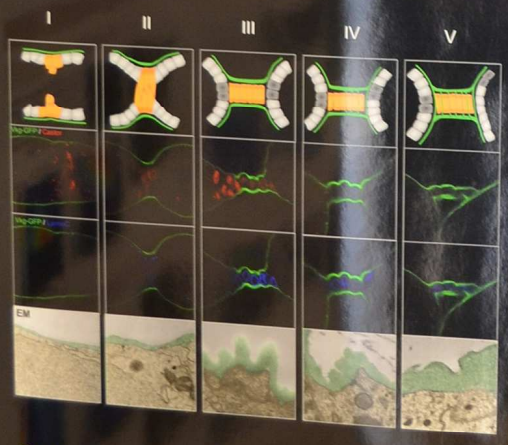

2 – Stalks' BM is produced by different tissus

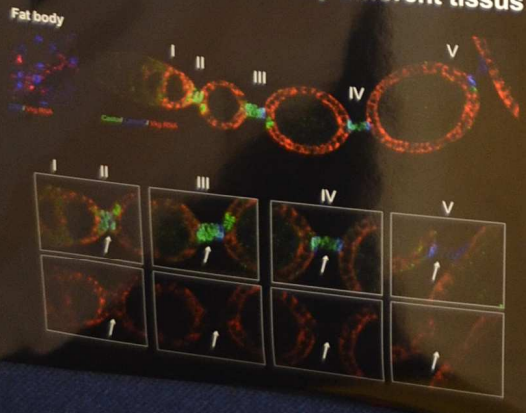

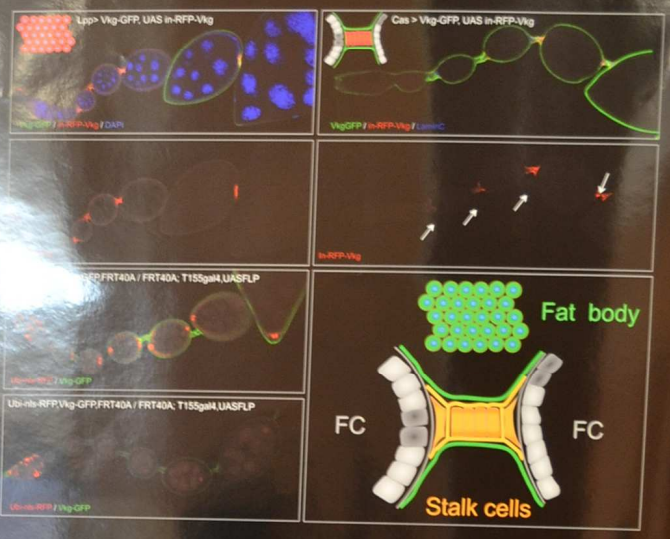

3 – BM deposition is required for stalks formation

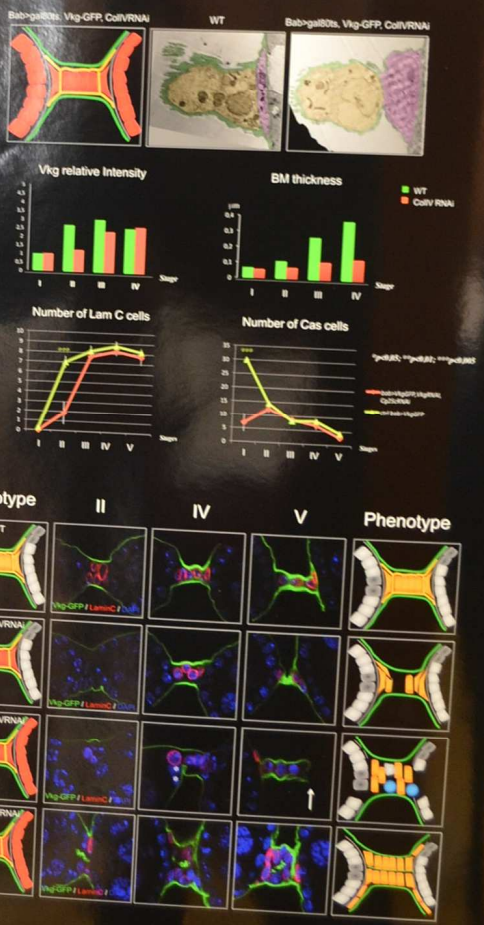

Conclusions and future work

The stalks' BM is thickening during the intercalation process and has multiple origins. The Col IV produced by the stalk cells and the FCs is not involved in stalk cells' differentiation but is essential for stalks and ovarioles integrity. Pcan is required for the intercalation process.

We are currently investigating whether Col IV produced by the fat body is important for the differentiation and the intercalation processes. Finally, we are investigating the role of other BM's components in these two processes.

The Role of Sidekick at Apical Vertices in Epithelial Morphogenesis

Tara Finegan[1], Nathan Hervieux[1], Alexander Fletcher[2], Guy Blanchard[1] and Bénédicte Sanson[1].
[1]Department of Physiology, Development and Neuroscience, University of Cambridge, UK.
[2]School of Mathematics & Statistics & The Bateson Centre, University of Sheffield, UK.
E-mail: tmf32@cam.ac.uk, nh480@cam.ac.uk, a.g.fletcher@sheffield.ac.uk, gb288@cam.ac.uk, bs251@cam.ac.uk.

UNIVERSITY OF CAMBRIDGE

1. We use the early *Drosophila* embryo as a model for tissue elongation

Drosophila embryos extend their body axis in a process called **germband extension (GBE)** using a common morphogenetic process found in animal development: **convergence and extension.**

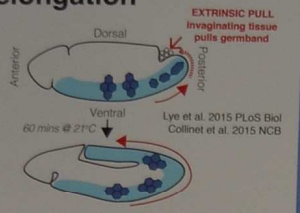

cell intercalation

a cell intrinsic process driven by active junction remodelling

\+

cell shape changes

PULL

a cell extrinsic process driven by tissue being pulled

=

tissue deformation

These contributing behaviours can be separated and quantified

Butler et al. (2009) NCB & Blanchard et al. (2009) Nat Met

2. Cell intercalation is driven by actomyosin activity and changes in adhesion

Intercalation occurs specifically at actomyosin enriched boundaries established by anteroposterior (AP) patterning (Tetley et al. 2016 eLife ; Paré et al. 2014 Nature) .

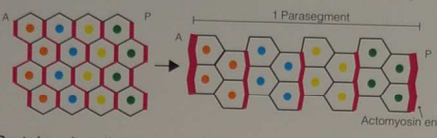

Epithelia are polarised

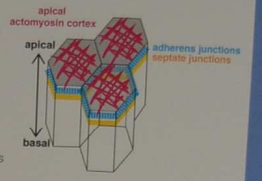

Proteins localised at apical adherens junctions drive intercalation.

Lecuit, Lenne, Wieschaus and Zallen labs

Apical view of cells intercalating in a "T1 transition":

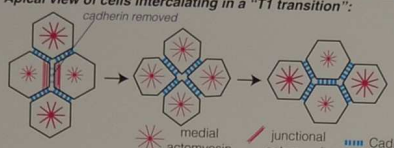

Actin-based protrusions basally also contribute to intercalation (Sun et al. (2017) NCB).

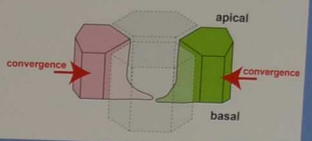

3. Research question: What is the role of vertices during epithelial morphogenesis?

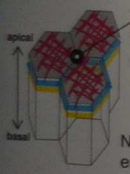

Vertices are points where 3 or more cells meet.

Vertices must be remodelled during cell intercalation:

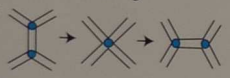

No vertex specific proteins found in the early embryo during GBE (no mature septate junctions).

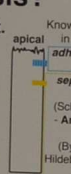

Known vertex proteins in other epithelia:

adherens junctions:
none

septate junctions:
- **Gliotactin** (Schulte et al. 2003)
- **Anakonda / Bark Beetle** (Byri et al. 2015 & Hildebrandt et al. 2015)
- **Mud** (Bosveld et al. 2017)

4. The Ig superfamily protein Sidekick defines apical vertices

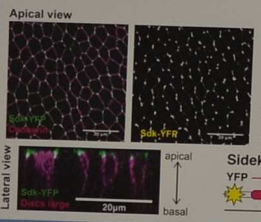

Screening YFP-tagged proteins, we discovered that Sidekick localises specifically to vertices at the level of adherens junctions (Lye et al. 2014 Dev).

Sidekick is the first protein found to localise at vertices at the level of adherens junctions in any epithelia.

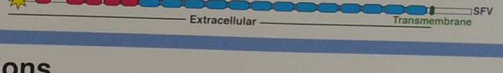

5. Sdk-YFP invades shrinking junctions

Super resolution SIM imaging reveals Sdk-YFP forms 'strings' at vertices:

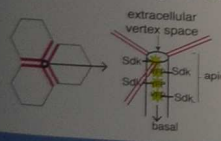

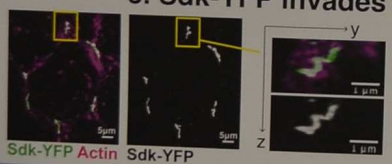

Shrinking junctions:

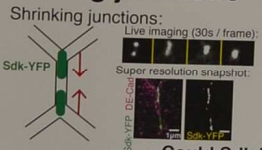

Growing junctions:

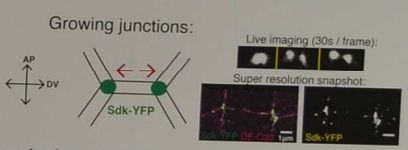

• Could Sdk be playing an active role in intercalation?

6. *sdk* mutants show severe intercalation defects, compensated for by an increase in cell shape changes

• AP patterning and actomyosin enrichments are maintained in *sdk*:

• *sdk* mutants show abnormal tissue geometry:

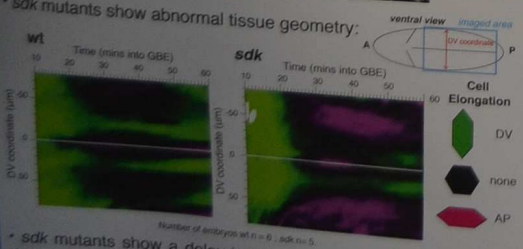

• *sdk* mutants show a delay in GBE and a severe intercalation defect, compensated for by an increase in cell shape changes:

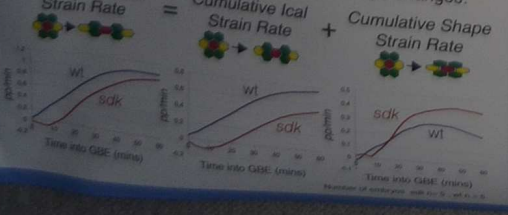

7. A computational vertex model recapitulates the *sdk* phenotype

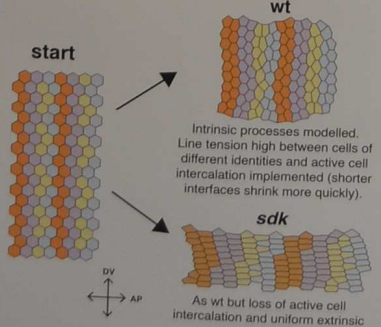

8. Sdk is required for epithelial tissue integrity during morphogenesis

Epithelial holes are more common and persist for longer in *sdk* mutants.

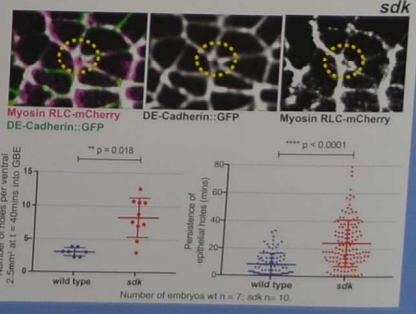

9. Conclusions and model

1. We discovered the first protein to localise to epithelial vertices at adherens junctions: Sidekick.
2. Sidekick is required for correct active cell intercalation driven at the apical domain.
3. *sdk* mutants complete GBE because the cell intercalation defect is compensated by cell shape changes, driven by the posterior extrinsic pull.
4. Epithelial holes are formed in *sdk* mutants undergoing epithelial morphogenesis.

sdk-

P221

Matching partners in a stochastic neuronal circuit

Maximilien Courgeon and Claude Desplan

Department of Biology, New York University, 100 Washington Square East, 9 New York NY 10003, USA

•Stochastic specification of photoreceptors in the fly retina:

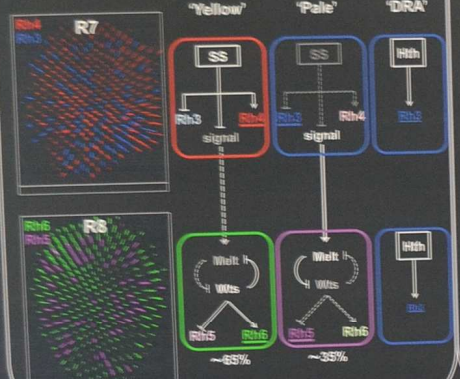

•Development and organization of the fly visual system:

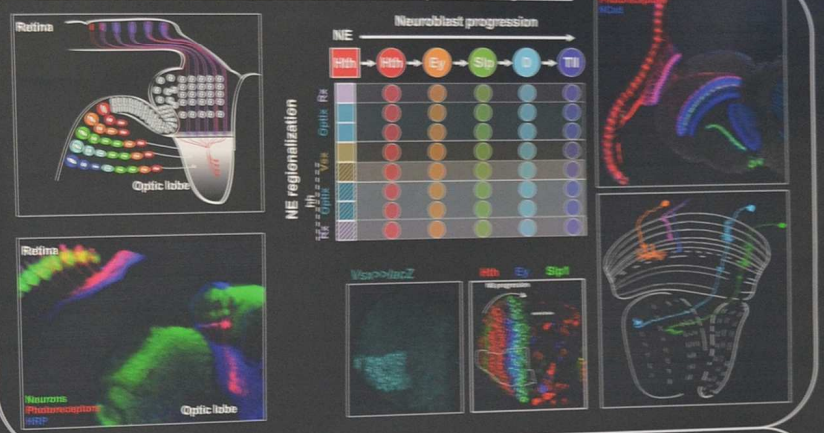

• A pair of cell adhesion molecules is expressed in $_{yellow}$R7s and their targets in the brain:

•Dprt1 is expressed in $_{yellow}$R7s:

•DIPγ is expressed in the medulla:

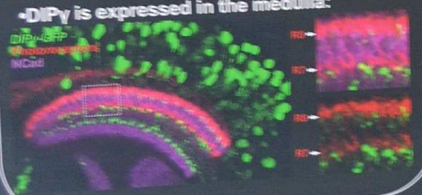

• A subset of Dm8s expressed DIPγ:

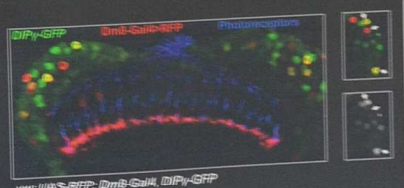

yw; UAS-RFP; Dm8-Gal4, DIPγ-GFP

• DIPγ$^+$Dm8s are paired with $_{yellow}$R7s:

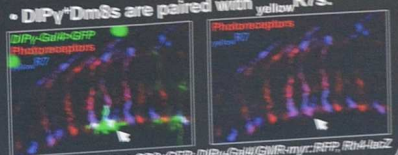

yw, hs-flp; UAS>stop>CD8::GFP; DIPγ-Gal80, Dm8-Gal4/GMR-myr::RFP, Rh4-lacZ

• $_{pale}$Dm8 do not express DIPγ:

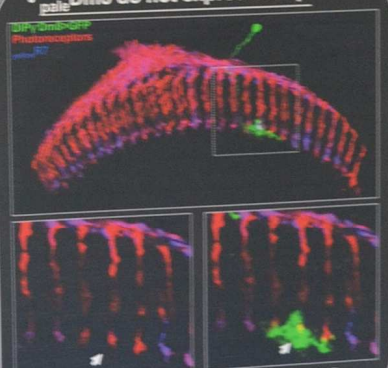

yw, hs-flp; UAS>stop>CD8::GFP; DIPγ-Gal80, Dm8-Gal4/GMR-myr::RFP, Rh4-lacZ

• $_{DRA}$Dm8 have a specific morphology:

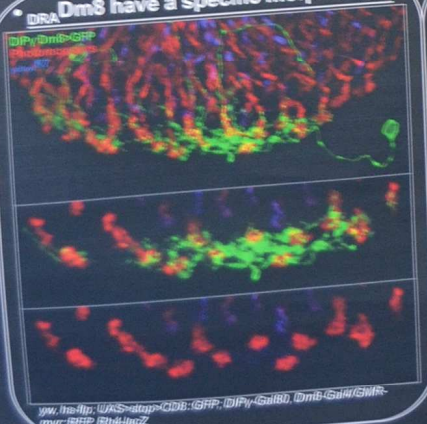

yw, hs-flp; UAS>stop>CD8::GFP; DIPγ-Gal80, Dm8-Gal4/GMR-myr::RFP, Rh4-lacZ

• Developmental origin of $_{yellow}$Dm8s:

•Dac+DIPγ+ neurons are $_{yellow}$Dm8s:

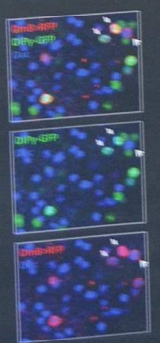

*$_{yellow}$Dm8s are produced by a specific region of the neuroepithelium:

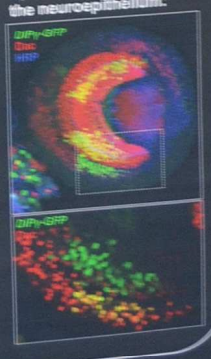

• Future directions:

- Function of Dprt1 and DIPγ (in collaboration with Kai Zinn and Kaushiki Menon, Caltech)
- Role of other Dprs and DIPs in matching photoreceptors and their targets
- What mechanisms ensure the right stoichiometry of photoreceptors and their targets?

• Acknowledgements:

- Our collaborators:
Kai Zinn and Kaushiki Menon
- For reagents:
Hugo Bellen
Larry Zipursky
- The Desplan lab
- Vilaiwan Fernandes for the schematics

46

Circadian Control of Mechanosensation

Jason Somers[1], Jake Cable[1] Ross EF Harper[1,2], Ariana Hübner[1,2], Jörg T Albert[1,2]

[1]Ear Institute, University College London, London, United Kingdom
[2]Centre for Mathematics and Physics in the Life Sciences and Experimental Biology (CoMPLEX), University College London, London, United Kingdom
[j.somers@ucl.ac.uk] [joerg.albert@ucl.ac.uk]

Abstract: The circadian rhythms of an animal's physiology are driven by molecular oscillations within a variety of tissues; some tissues are under hierarchical control of central pacemakers, but several tissues in *Drosophila* display autonomous, molecular and functional, oscillations[1]. This project will investigate a similar phenomenon in chordotonal organs focussing on the fly ear, i.e. the Johnston's organ (JO), which is located in the second antennal segment (a2). The JO is a cluster of mechanosensitive neurons that transduce antennal motions into nerve impulses. Here, the daily profiles of their energy expenditure should ideally be matched to the daily profiles of their corresponding mechanosensory behaviours.

Gene expression in JO

Is there a molecular clock in the JO?

Clock genes are expressed in the JO in phase with clock gene expression in the head

Mechanosensory gene expression show no clear oscillations

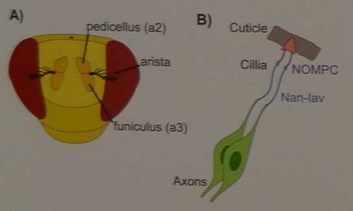

(A - B) Anatomy of fly antenna and chordotonal neurons

(C - E) qPCR results of clock gene and mechanosensory TRP channel genes expression in adult head and JO over a day. Values are normalised by Z-score +/- SEM for three biological repeats.

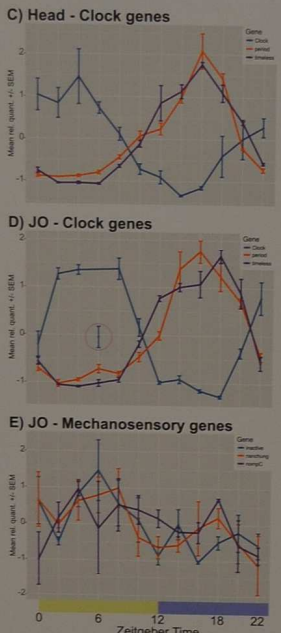

Sensitivity to mechanical vibrations

Mechanosensation also allows the fly to response to less subtle stimuli while also providing proprioceptive feedback during flight and locomotion. Oscillations in response to mechanical stimuli were investigated.

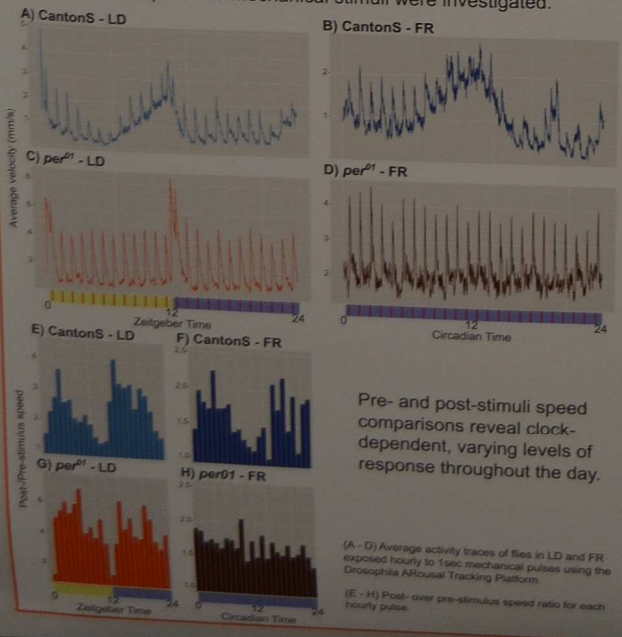

Pre- and post-stimuli speed comparisons reveal clock-dependent, varying levels of response throughout the day.

(A - D) Average activity traces of flies in LD and FR exposed hourly to 1sec mechanical pulses using the Drosophila ARousal Tracking Platform.

(E - H) Post- over pre-stimulus speed ratio for each hourly pulse.

Clock controlled biophysics of the antennal ear

Drosophila antennal ears are finely tuned to their conspecific courtship song via an active process that requires an injection of energy. As auditory dependent behaviours (e.g. courtship) exhibit circadian rhythms, rhythms of antennal biophysics of the antenna were explored.

Changes were observed in some parameters but not consistent in FR conditions.

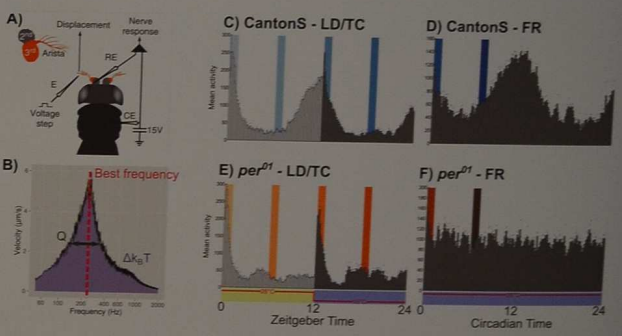

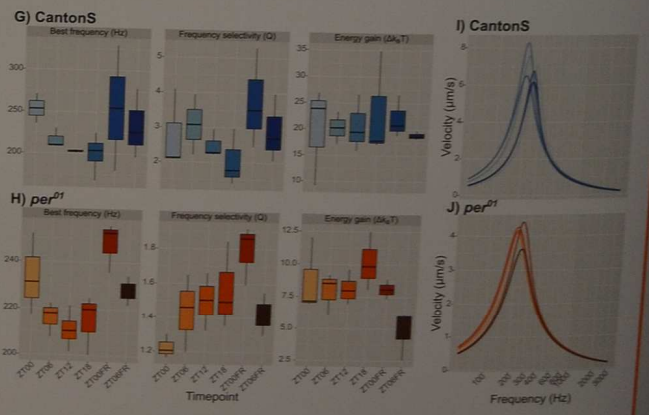

(A) Diagram of Laser Doppler Vibrometry set up. Laser is focussed on the arista tip and motion is recorded.
(B) Example FFT generated frequency velocity data demonstrating extracted parameters.
(C - F) Average activity hisograms for CantonS and *per*^{01} clock mutant entrained to in-phase 12-hour light:dark temperature cycles. Flies were entrained for at least 4 days before being measured or released into FR conditions.
(G - H) Box-plots of extracted parameters measured from 6 separate timepoints see (B) for visual representation of parameters.
(I - J) Median fit of each timepoint for both genotypes. Fit uses a dampened harmonic oscillator model.

Future work

Investigate mechanosensory protein levels/ localisation

Biophysics assays with females

White noise and/or step stimulus experiments to dissect motor/transducer contribution to antenna tuning

Entrainment using pure mechanical stimulus

Funding

UCL CoMPLEX
erc
European Research Council

References

1 - Krishnan, B. *et al.* Nature **400**, 375-378 (1999)
2 - Faville, R. & Kottler, B. *et al.* Sci. Rep. **5**, (2015)
3 - Riabinina, O. *et al.* Curr. Biol. **21**, 658-664 (2011)

P24

Motor Neurons and the Path to Synaptic Specificity

Lalanti Venkatasubramanian, Jonathan Enriquez and Richard S. Mann

COLUMBIA UNIVERSITY IN THE CITY OF NEW YORK

COLUMBIA | ZUCKERM
Mortimer B. Zuckerman Mind Br

OVERVIEW : DEVELOPMENT OF DROSOPHILA LEG MOTOR NEURONS

LATE LARVA – 96hrs AEL

PUPA – 125hrs AEL

ADULT – 240hrs AEL

VENTRAL NERVE CORD

T1 LEG

COMBINATORIAL TRANSCRIPTION FACTOR CODES TO IDENTIFY INDIVIDUAL LEG MOTO

Late L3 CNS

LinB
7 MNs

LinA
29 MNs

Birth order of MNs

Co1
Tr1
Fe1
Tr2
Co2
Co3
Co4

Eve
Eve Pb Zfh1
Eve Pb Zfh1
Eve Pb Zfh1
Zfh1 Toy
Zfh1 Toy Prox
Zfh1 Toy Prox

Distal Fe STi
Proximal Fe STi

TRANSCRIPTION FACTOR CODES SPECIFY LEG MOTOR NEURON TARGETING

LinB
T1 Leg

LinA
T1 Leg

WT

Co1
Tr1
Fe1
Tr2
Co2
Co3
Co4

Co
4 MNs

Fe
1 MNs

Tr
2 MNs

UAS-ems, UAS-ab

Cox to Fe

ab^{5}, zfh1^{5}, UAS-zfh2

Fe
13 MNs

Ti
15 MNs

Tr
1 MN

UAS Zfh1

Di to Pr Fe

Proximal Fe STi
Distal Fe STi
Zfh1
Cas

A NOVEL GROUP OF IG DOMAIN TRANSMEMBRANE PROTEINS AND THEIR INVOLVEMENT IN LEG MOTOR NEURON TARGETING

DPR-ome NETWORK

cDIP
DPR
DIP
cDIP

Ozkan et al., 2013
Carrillo et al., 2015

DIP-ALPHA AFFECTS TARGETING OF LEG MOTORNEURONS TO LONG TENDON MUSCLES

Ab-Gal4 > GFP

DIP-Alpha-T2AGal4 > GFP

DIP-Alpha$^{-/-}$
Ab-Gal4 > GFP
DIP-Alpha$^{-/-}$
Zipursky Lab

αFe
αTi-a
αTi-b

N=3/9
N=9/9

EXPRESSION OF DIP-ALPHA BINDING PARTNERS IN ADULT LE

Dpr6-T2AGal4 > GFP

Dpr10-T2AGal4 > GFP

Acknowledgement: DIP and Dpr MiMIC T2A Gal4 lines were generated in a collaboration between the Bellen, White, Zuker, Dreyfus and Zipursky labs.

CHARACTERISATION OF DIP-ALPHA EXPRESSING LEG MOTOR NEURONS

DIP-Alpha 84,805bp

Enhancer
Ab
GAL4

MiMIC Cassette
Venken et al., 2011

RMCE T2A-Gal4
Diao et al., 2015

SA
T2AGAL4
pA
SD

Late L3 T1 LinA

Dorsal
Ventral

Early Pupa T1 LinA

Late Pupa T1 LinA

Adult VNC
T1 - Hemisegment

MN Cell Body

Ab-Gal4 > MCFO

Adult VNC

Ab-Gal4 > GFP

DIP-Alpha-T2AGal4 > GFP
DIP-Beta-T2AGF-2 > mCherry

αTi-b
αTi-a
αFe

WORKING MODEL AND FUTURE DIRECTIONS

Early Larva
Late Larva
Pupa
Leg Disc

NB

Sub-cellular Localisation?
DIP-Alpha
dpr6, dpr10

Axon targeting gene(s) are turned on

Adult VNC

T1 Leg

References

1. Baltz et al., 2004
Baek and Mann, 2009
2013
3. Enriquez et al., 2015
Neurons and combinatorial
Stewart et al., 2014
mCherry) 5. Venken et al., 2011
library) 6. Diao et al., 2015
Gal4) 8. Ozkan et al., 2013
2015; Tan et al., 2015
Nern et al., 2015 (MCFO)

Unpublished
1. DIPalpha T2A-Gal4s
Bellen, White, Zuker, Dreyfus Labs
2. DIP-Alpha -/- Zipursky Lab

P360

More than black or white: Variable roles of the melanization reaction in *Drosophila* immunity

J.P. Dudzic, D. Main, B. Lemaitre
Ecole Polytechnique Fédérale de Lausanne (EPFL), Global Health Institute, Lausanne, Switzerland
jan.dudzic@epfl.ch

Abstract The arthropode immune mechanism of melanization is catalyzed by enzymes called Prophenoloxidases (PPOs)[1]. After an initial stimulus these PPOs are activated by a cascade of serine proteases (SPs)[2]. We investigated the role of two SPs previously connected to melanization: *Hayan* and *Sp7*[3,4]. We found two distinct modes of melanization depending on the involved SP. *Hayan* is involved in the local melanization of the wound site, while *Sp7* dependent melanization is necessary for the clearance of septic infections.

Fig. 1

Fig.1: Clean injury confirms alternating phenotypes in two serine proteases involved in melanization. Wild-type animals show rapid melanization of wound sites. *Hayan* mutant flies show a loss of melanization (arrow) while larval melanization is only partially impaired. Flies mutant for *Sp7* show an alternating phenotype: melanization in adult flies is not impaired while larvae show a complete loss of melanin deposition (arrow). The *PPO1,2,3* mutant acts as control for the total loss of melanization[5].

Fig.2: Survival experiments with *S. aureus* show susceptibility of *Sp7* mutants. While wound melanization seems intact in adults, *Sp7* mutants phenocopy the survival defect of melanization deficient flies. In contrast: *Hayan* flies which do not show wound melanization show no survival defect. Flies with defective IMD or Toll pathway are not susceptibility against *S. aureus* revealing a melanization specific phenotype.

Fig. 2

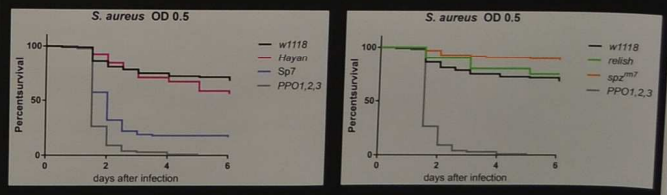

Fig.3: Infection with fluorescent *S. aureus* reveals that *Sp7* mutants can not control infections albeit wound melanization seems not affected. *Hayan* mutants clear infections quickly although wound melanization is not apparent. Flies mutant for melanization (*PPO1,2,3*) show the same

Fig. 3

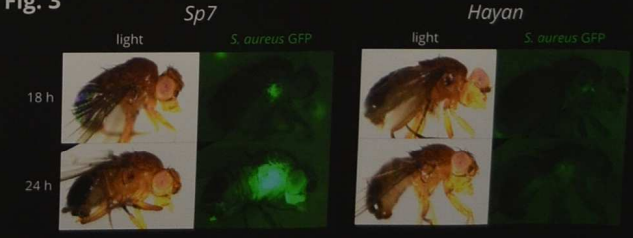

Fig. 4

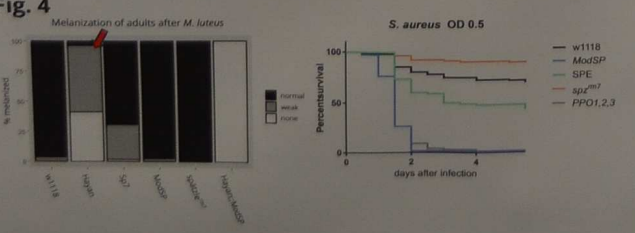

Fig.4: Gram positive *M. luteus* can induce wound melanization in absence of *Hayan* compared to clean injury wounding (see Fig. 1), which suggests a role of the Toll pathway in melanization. Combined melanization and survival experiments reveal further evidence for the Toll pathway activating serine protease *ModSP* which might branch to the melanization pathway to activate *Sp7* dependent clearance of *S. aureus*.

Conclusion: Two distinct types of the melanization reaction can be assumed by the shown evidence. While *Hayan* seems essential for proper melanization of wound sites in adult flies, it does not show any defect in the melanization dependent clearance of *S. aureus*. Sp7 on the contrary seems to be dispensable for the melanization of wound areas, but is mandatory for surviving *S.aureus* infections in adult flies. Elements of the Toll pathway activating cascade seem to be involved in the differential activation of those two, non-redundant melanization functions, which are dependent on the activating SP.

References: 1: Cerenius, L. and Söderhäll, K. (2004). The prophenoloxidase-activating system in invertebrates. Immunological Reviews, 198.
2: Kanost, MR., Jiang, H., Wang, Y., Yu, XQ., Wu, C. et al (2001). Hemolymph proteinases in immune responses of Manduca sexta. Adv Exp Med Biol, 484
3: Ligoxygakis, P., Bulet, P. and Reichhart, JM. (2002). The serine protease Sp7 is expressed in blood cells and regulates the melanization reaction in Drosophila. Biochemical and Biophysical Research Communications
4: Buchon, N., Broderick, NA., Poidevin, M., Pradervand, S. and Lemaitre, B. (2009). Drosophila intestinal response to bacterial infection: activation of host defense and stem cell proliferation. Cell Host Microbe, 5
5: Dudzic, JP., Kondo, S., Ueda, R., Bergman, CM., Lemaitre, B. (2015). Drosophila innate immunity: regional and functional specialization of prophenoloxidases. BMC Biol 13

Functional characterization of *Drosophila* adenosine deaminase-like protein (ADAL) in embryogenesis

Yu-Hsien Lin[1], Michal Zurovec[2]

Faculty of Science, South Bohemia University, Czechia
Entomology Institute, Biology Centre CAS, Czechia
(r99632012@gmail.com[1]; zurovec@entu.cas.cz[2])

Introduction

Adenosine deaminase-like protein (ADAL) has been shown to be involved in the metabolism of N_6- or O_6- substituted purine nucleoside monophosphates in humans (Murakami et al., 2011; Schinkmanova et al., 2006). However, the physiological roles of ADAL are still unclear in any kind of model organism. In the present study, we generated a null *adal* mutant by CRISPR/Cas9 approach and described the function of *Drosophila adal* gene (CG11194) in *Drosophila* embryogenesis.

adal mutagenesis by CRISPR/Cas9

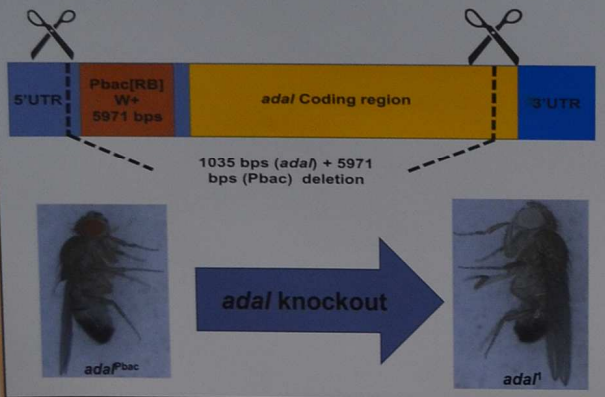

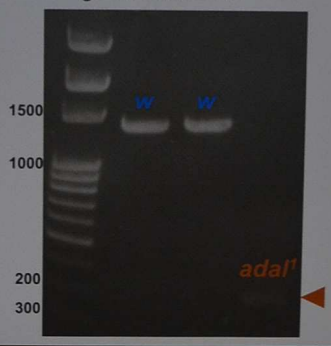

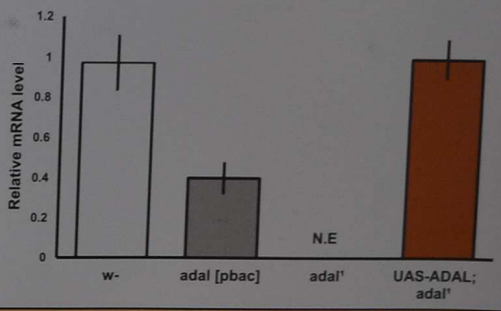

Larval development and eclosion rate

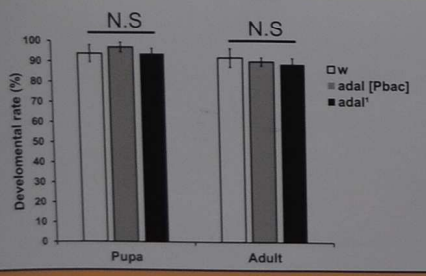

Hatching rate in *adal* mutant

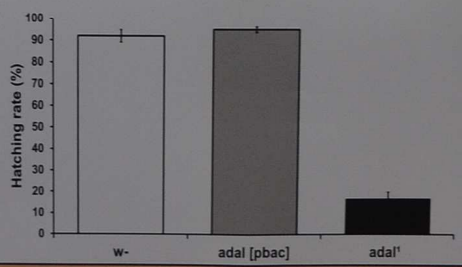

adal expression in early embryogenesis

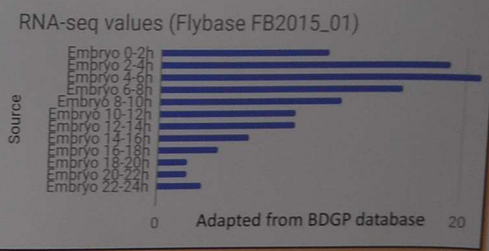

adal as a maternal effect gene

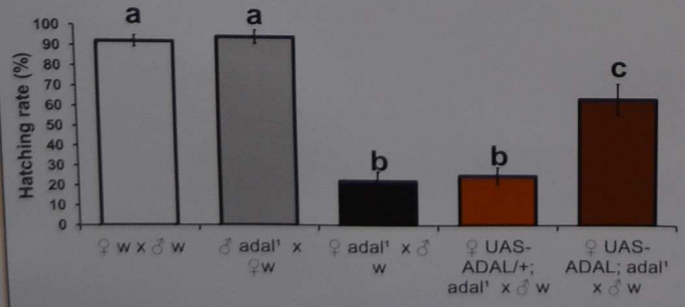

Embryogenesis interruption (5-6 hours embryo)

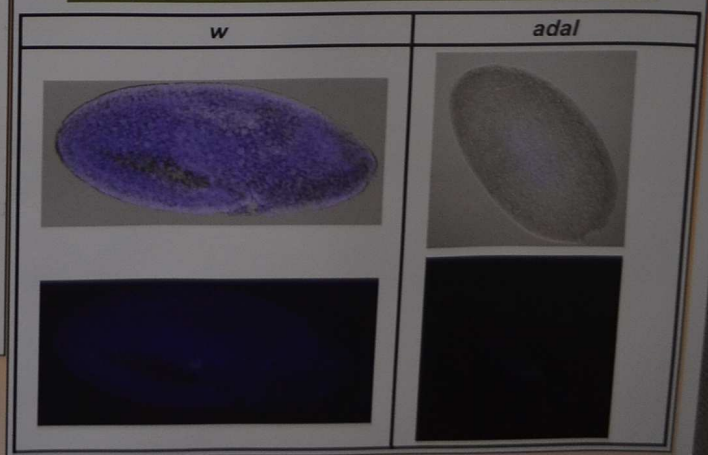

Conclusion

1. *adal* loss of function significantly reduced embryo viability (~16% hatch rate).
2. The reduced hatch rate of *adal* mutant eggs fertilized by wild-type males indicates that *adal* is maternally provided.
3. *adal* mutant embryogenesis fails to proceed the early nuclear division.

Reference

1. Murakami, E. *et. al.* 2011. Adenosine deaminase-like protein 1 (ADAL1): characterization and substrate specificity in the hydrolysis of N(6)- or O(6)-substituted purine or 2-aminopurine nucleoside monophosphates. J Med Chem 54, 5902-5914.
2. Schinkmanova, M. *et. al.* 2006. N6-methyl-AMP aminohydrolase activates N6-substituted purine acyclic nucleoside phosphonates. Biochem Pharmacol 71, 1370-1376.

Revealing the interplay between Hedgehog signaling and metabolism during growth control of the *Drosophila melanogaster* wing disc

Ioannis Nellas[1], Venkatesan Iyer[1], Stephanie Spannl[1], Stefanie Schirmeier[2], Suzanne Eaton[1]

[1] Max Planck Institute of Molecular Cell Biology and Genetics, Pfotenhauerstraße 108, 01307, Dresden, Germany

[2] University of Münster, Institute of Neuro- and Behavioral Biology, Badestraße 9, 48149, Münster, Germany

Introduction

Hedgehog (Hh) proteins regulate growth and patterning during development and regeneration. Tissue differentiation is controlled by the establishment of gene expression patterns mediated by the Gli family transcription factors. While the pattern of differentiation controlled by morphogens has been well characterized, we lack the understanding of how they promote growth during normal development. Metabolic shifts are key drivers of growth during tumorigenesis, but whether metabolic regulation plays a role during normal growth is not clear. Here we investigate the role of Hh signaling in controlling specific patterns of metabolic activity during growth in the wing imaginal disc of *Drosophila melanogaster*. Cells at the organizer regions have unique metabolic properties and we need to define and understand how metabolic patterning contributes to the growth of the wing disc.

Scientific questions

- ***How does morphogen signaling interface metabolism?***
- ***What is the metabolic state induced by Hh signal in the A/P boundary?***

1

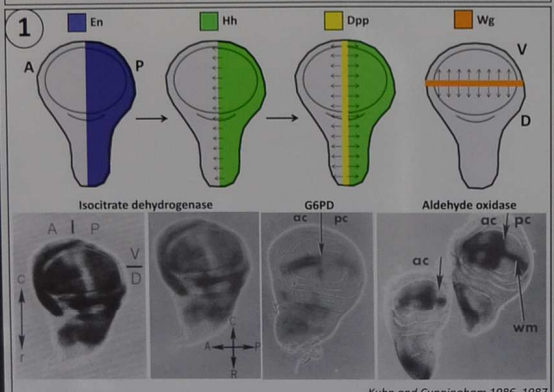

Kuhn and Cunningham 1986, 1987

- A/P boundary–like pattern of metabolic enzymes (!)
- Does Hh or other morphogens regulate their expression or activity?
- What is the role of metabolic patterning in growth control?

2 **Knock down of GAPDH2 activates Hedgehog signaling in the wing disc.**

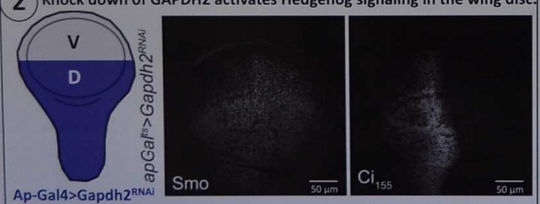

Gapdh2 KD elevates the levels of the signal transducer Smoothened and Ci.

Study goal

My aim is to study the interplay between Hh signaling and metabolism in growth control of the *Drosophila* wing disc and reveal the metabolic status of cells at the A/P boundary where Hh signal takes place.

Experimental approach

3 **Hh** → **Metabolism** — Steps

Metabolic enzyme levels and localization — Protein level
- Monitor protein levels of GFP-protein fusions
- Localization after Hh perturbation

Genetically encoded FRET sensors from reporter flies — Metabolites level
- ATP, lactate, pyruvate and glucose
- Effect of Hh perturbation on metabolite levels?

Adapted from San Martin *et al., 2013*

4 **Metabolism** → **Hh**

Feedback on morphogen signaling
- UAS/Gal4 system to knockdown metabolic enzymes using RNAi
- Immunohistochemistry for Hh signal components (Ptc, Smo, Ci_{155})

Results

5 **Mitochondrial membrane potential is stable throughout the wing disc pouch in wild type flies, as indicated by the TMRE staining.**

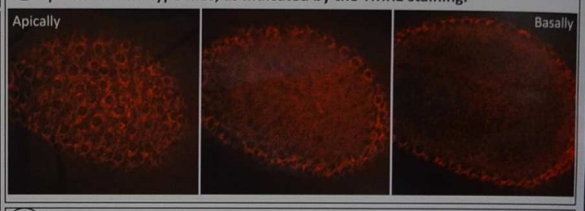

6 **ATP levels are mostly homogeneous throughout the wing disc pouch.**

Color code: High ATP levels — *Low ATP levels*

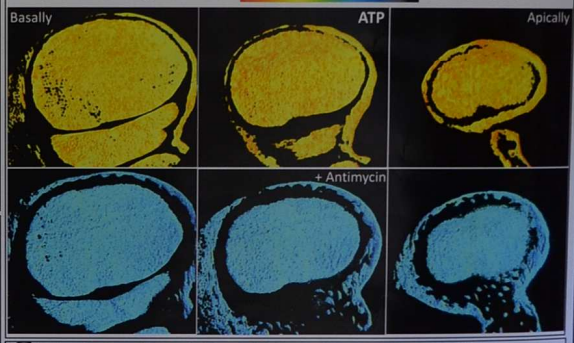

7 **Distribution of metabolites (glucose and lactate) from glycolysis appears to be mostly homogeneous throughout the imaginal wing disc pouch.**

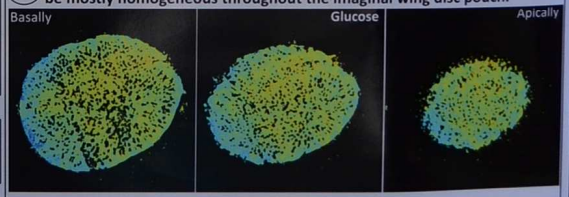

Color code: High Glucose levels — *Low Glucose levels*

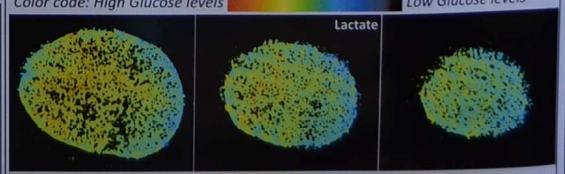

Color code: Low Lactate levels — *High Lactate levels*

Conclusions & Future plans

- MMP and ATP levels are homogeneous throughout the wing disc pouch, so do some metabolites. Thus, which aspect of metabolism changes?
- What is the contribution of the metabolic patterning in growth control of the wing disc? How are these regions metabolically different?
- Once we understand how they are different, we can ask what happens to the remaining tissue compartments of the wing disc!

References

- Alejandro San Martín *et al.* PLoS One. 2014; 9(1): e85780.
- Alejandro San Martin *et al.* PLoS One. 2013;8(2):e57712.
- Sprey and Kuhn, Genetics. 1987 Feb;115(2):283-94.
- Kuhn and Cunningham. Dev. Genet. 1986;7(1):21-34.

Gelatin and Starch Media Stabilize Bacterial Luciferase and Oxidoreductase

Anna BEZRUKIKH[1], Elena ESIMBEKOVA[2,1], Valentina KRATASYUK[1,2]

[1] Siberian Federal University, pr. Svobodnyi 79, Krasnoyarsk, 660041, Russian Federation, *Aebezrukih@gmail.com*

[2] Institute of Biophysics SB RAS, Akademgorodok, Krasnoyarsk, 660036, Russian Federation

The aim of the work was:

To examine the effect of the viscous gelatin and starch microenvironments on the stability of coupled enzyme system of luminous bacteria NADH:FMN-oxidoreductase-luciferase *(R+L)* when exposed to various physical and chemical environmental factors.

Results:

1. Adding of R+L to gelatin sol makes bioluminescence intensity weaker, while including of R+L in the gelatin gel matrix increases its activity. For instance, at 20°C in case of 1% gelatin and at 25°C in case of 5% gelatin the luminescence intensity increases by two times. In the presence of starch the bioluminescence intensity of R+L barely changes with temperature variation, and the temperature optimum remains 25°C.
2. Thermal inactivation of R+L includes two stages, which correspond to the processes of enzyme dissociation into subunits and their subsequent denaturation.
3. Gelatin and starch viscous microenvironments do not change the thermal inactivation rate constants of R+L in a temperature range from 23 to 43°C.

Reactions catalyzed by oxidoreductase (R) and luciferase (L):

$$NADH + H^+ + FMN \xrightarrow{R} NAD^+ + FMNH_2$$

$$FMNH_2 + RCHO + O_2 \xrightarrow{L} FMN + RCOOH + H_2O + h\nu$$

Methods:

The thermal stability of R+L in a gelatin and starch containing media and the effect of gelatin and starch on the stability of R+L under conditions of varying environmental pH and ionic strength were studied. A reagent composed of R+L immobilized in gelatin gel by dosing in drops and drying was prepared.

Thermal inactivation kinetic curves of R+L at different temperatures in the presence of 1% gelatin (b) and in its absence (a)

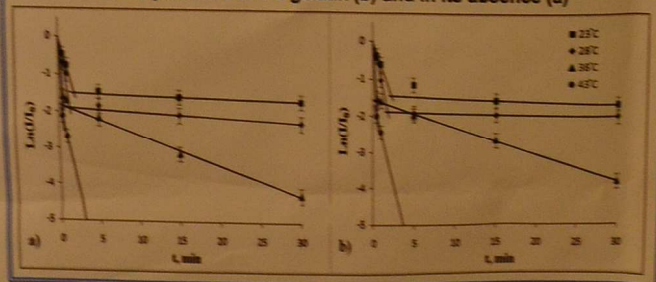

Dependence of the luminescence intensity of R+L on temperature in buffer solution (control) and in the presence of 1% or 5% gelatin, 2% starch

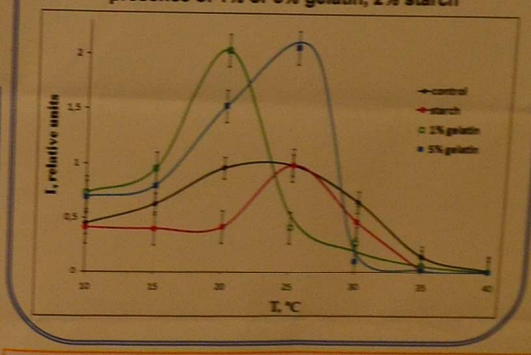

4. R+L surrounded by both gelatin and starch increases its resistance in an alkaline pH region and its optimum ionic force expands to lower values.
5. Gelatin immobilized reagent retains its activity for more than two years when stored at 4°C.

Effective rate constants of the first (k_1) and second (k_2) thermal inactivation stages of R+L in the presence of 1% gelatin and in buffer solution (control) at different temperatures

T, °C	Buffer		Gelatin	
	$k_1 \times 10^2$, min^{-1}	$k_2 \times 10^2$, min^{-1}	$k_1 \times 10^2$, min^{-1}	$k_2 \times 10^2$, min^{-1}
23	76±11	0,7±0,1	61±9	0,9±0,2
28	140±20	1,4±0,6	100±20	0,5±0,3
33	220±40	1,4±0,6	290±40	0,8±0,3
38	>>1	8,3±1,2	>>1	7,5±1,1
43	>>1	110±20	>>1	93±14

The immobilized reagent based on R+L is a disc-shaped dried film with a diameter of 6-7 mm; its dry weight is 1,5÷0,2 mg.

pH dependence of the normalized luminescence intensity of R+L in buffer solution (control) and in the presence of 1% gelatin or 2% starch

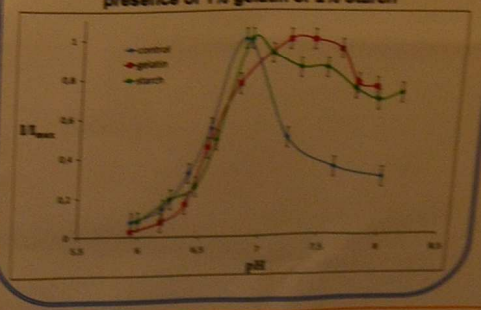

Conclusions:

This work demonstrated that both gelatin and starch have a stabilizing effect on the enzymes of luminous bacteria under certain conditions. The results obtained are helpful to improve the preparation procedure of gelatin and starch immobilized reagents for bioluminescence analysis and as a result to increase their stability and activity.

The work was supported by the Russian Academy of Sciences (Program "Molecular and Cell Biology", grant No 8.8) and the state contract between Ministry of Education and Science and Siberian Federal University No 1762.

Opsin-based photoreception in a luminous brittle-star

Jérôme Delroisse [1], E. Ullrich-Lüter [2], O. Ortega-Martinez [3], J. Mallefet [4], P. Flammang [1]

1 Marine Organism Biology & Biomimetics Lab, UMONS, Belgium ; 2 Museum für Naturkunde, Berlin, Germany , 3 Department of Biological and Environmental Science, University of Gothenburg, Kristineberg, Sweden ; 4 Marine Biology Lab, UCL, Louvain-La-Neuve, Belgium

Corresponding author: jerome.delroisse@umons.ac.be

Introduction

Extraocular photoreception in Echinoderms

- In metazoans, opsins are photosensitive proteins involved in both vision and non-visual photoreception [1].
- Echinoderms are no exception to the rule even though they have no eyes [2]
- Sea urchin genome : 8 opsins genes , of which 4 are homologous to metazoan visual opsin [3]
- No data for other echinoderm classes!

Bioluminescence & Extraocular photoreception

- Molecular markers of photoreception were identified in the light-producing organs of a sepiolid squid [6] and a ctenophore [7], suggesting a link between bioluminescence and photoreception in these phylogenetically distant organisms.
- Extraocular photoreception would constitute an adequate control of photogenesis in these species.
- *Could such a mechanism be present in ophiuroids?*

Case of a luminous brittle star...

- Project focused on the luminous brittle star *Amphiura filiformis (blue emission)* [4].
- Infaunal ophiuroid, large densities on soft bottoms all around Europe [5].

Goals of this study

- Opsin diversity estimation in the luminous brittle star *A. filiformis*
- "Classical opsins" (rhabdomeric and ciliary) immunodetections
- Functional link between bioluminescence and photoreception?

Methodology

1. Organism collection

- Gullmar Fjord
- Kristineberg Marine Station (Sweden)

≈30m depth

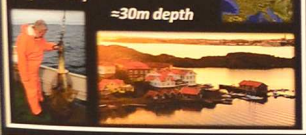

2. Data acquisition

Genome-seq → Univ. of Gothenburg Centre for Marine Evolutionary Biology (Olga Ortega Martinez)

RNA-seq → Total RNA extraction + mRNA selection → Library construction → Sequencing HiSeq Illumina → De novo Assembly

3. Genome & Transcriptome analysis

Opsin research

Genomic sequence database from *A. filiformis* (957.749.165 nucleotides, 1.407.676 sequences) → tBLASTx hits from reference opsin sequences (Reference opsin sequences) → Reciprocal BLASTx against GenBank Nt/Nr database → Opsin-like candidate contigs → Gene/Protein prediction (Expasy translate & Genescan) → Multiple alignment & *Opsin status confirmation* → 14 *A. filiformis* opsin genes

HiSeq Illumina transcriptome sequence database from *A. filiformis* adult arms (90.186.310 nucleotides, 457.352 sequences) → tBLASTx hits from 14 *A. filiformis opsin* gene sequences & reference opsin sequences → Protein prediction (Expasy translate) → Multiple alignment & *Opsin status confirmation* → 3 *A. filiformis* opsin mRNAs

4. Phylogenetic analysis

Maximum likelihood analysis

Software: *Seaview 4.2.12*

Evolution model : WAG (tested with *Mega 4.0*)

5. Whole-mount immunofluorescence

Anti-[sea urchin rhabdomeric opsin] Abs
Anti-[sea urchin ciliary opsin] Abs
?Anti-acetylated alpha-tubulin Abs (Nervous system)

C-opsin & R-opsin

Sea urchin (*S.purpuratus*)

Opsin diversity in *A. filiformis*

- **14 new putative opsin genes** against 8 *bona fide* opsin genes in the purple sea urchin *(Strongylocentrotus purpuratus)* genome.
  - 6 rhabdomeric opsin (R-) homologue to the Sp opsin4
  - 1 putative ciliary opsin (C-) showing high similarity with the homologous Sp opsin1 *(encephalopsin group)*
  - 2 basal-branched opsins homologue to the Sp opsins 2 & 5
  - 1 G0-opsin homologue to the Sp G0-opsins
  - 2 neuropsins homologue to the Sp neuropsin
  - 2 putative peropsin/RGR-opsins homologue to the Sp peropsin/RGRopsin
- Adult arm transcriptome analysis pinpointed opsin mRNAs corresponding to a R-opsin, a neuropsin and a basal-branched opsin.

Figure 2: Phylogenetic tree of metazoan opsins including the new A. filiformis opsins (★). Consensus bootstrap tree was calculated from 500 bottstrap replicates. Representative bootstrap supports are marked in the tree.

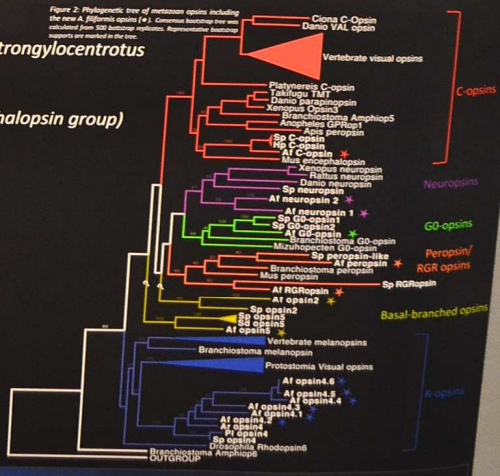

Rhabdomeric and ciliary opsin expression in *A. filiformis*

- R-opsin positive cells at the tip (cone shape) and at the base of the tube feet
- R-opsin positive cells also identified in the radial nerve of the arm.
- No associated shading pigment

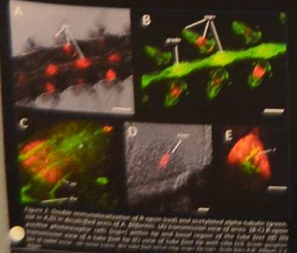

- C-opsins positive cells at the level of the spine stroma
- Close association with the spinal nerve + pigments

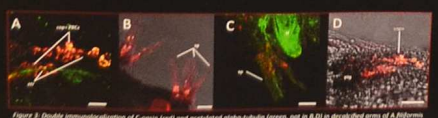

Figure 3: Double immunolocalization of C-opsin (red) and acetylated alpha-tubulin (green, not in B,D) in decalcified arms of A.filiformis (A) High magnification reveals connection of the ciliary opsin positive cells (cop+PRCs) to the nerve tracts (nt) (B) C-opsin localized in an inner portion of the spine (sp) (C) tube feet (tf) show no ciliary opsin signal (D) Transmission view showing dark pigment (pig) and ciliary at the base of the spine. Scale bars in A,B,pm: 0.1 100µm, F: 10µm

- Colocalization "bioluminescence"/C-opsin in the spines

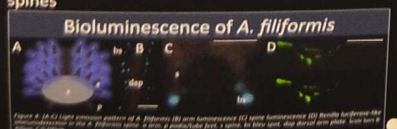

Figure 4: (A-C) Light emission pattern of A. filiformis (B) arm luminescence (C) spine luminescence (D) Results facilitated the colocalization in the A. filiformis spine. b: brain, p: podia/tube feet, s: spine, bs: bivo spot, dap: dorsal arm plate. Scale bars B: 100µm, C-D: 100µm

In conclusion,

- Opsin-based photoreception in brittle stars
- High opsin diversity in a non-visual infaunal brittle star
  - 14 new putative opsin genes
  - R-opsin gene multiplication in the brittle star lineage
- Complex expression pattern of opsins
  - R-opsin in tube feet & in the radial nerve cord
  - C-opsin in spines
  - 3 opsins mRNA expressed in adult arm transcriptome
- Photoreception (c-opsin) & Bioluminescence colocalization in spines
  - Photoreception as a "control tool" for bioluminescence?

P
0010

Development of a highly sensitive and rapid chemiluminescent assay for hydrogen sulfide

Showa University, School of Pharmacy
○Hidetoshi Arakawa, Chiaki Nishijima

【Abstract】

Hydrogen sulfide (H_2S) is attracting attention as one of three endogenously generated gaseous signaling compounds, the others being carbon monoxide and nitric oxide. The hydrogen sulfide in live cells is generated by the following three enzymes: cystathionine β-synthase (CBS);cystathionine γ-lyase (CSE);and 3-mercaptopyruvate sulfurtransferase (3MST).

These enzymes are involved in neurotransmitter regulation and vasodilatation. However, hydrogen sulfide, the odorous component of waste and sewage, is a toxic gas; therefore, a highly sensitive and specific method for monitoring H_2S is desired in order to protect human health and the environment.

Hydrogen sulfide is generally measured by gas chromatography, but this method requires special equipment. Fluorescent probes for hydrogen sulfide have also been recently developed as a simpler method.

In order to analyze hydrogen sulfide rapidly and sensitively, we have developed a novel method using lucigenin chemiluminescence in the presence of copper ion (II).

Cu^{2+}concentration

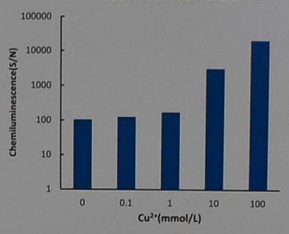

ESR spectrum

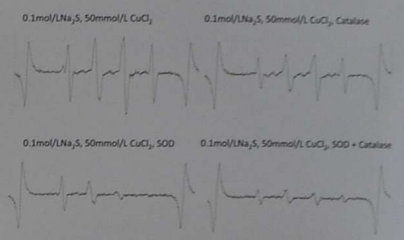

Principle

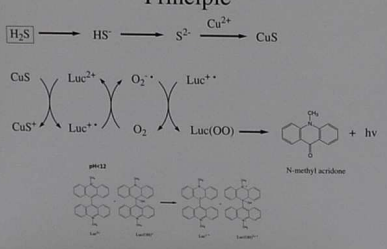

pH

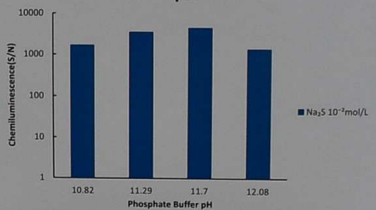

Standard Curve for Na_2S

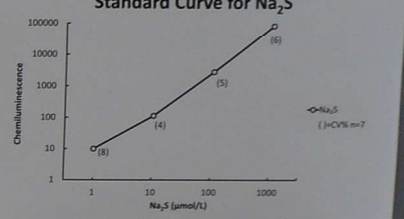

Assay method

Lucigenin chemiluminescent solution (0.2 mL: 5 μmol/l copper chloride (II), 0.04 mg/mL lucigenin, 0.1 mg/mL TritonX-100) was added to Na_2S solution (20 μl) diluted with phosphate buffer (pH 11.7).

Chemiluminecence intensity was measured using an Aloka luminescence reader (Aloka Co. Japan) (waiting time, 10 s; integration time, 10 s).

Buffer salt

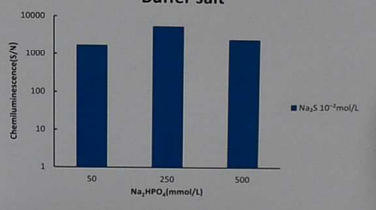

Specificity

1×10⁻⁴mol/L	CL(%)
Na_2S	100
L-Cystein*1)	20.1
Glutathion*2)	4.1
Dithiothreitol	9.0
$NaNO_2$	7.0
NADH	3.4
Vitamin E	2.1
NO (NOC7)	1.8

*1) L-Cystein 1x10⁻²mol/L correspod to 0.58% of CL of Na_2S
*2) Glutathion 1x10⁻²mol/L correspod to 2.7% of CL of Na_2S

Metal ion

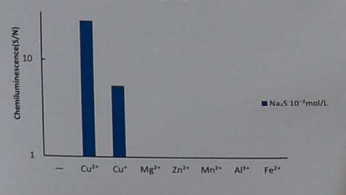

Effect by Catalase & SOD on CL intensity

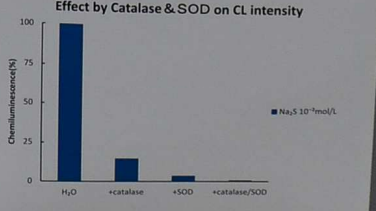

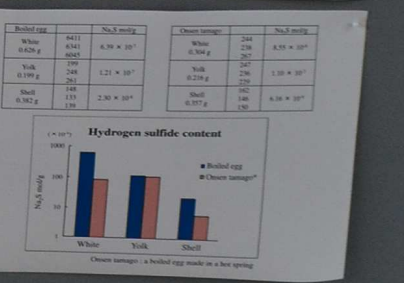

【Discussion】

- This is a novel chemiluminescence method based on the principle that light is emitted by metal ions and hydrogen sulfide in the presence of lucigenin.
- The effects of several metal ions (copper (II), copper (I), zinc, magnesium and aluminum) were studied. Intense luminescence was generated with copper (II).
- Reactive oxygen involved in this chemiluminescent reaction was analyzed using ESR by the addition of a scavenging enzyme, SOD. Lucigenin was essential for the generation of reactive oxygen. With the addition of both catalase and SOD, this signal essentially disappeared. This result indicates that the radical species is a superoxide anion. The concept is shown in Fig.1.

- Detection limit of Na_2S was 20 pmol / assay.
- Reproducibility was from 1.5 to 11.7% (n = 7), with 6.0% as the mean.
- The specificity of the method was examined using cysteine and glutathione as SH compounds.
- Further, by adding maleic imide to the luminescent reagent, the specificity was able to be improved. Thus, this method was found to show high specificity for Na_2S.

P
0052

P0052

First-Principles Investigation on Optical Properties of Firefly Luciferin Anion

Yoshifumi Noguchi, Miyabi Hiyama, and Hidefumi Akiyama
(ISSP, the University of Tokyo)

Nobuaki Koga
(Nagoya University)

June 23-28, 18th ISBC 2014, Uppsala, Sweden

Introduction

Electron-hole two-particle Green' s function, for which the Bethe-Saleter equation (BSE) is solved within the *GW* approximation (GWA) (the so-called *GW*+Bethe-Salpeter method), has proven to be a versatile method for simulating photoabsorption spectra. In actuality, the theoretically observed photoabsorption spectra have been confirmed to be comparable with the available experimental spectra at low energy range [1].

The next theoretical step would be a treatment for the Rydberg and resonance excitations, whose corresponding peak positions are located at slightly higher photon energies than the first isolated peaks. A first-principles treatment of the free electron states or the Rydberg excitation is an interesting topic, especially from the viewpoint of basis set dependency.

[1] K. Stechkel, et al., J. Phys. Chem. A, 115, 2155 (2011).

Purpose

In this study, the isolated firefly luciferin anion in vacuumwhich is perhaps the simplest model system for firefly bioluminescence for which experimental data are available is considered for further investigation. Optical properties are calculated by using the all- electron GW+Bethe-Salpeter method, and the results are compared with those of time-dependent DFT (TDDFT) calculations employing the localized AO basis sets and the expeiment in vacuum.

The present method replicates the line shape and peak positions of the first few excitons. We also investigate the basis set dependency in describing the Rydberg and resonance excitations.

Methodology – all-electron mixed basis program -

One-particle wave function

Whole electronic states from **core electron states** to **free electron states** above vacuum states can be described efficiently.

Various materials, not only **isolated systems** such as molecules and clusters but also **extended systems** such as crystals can be treated with small number basis sets.

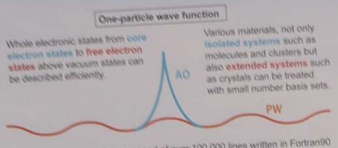

- Original source code composed of over 100,000 lines written in Fortran90
- All-electron first-principles approach
- Green's function methods (GW, T-matrix, Bethe-Salpeter, MP2, etc)
- Simple user interface
- Massively parallel (hybrid parallel by OpenMP and MPI)
- Portability (FUJITSU, NEC, SGI, HITACHI, HP)

Methodology – one-particle Green's function *GW* approximation (GWA)

L. Hedin, Phys. Rev. **139**, A796 (1965).

GW self-energy operator

$$\Sigma = iGW$$

Fock-exchange *GW* correlation

Dynamically screened Coulomb interaction within RPA

$$W(\omega) = \epsilon^{-1}(\omega)v = (1 - vP^{\mathrm{RPA}}(\omega))^{-1}v$$

GW quasiparticle energy

$$E_\nu^{GW} = E_\nu^{\mathrm{LDA}} + Z_\nu < \nu|\Sigma^{GW} - \mu^{xc}|\nu >$$

LDA Kohn-Sham energy; renormalized factor; LDA exchange correlation potential

Renormalization factor

$$Z_\nu = \frac{1}{1 - < \nu|\partial\Sigma^{GW}(E_\nu^{\mathrm{LDA}})/\partial E_\nu^{\mathrm{LDA}}|\nu >}$$

Methodology – two-particle Green's function - Bethe-Salpeter equation (BSE)

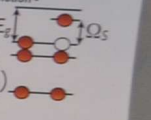

Electron-hole interaction kernel within GWA

$$\Xi = \frac{\delta}{\delta G_1}(V_H + \Sigma^{GW}) = \frac{\delta}{\delta G_1}$$

Eigenvalue problem for electron-hole two-particle Hamiltonian

$$(E_{\epsilon'}^{GW}\delta_{\epsilon,\epsilon'} - E_{\epsilon''}^{GW}\delta_{\epsilon'',\nu'})A_{\epsilon,\nu}^S + \sum_{\epsilon',\nu'} K_{\epsilon,\nu;\epsilon',\nu'}(\Omega_S)A_{\epsilon',\nu'}^S = \Omega_S A_{\epsilon,\nu}^S$$

GW gap; Matrix elements of electron-hole interaction kernel

$$K_{\epsilon,\nu;\epsilon',\nu'}(\Omega_S) = i\int d3d3'd4d4'\,\psi_\epsilon^*(r_3)\psi_{\epsilon''}^*(r_3')\,v(r_3 - r_4)\,\chi(3,3',4,4';\Omega_S)\,\psi_{\epsilon'}(r_4)\psi_{\nu'}(r_4')$$

Electron-hole two-particle Green's function:

Methodology – calculation cost & parallel efficiency -

Intel Xeon E5-2690 × 4 (= 172.8GFlops × 4)
Target system: isolated C_{60}

	LDA	GWA	BSE
Elapse time (h)	0.6	19.6	> 48

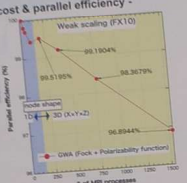

GWA and BSE calculations require much more expensive computational cost than that of DFT, however they are highly scalable for massive # of CPU cores.

Results – Atomic geometry -

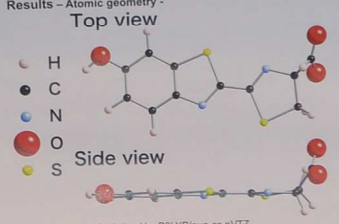

Optimized by B3LYP/aug-cc-pVTZ

Results – basis set dependency -

Left figure shows the LDA Kohn-Sham orbital energies at the lowest 50 empty levels calculated by using the all-electron mixed basis (PW+AO) and aug-cc-pVTZ (AO-only). LUMO is set to be zero electron volts for comparison.

Results – basis set dependency -

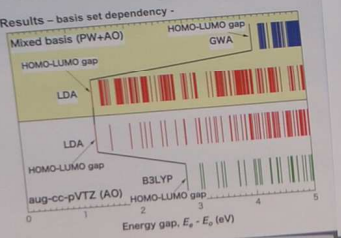

Results – basis set dependency -

Figure shows how the calculated energy gap depends on the basis set. The mixed basis shows a dense population, with 400 states found in the energy range up to 5 eV, and aug-cc-pVTZ shows a sparse population, with only 73 states found there. This tendency is also the same for the high- level calculations. GWA with a mixed-basis finds 83 states in the energy range up to 5 eV and B3LYP with aug-cc-pVTZ finds only 30 states.

Results – basis set dependency -

The population of the mixed basis is dense and 50 empty states are densely located in the small energy range of 0.0–0.7 eV, where LUMO +49 is about 0.7 eV. In contrast, the population of aug-cc-pVTZ is too sparse to regard these states as the free electron states and LUMO +49 is about 6.14 eV. The strong basis set dependency is observed between all-electron mixed basis and aug-cc-pVTZ.

Results – Photoabsorption spectra -

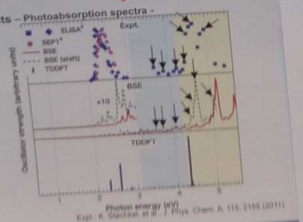

Expt.: K. Stechkel, et al., J. Phys. Chem. A, 115, 2155 (2011).

Results – Photoabsorption spectra -

Left figure shows the theoretical and experimental photoabsorption spectra. Photon energy is divided into three areas according to the type of excitons: a sparse population of excitons up to 3.1 eV (white background color), the Rydberg excitation (sky blue background color), and the resonance excitation (yellow background color).

Results – exciton profile -

Results – exciton profile -

Table shows exciton profile of first six low-lying excitons. The main transitions and the ratio of the contributions are different between the BSE and TDDFT for example, S1 is composed of the transitions from HOMO-1 to LUMO+2, LUMO+10, and LUMO+19 in BSE and the transitions from HOMO-1 or HOMO to LUMO in TDDFT. In the case of TDDFT, the exciton involving the transition from HOMO-3 first appears at 7th, which is not shown here. Such inconsistencies in the main transitions are also seen in following exciton states. So in S1 to S5,

Summary

- We have applied the first-principles GW+Bethe-Salpeter method to an isolated firefly luciferin anion in vacuum.
- Our GW+Bethe-Salpeter method employing the all-electron mixed basis approach describes the Rydberg and resonance excitations accurately.
- The BSE spectra well replicate the line shape of the experimental spectra. However these spectra show a blueshift of the overall peak positions by about 0.5 eV from the experiments.

Current ecological knowledge about *Mus spicilegus* Petényi, 1882 (Rodentia) in Slovakia

Csanády A.[1], Stanko M.[2, 3] & Mošanský L.[2],

[1] University of Prešov, Faculty of Humanities and Natural Sciences, Department of Biology
[2] Institute of Parasitology, Slovak Academy of Science, SK-04001 Košice, Slovakia
[3] Institute of Zoology, Slovak Academy of Science, SK-040 01 Košice, Slovakia

INTRODUCTION

➢ ecological research in the years 2002 - 2010 from four orographic units of Slovakia (Východoslovenská rovina plain, Košická kotlina basin, Ipeľská pahorkatina upland and Hronská pahorkatina upland).

➢ focus on autumn-winter and spring-summer ecology, reproduction, mounds morphology and morphometric analyses.

A

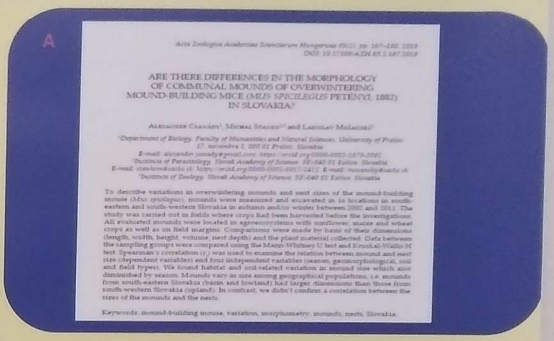

ARE THERE DIFFERENCES IN THE MORPHOLOGY OF COMMUNAL MOUNDS OF OVERWINTERING MOUND-BUILDING MICE (*MUS SPICILEGUS* PETÉNYI, 1882) IN SLOVAKIA?

B

First Knowledge of Winter Ecology of the Mound-building Mouse (*Mus spicilegus* Petényi, 1882) from Slovakia

E

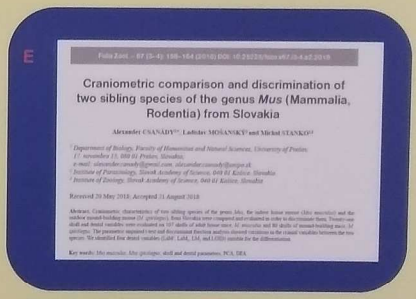

Craniometric comparison and discrimination of two sibling species of the genus *Mus* (Mammalia, Rodentia) from Slovakia

C

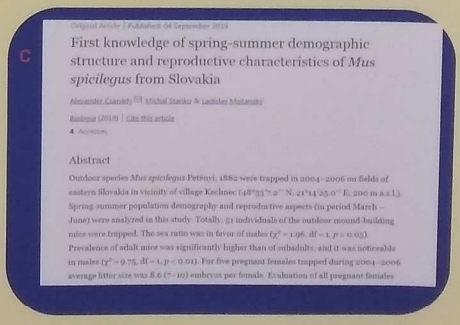

First knowledge of spring-summer demographic structure and reproductive characteristics of *Mus spicilegus* from Slovakia

RESULTS

➢ the variability of the overwintering mounds (n = 376) and the nest size (n = 83) were confirmed between the orographic regions and between the habitat type (***Csanády et al. 2019, Acta Zool. Acad. Sci. Hung. 65***); A

➢ winter prevalence of juveniles (χ^2 = 52.74, p <0.01) and males were confirmed for the autumn-winter period (χ^2 = 5.47, p <0.05) (***Čanády et al. 2009, Acta Zool. Bulg. 61(1)***); B

➢ spring-summer sex ratio was in favor of males (χ^2 = 1.96, df = 1, p > 0.05) (***Csanády et al. in press, Biologia***); C

➢ we confirmed higher testicular values in *M. spicilegus* males than in *M. musculus* males (***Csanády et al. 2019, Mamm. Res. 64);*** D

➢ average litter size (n = 9) was 8.3 (6-10) embryos per female (***Csanády et al. in press, Biologia***); C

➢ four dental variables (LaM^1, LaM_1, LM_1 and LOID) suitable for the differentiation two *Mus* species (***Csanády et al. 2018, Fool. Zool., 67(3-4)***); E

➢ *M. spicilegus* population significant morphologically differ by longer head-and-body length and shorter of tail length from *M. musculus* (***Čanády et al. 2008, VOCS VIII., 2007***)

D

Are differences in variation and allometry in testicular size of two sibling species of the genus *Mus* (Mammalia, Rodentia) caused by female promiscuity?

CONCLUSION

Long-term research significantly expanded our knowledge about morphology and ecology of *M. spicilegus* at the margin of the species distribution

ACKNOWLEDGEMENTS

We would like to express our sincere thanks to all colleagues for their help in both the field and laboratory work.
Research was supported by the VEGA projects 1/0084/18 and 1/0277/19 .

PAR6

Aktivita klíšťat u Brněnské přehrady v minulých letech

H. Nejezchlebová, A. Žákovská, V. Nesnídalová, K. Bečárová, B. Kolářová, R. Horáková

Oddělení fyziologie živočichů a imunologie, PřF MUNI, Kotlářská 2, 611 37 Brno

Cílem příspěvku je podat přehled o aktivitě klíštěte obecného (*Ixodes ricinus*) v průběhu minulých let na lokalitě Ruda (234 m. n. m., 49°14'18" s. š., 16°31'29" v. d.). Lokalita se nachází asi 200 m na západ od Brněnské přehrady. Jde o oblast navštěvovanou turisty i místními lidmi, kteří zde sportují a tráví volný čas (obr 1).

Obr. 1: Brněnská přehrada a okolí: oblíbené místo k rekreaci

Foto: www.pruvodcebrnem.cz/brnenska-prehrada

Sběry klíšťat probíhaly intermitentně v letech 2012, 2015, 2016 a 2019 v pravidelných intervalech jednou za 14 dní metodou vlajkování od března do října / listopadu (obr. 2). Výsledky jsou uvedeny v tab. 1.

Obr. 2: Vlajkování na lokalitě Ruda

Foto: Veronika Nesnídalová

	celkem	larvy	nymfy	samice	samci	kritický	závislost na		
						měsíc	teplotě	vlhkosti vzduchu	tlaku vzduchu
2012	321	64	236	7	14	červen	ne	ne	ne
2015	255	12	232	6	5	květen	ne	ne	ne
2016	364	77	261	16	10	duben	ano	ne	-
2019	554	134	411	2	7	květen	ne	ano	ano

Tab 1: Výsledky sběrů v jednotlivých letech

- Roční úhrny nasbíraných klíšťat značně kolísaly a statisticky se od sebe liší.
- Nejvyšší aktivita klíšťat byla vždy zaznamenána v jarních měsících, s tím je spojena i míra rizika přisátí klíštěte na člověka/zvíře.
- Nejpočetnějším stádiem byly nymfy, průměrně tvořily 76 % odchycených jedinců.
- Nejméně zastoupení byli dospělci (5 %). 19 % odchycených klíšťat tvořily larvy. I zde nacházíme statisticky významné rozdíly mezi jednotlivými lety.
- Závislost celkového počtu odchycených jedinců na teplotě, relativní vlhkosti vzduchu a atmosférickém tlaku nebyla ve většině případů statisticky potvrzena.

Podpořeno ze Specifického výzkumu MUNI /A/1397/2019

Tvorba specifických protilátek třídy IgM a IgG proti *Borrelia afzelii* u laboratorně očkovaných myší

H. Ruščáková, J. Benešová, A. Žáková
(Katedra srovnávací fyziologie živočichů Přírodovědecké fakulty Masarykovy univerzity, Brno, Česko)

ÚVOD

V rámci této studie bylo řešena problematika imunitní reakce drobných savců na patogenní bakterie *Borrelia sensu lato* pocházející z různých zdrojů izolace (vektor, hostitel). Cílem bylo sledovat dynamiku a množství vytvořených antiborrelových protilátek v krvi samců laboratorních myší.

MATERIÁL A METODY

K pokusu, který trval celkem 9 týdnů (červen – srpen), bylo použito 22 myší

Uspořádání experimentu:

K intraperitoneálnímu očkování byla použita suspenze usmrcených bakterií druhu *Borrelia afzelii*

kontrolní skupině (4 jedinci) byl očkován 0,1% roztok aluxidu doplněný fyziologickým roztokem

k očkování pokusné skupiny (7 jedinců) BRZ 9 byl použit antigen izolovaný z *Ixodes ricinus* - Klíště obecné (Písárky)

k očkování pokusné skupiny (5 jedinců) BRZ 14 byl použit antigen izolovaný z *Culex pipiens molestus* - Komár (Vysoké Mýto)

k očkování pokusné skupiny (6 jedinců) BRZ 21 byl použit antigen izolovaný ze samce *Apodemus flavicollis* – Myšice lesní (Lanžhot)

IMUNIZACE

Šest týdnů staré myši byly očkovány ve třítýdenních intervalech podle Harlowa a Laneho, 1988

Schéma: Ideální průběh imunitní reakce

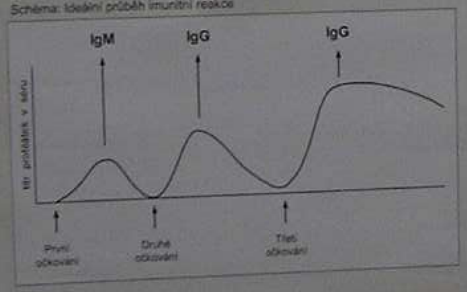

K injikaci byly použity celobuněčné bakterie rodu *B. afzelii* (poskytnuto ÚBO AV ČR, Vestec). Pokusným jedincům byl intraperitoneálně injikován objem 300 µl. Tento objem obsahoval 7,5 µg bakterií a 0,1 % roztok aluxidu, který napomáhá k dosažení optimálního imunogenního účinku. Kontrolním myším byl očkován 0,1% roztok aluxidu doplněný fyziologickým roztokem.

ODBĚR KRVE

Krev byla pokusným zvířatům odebírána v celkové narkóze (ethylether) 14. den po každém očkování. Při prvních dvou odběrech byla myším odebrána krev z periferní ocasní žíly do hematokritových kapilár s heparinem. Při posledním odběru byla krev odebrána z krkavice (arteria carotis externa)

DETEKCE PROTILÁTEK: NEPŘÍMÝ TEST ELISA

Tato metoda slouží k průkazu protilátek. Antigen vázaný na pevnou fázi reaguje se specifickými protilátkami přítomnými v testovaném vzorku. V našem případě byly používány konjugáty anti-Mouse IgM a IgG – whole molecul (sigma)

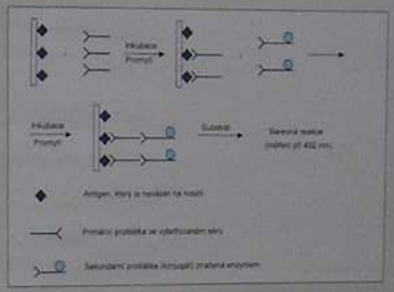

VÝSLEDKY

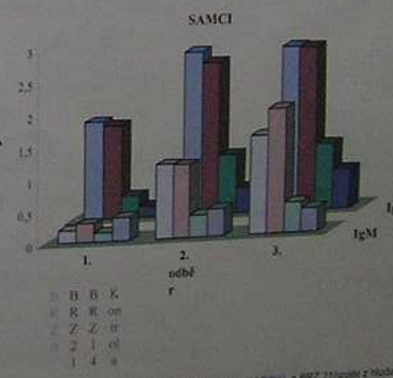

Krev myší očkovaných antigenem BRZ 9 (izolát z klíštěte) a BRZ 21(izolát z hlodavce) vykazovala vysoký titr hladiny protilátek třídy IgM, IgG. Hladina protilátek u myší očkovaných antigenem BRZ 14 (izolovaného z komára) byla o polovinu nižší. Tyto výsledky naznačují, že antigeny borrelií izolovaných z klíšťat a hlodavců jsou schopné vyvolat silnou imunitní reakci, kdežto antigeny borrelií izolovaných z komárů vyvolávají imunitní reakci poloviční intenzity. Znamená to, že antigenní vlastnosti borrelií stejného druhu, ale izolovaných z jiných živočichů se liší.

Studie vznikla za podpory výzkumného záměru J07/98: 143100008

Host response to *Borrelia afzelii* in BALB/c mice

Department od Comparative Animal Physiology and General Zoology, Faculty of Science, Masaryk University, Kotlářská 2, CZ-61137 Brno, Czech Republic; tel.: ++ 420 5 41129396,
email:

INTRODUCTION

The aim of the study was to find the vaccination effect in the formation of antiborrelian antibodies against three individual *Borrelia afzelii* antigen doses (dead cell suspension) isolated from three different sources: *Ixodes ricinus* tick (BRZ 9), Cuiro (Cuiro) *pipiens molestus* mosquitoe (BRZ 14) and *Apodemus flavicollis* wild rodent (BRZ 21). We have investigated the specific humoral immune response after experimental inoculation of *Borrelia afzelii* by *ELISA* method and individual proteins responsible for antibodies formation by *Western blot* method.

MATERIAL AND METHODS

Animals

Male BALB/c mice, were housed in plastic cage in a conditioned room at 20 - 24 ± 1 °C with the illumination from 7 AM to 7 PM. All animals were allowed to adapt to the environment for at least 2 weeks prior to immunization. Mice were fed a standard diet (Fábry 1959). The initial body weight of the animals was approximately 25 g. The duration of experimental treatment was 9 weeks.

Figure 1 BALB/c mice

Male mice were divided into four groups. Group 1 was injected by BRZ 9 (BRZ means the internal mark of individual isolated strain) *B. afzelii* whole cell antigen isolated from *Ixodes ricinus* (Praděd I. t. Brno) completed 0,1% Freund's adjuvant ; group 2 was injected by BRZ 21 *B. afzelii* whole cell antigen isolated from *Apodemus flavicollis* (Studenka, I. t.) completed 0,1% Freund's adjuvant, group 3 was injected by BRZ 14 *B. afzelii* whole cell antigen isolated from Cuiro *pipiens molestus* (Vyškov mýto, I. t.) completed 0,1% Freund's adjuvant, group 4 (control group) was injected saline completed 0,1% Freund's adjuvant.

Cultivation of isolated strains

Three individual species of *B. afzelii* (BRZ 9, BRZ 21, BRZ 14) were identified by using PCR, PCR - RFLP and gradient PAGE methods as reported in Zakovska et al., 2002. Isolated strains were cultivated in BSK-H medium (Sigma) enriched with 6% rabbit serum, Rifampicin (50 µg/ml), Phosphomycin disodium salt (100 µg/ml) under 33 °C. The correct sample of spirochetes was observed by dark-field microscopy (DFM) at 400x magnification. Dead isolated strains were prepared until the density of bacterial suspension reached 10^8 - 10^9 cells/ml.

Immunization

Male BALB/c mice, 6 weeks old were intraperitoneal injected 3 times. After each 3 weeks the injection was repeated. For injection were used plastic disposable syringe. All injections contained Freund's adjuvant. For immunization lower antigen level was used to induce a strong immune response (Harlow, Lane 1988). Each mouse was injected by mixture of 300 µl of antigen solution completed with 0,1% Freund's adjuvant.

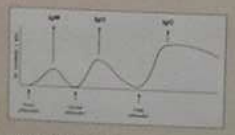

Figure 2 Kinetics of immune response

Sample collection and analytical procedures

Mice were anaesthetized with diethyether and blood was collected from tail vein from each mouse. Blood is easily accessible and does not have high numbers of nerve endings. At the end of experimental period, all animals were killed and blood was collected from carotis (arteria carotis externa). Blood samples were taken 14 days after each injection to check the production of specific antibodies (Harlow, Lane 1988). Sera were separated from other blood fractions by precipitation and centrifugation. Samples of serum were determined using enzyme - linked immunosorbent assay (ELISA).

ELISA

The sera were examined by ELISA modified to our conditions, available in commercial sets (TestLine, Prague) used for diagnosis of Lyme borreliosis in human medicine (Vostal, Zakovská, 2003). The test was performed using 96-well microplates coated 2 µg/ml *Borrelia afzelii* antigen. As secondary antibodies peroxidase - conjugated (Sigma) goat anti-Mouse IgG, IgM antibodies were used. Absorbance was measured at a wave length of 492 nm. The serum samples from immunized mice were evaluated as positive. The serum samples from control mice were evaluated as negative.

Western blotting

Whole cells suspension of *Borrelia afzelii* were separated by SDS-PAGE on 10% polyacrylamide gels and transferred to nitrocellulose. After blocking with 3% casein, individual strips were incubated with respective sera from immunized mice (diluted 1:40 for IgG and 1:100 for IgM). Bound antibodies were visualized using a peroxidase conjugate labeled goat anti-Mouse IgG, IgM antibodies and TBS.

ACKNOWLEDGEMENT

This work was partially supported by FRVŠ 1413/G4/4427, MSM 143100010 (formerly CEZ: J07/98:143100010) and by MŠMT 143100008.

LITERATURE

Fábry P.: Antibodies: source, metabolism, laboratory work, that a synopsis problem through from 14. simple course of standard laboratory mice with various preparations of some substances.). Ce Fysiol. 6: 129-151, 1959

Harlow E., Lane D.: Antibodies (a laboratory manual). Cold Spring Harbor Laboratory, 1988

Vostal K., Zakovská A.: Two-years study of examination of blood from wild rodents for the presence of antiborrelian antibodies. Ann Agric Environ Med 2003; 10:13-16

Zakovská A., Čapková L., Hořínková A., Šery O.: The presence of *Borrelia burgdorferi* in Calex *B.*(sec) patient have proved by the PCR method. Sborník Fac. Sci. Nat. Univ. Masaryk Brno, 2/E Biologie 11-16, 2002

RESULTS

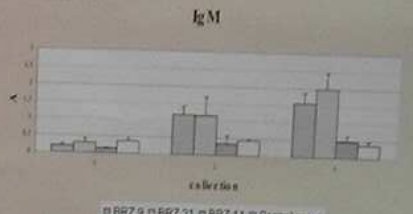

Figure 3 IgM responses to *Borrelia burgdorferi* antigens during experimental period. Data points represent the mean absorbance ± the standard error of the mean of serum samples from all 6 mice.

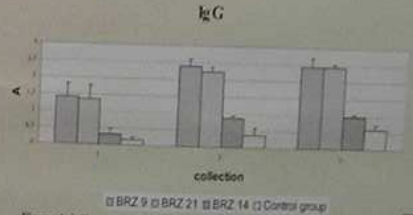

Figure 4 IgG responses to *Borrelia burgdorferi* antigens during experimental period. Data points represent the mean absorbance ± the standard error of the mean of serum samples from all 6 mice.

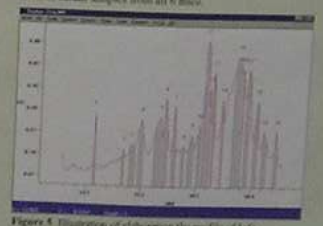

Figure 5 Illustration of elaboration the profile of IgG antibodies from BRZ 21 sample. Analysis were performed by Molecular analyst software, verse 1.1.1., Bio-Rad

Figure 6 Illustration of protein fractions IgG antibodies on nitrocellulose from BRZ 21 sample. (s-standard, 1,2 - samples)

Two mice tested by BRZ 9 and BRZ 21 showed a statistically significant values in the increasing amounts of specific IgG antibodies during the three-times vaccination and three-step testing. Results of mice tested by BRZ 14 were statistically significant after the second and the third testing. IgM antibodies statistically increased in BRZ 9 and BRZ 21 after the second and the third sera testing. IgM antibodies did not increase statistically in mice vaccinated by BRZ 14 because of half of the antigen dose did not increase conclusive rise of IgM antibodies, although the antibody level was proportional to the dose amounts.

The data presented here show that immunization of BALB/c mice with *Borrelia* antigens induced specific antibodies and protective immunity against infection. The immunization resulted in the development of an immune response to each of three antigens. Levels of IgM and IgG antibodies were monitored in individual mice in days - 14, 35 and 56 after infection.

In conclusion, these results indicate that the amounts of antibodies dependend on amount of sorve antigens and that mice were susceptible to low dose of antigen. *Borrelia afzelii* antigens ostmung from different source did not differ in antibodies formation.

Proteins	BRZ 21		BRZ 14		BRZ 9	
	IgM	IgG	IgM	IgG	IgM	IgG
	56 (kDa)		56 (kDa)		56 (kDa)	
P79						
Hypo66						
P54						
P48						
P36						
P45						
P18						
Flagellin						
P39						
P35						
OspB						
OspA						
OspB						
OspB						
OspC						
OspB						
OspA						
P21						
P18						
P18						

Table 1 WB results of examined mice for the presence of *B. afzelii* antibodies. There were detected protein fractions in the range of molecular weight (MW) from 17 kDa to 200 kDa.

Western blots were performed after 56 days of triple infection. WB analysis revealed that mice inoculated by BRZ 21 antigen were able to generate amounts of specific antibodies. **IgM** antibodies to **Hypo6** and **OspC** were found in sera of all three group of mouse inoculated three different sources of antigens. IgM antibodies to **OspB** were presented only in sera of group BRZ 21 and BRZ 14. **IgG** antibodies to **OspA** and **OspC** were found in sera of all three groups of mouse IgG antibodies to **OspB** were presented only in sera of group BRZ 21 and BRZ 9.

6-year's study of the presence of *Borrelia burgdorferi* sensu lato in *Ixodes ricinus* ticks in the town-park locality Brno, Czech Republic using DFM, PCR, PCR-RFLP and PAGE methods

Nejedlá Petra, Mejzlíková Marie, Žákovská Alena, Holíková Alena, Martiníková Hana, Justinová Lenka

Department of Comparative Animal Physiology and General Zoology, Faculty of Science,

Masaryk University, Brno, Czech Republic

Introduction

The agents of the tick-borne disease, Lyme borreliosis, form a complex, *Borrelia burgdorferi* sensu lato, including 11 genospecies. In Europe, five genospecies (*B. burgdorferi* sensu stricto, *B. garinii*, *B. afzelii*, *B. valaisiana*, *B. lusitaniae*) have been reported in the main European tick vector, *Ixodes ricinus*. Three of these genospecies (*B. burgdorferi* sensu stricto, *B. garinii*, *B. afzelii*) are known to cause disease to humans. The aim of our study was to monitor the positivity and activity of *Ixodes ricinus* ticks for the presence of pathogenic *Borrelia burgdorferi* sensu lato in the town-park locality Brno, Czech Republic.

Materials and Methods

In the years of 1996 - 2002 a total of 3170 *Ixodes ricinus* ticks were collected by dragging of white flannel cloth over the vegetation. The ticks were examined for the presence of spirochetes by dark-field microscopy (DFM), samples with more than 50 spirochetes were transferred into BSK-H medium and cultivated under 33°C. For the detection of spirochetes were used also PCR (1998-2000) - from the tick midgut harboured more than 100 spirochetes two samples (one for PCR and second for the cultivation in BSK-H medium) were prepared. In 2001 only PCR was used, in 2002 three types of methods were used (PCR, DFM and cultivation with following DFM and PCR). All the methods were performed to obtain spirochete strains for further detailed detection.

For the genospecies identification single-tube nested PCR and restriction fragment length polymorphism (RFLP) were used. PCR assay was based on specific flagellin sequence amplification for detection of *B. burgdorferi* s. l. RFLP analysis of amplified PCR products was performed by Alu1 endonuclease digestion. The restriction fragments were separated in 2.5% agarose gel and stained with ethidium bromide.

The characterization of yielded isolates was performed also by comparison of the protein composition to standard stems *Borrelia burgdorferi* s. s., *B. garinii* and *B. afzelii* using SDS-gradient PAGE. Unknown spirochete and standard samples were separated by electrophoresis in 7,5% - 20,02% gradient gel in the surrounding of Tris-glycin-EDTA, pH 8,3 at voltage 400-610 V. Gels were stained with $AgNO_3$ by Rabilloud and evaluated using videodensitometr and software of Molecular Analyst (Bio-Rad).

Town-park locality Brno in autumn

Locality

Ixodes ricinus ticks were collected in the town-park locality Brno, Czech Republic, 2 km far from the centre of the town, 197 – 210 m above sea level on a 150 x 300 m study plot in a mixed wood for the people holiday utilization. In this biotype predominate *Quercus petrae*, *Quercus robur*, *Carpinus betulus*, *Pinus sylvestris* and less frequent are *Picea abies* and *Fagus sylvatica*. Other such as *Betula pendula*, *Populus tremula*, *Robinia pseudacacia*, *Picea pungens*, *Larix decidua* are present sporadically. The shrub layer is composed primarily of *Sambucus nigra* and less frequent *Sambucus racemosa*, *Symphoricarpos rivularis*, *Swida sanguinea* and *Crataegus*. Herbal undergrowth contains *Allium ursinum*, *Corydalis cava*, *Ficaria verna*, *Anemone ranunculoides*, *Pulmonaria officinalis*, *Poa nemoralis*, *Melampyrum nemorosum* and other species.

Year	Male n/N P (%)			Female n/N P (%)			Nymph n/N P (%)			Larva n/N P (%)			Total n/N P (%)			Total number of colected ticks
	DFM	PCR	cultivation	DFM	PCR	cultivation	DFM	PCR	cultivation	DFM	PCR	cultivation	DFM	PCR	cultivation	
1996	0/5 (0.0)	-	-	1/8 (12.5)	-	-	2/32 (6.3)	-	-	0/3 (0.0)	-	-	3/48 (6.3)	-	-	48
1997	6/34 (17.7)	-	-	3/45 (6.7)	-	-	32/332 (9.6)	-	-	2/34 (5.9)	-	-	43/445 (9.7)	-	-	445
1998	14/73 (19.2)	-	-	7/70 (10.0)	-	-	31/279 (11.1)	-	-	0/1 (0.0)	-	-	52/423 (12.3)	30/257 (11.7)	-	423
1999	2/20 (10.0)	-	-	2/22 (9.1)	-	-	9/318 (2.8)	-	-	0/0 (0.0)	-	-	13/360 (3.6)	10/360 (2.8)	-	360
2000	8/111 (7.2)	-	-	10/127 (7.9)	-	-	13/486 (2.7)	-	-	1/73 (1.4)	-	-	32/797 (4.0)	17/797 (2.1)	-	797
2001	-	2/32 (6.3)	-	-	2/9 (22.2)	-	-	6/82 (7.3)	-	-	1/78 (1.3)	-	-	11/201 (5.5)	-	201
2002	0/9 (0.0)	4/40 (10.0)	3/13 (23.1)	0/9 (0.0)	3/36 (8.3)	5/10 (50.0)	14/86 (16.3)	43/569 (7.6)	21/157 (13.4)	0/0 (0.0)	1/147 (0.7)	2/21 (9.5)	14/104 (13.5)	61/792 (6.4)	31/201 (15.4)	896
Total positivity	30/253 (11.9)			23/281 (8.2)			101/1533 (6.6)			3/111 (2.7)			157/2177 (7.2)	119/2407 (4.9)	31/201 (15.4)	3170

Table 1: Prevalence of *Borrelia burgdorferi* sensu lato in *Ixodes ricinus* ticks (n - Number of positive ticks, N - Number of examined ticks, P - Prevalence of *B. burgdorferi* in *I. ricinus* ticks)

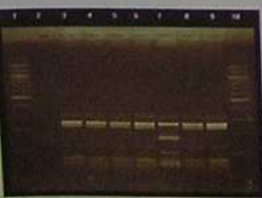

Figure 1: PCR-RFLP genetic characterisation [illegible]

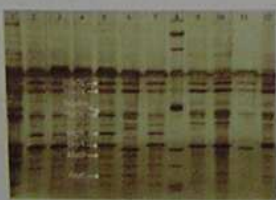

Figure 2: SDS-gradient PAGE protein profiles. [illegible]

	Isolate	Stage	Year of isolation	Identification
1.	BRZ 1	F	1997	*B. afzelii*
2.	BRZ 2	N	1997	*B. garinii*
3.	BRZ 4	F	1997	*B. afzelii*
4.	BRZ 7	N	1998	*B. garinii*
5.	BRZ 9	M	1998	*B. afzelii*
6.	BRZ 15	M	2000	*B. afzelii*
7.	BRZ 16	M	2000	*B. afzelii*
8.	BRZ 17	F	2000	*B. afzelii*
9.	BRZ 18	F	2000	*B. garinii*
10.	BRZ 19	F	2000	*B. afzelii*
11.	X 5	N	2002	*B. burgdorferi s.l.*
12.	X 8	N	2002	*B. burgdorferi s.l.*
13.	X 12	N	2002	*B. burgdorferi s.l.*
14.	X 16	N	2002	*B. burgdorferi s.l.*
15.	X 18	F	2002	*B. burgdorferi s.l.*
16.	X 19	N	2002	*B. burgdorferi s.l.*
17.	X 23	M	2002	*B. burgdorferi s.l.*
18.	X 24	N	2002	*B. burgdorferi s.l.*
19.	X 27	N	2002	*B. burgdorferi s.l.*
20.	X 29	N	2002	*B. burgdorferi s.l.*
21.	X 41	N	2002	*B. burgdorferi s.l.*
22.	X 54	N	2002	*B. burgdorferi s.l.*
23.	X 58	N	2002	*B. burgdorferi s.l.*
24.	X 94	N	2002	*B. burgdorferi s.l.*
25.	X 166	N	2002	*B. burgdorferi s.l.*
26.	X 192	N	2002	*B. burgdorferi s.l.*
27.	K 16	N	2002	*B. burgdorferi s.l.*
28.	K 46	N	2002	*B. burgdorferi s.l.*
29.	K 79	N	2002	*B. burgdorferi s.l.*
30.	K 81	N	2002	*B. burgdorferi s.l.*
31.	K 94	N	2002	*B. burgdorferi s.l.*

Table 2: Identification of 31 isolated strains of *Borrelia burgdorferi*

Results

The results of 6-year's study of the presence of *Borrelia burgdorferi* sensu lato in *Ixodes ricinus* ticks in the town-park locality Brno, Czech Republic, are presented in tab. 1. Mean annual proportion of infected ticks as DFM results was 7.2 % (males 11.9 %, females 8.2 %, nymphs 6.6 %, larvae 2.7 %). The PCR results are little different, but the total positivity of study locality is similar and with relatively low values.

From the total of 3170 collected ticks 157 tick homogenates were found to be infected by spirochetes. A total of 31 spirochete isolates from ticks were yielded. All the isolates were identified by single-tube nested PCR as *Borrelia burgdorferi* sensu lato and their protein composition was determined using SDS-gradient PAGE. 10 tick isolates were identified by PCR-RFLP (Fig. 1) as *B. garinii* and *B. afzelii*. SDS-gradient PAGE results (Fig. 2) correlate with PCR and RFLP results. Samples from the year 2002 are identificated in this time.

Acknowledgement

This work was partially supported by CEZ: J 07/98: 143100010, 143100008 and FRVŠ 541/03-G0427

Isolation and characterization of a novel subspecies of *Photorhabdus asymbiotica* isolated from *Heterorhabditis indica*

Ryusei Kuwata, Toyoshi Yoshiga, Mutsuhiro Yoshida* and Eizo Kondo
Department of Applied Biological Sciences, Saga University, Honjo 1, Saga 840-8502, Japan.
**National Agricultural Research Center, 3-1-1 Kannondai, Tsukuba, Ibaraki 305-8666, Japan.*

Introduction

Photorhabdus luminescens and *P. temperata* form a mutualistic symbiosis with heterorhabditid entomopathogenic nematodes. On the other hand, *P. asymbiotica* is a human pathogenic bacterium that has been isolated only from human clinical specimens in the USA and Australia. There is no assertive information available on the origin and the natural habitat of this clinical species.

In the study of *Photorhabdus* bacteria isolated from Japan, we found that two bacterial isolates from *H. indica* show high similarity to the clinical isolates of *P. asymbiotica*. Here we show the phylogenetic relationships of the *Photorhabdus* bacteria and *H. indica* associated with the bacteria. To investigate if the *H. indica* isolates are able to form mutualistic relationship with clinical isolates of *P. asymbiotica*, we monoxenically cultured Japanese *H. indica* isolates with some *P. asymbiotica* on the nutrient lipid agar plates. Pathogenicity of IJs obtained from the monoxenic culture was also examined.

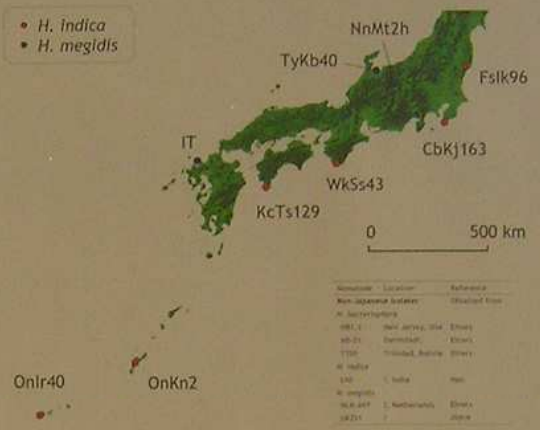

Results

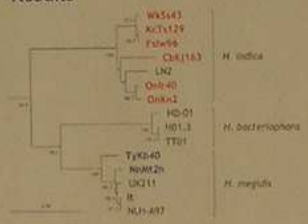

Phylogenetic relationships among *Heterorhabditis* isolates based on the sequences of COI region.

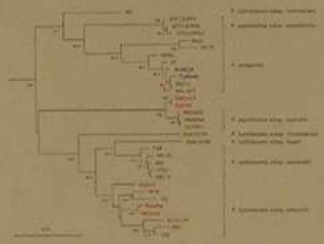

Phylogenetic relationships among *Photorhabdus* isolates based on the 16S rDNA sequences.

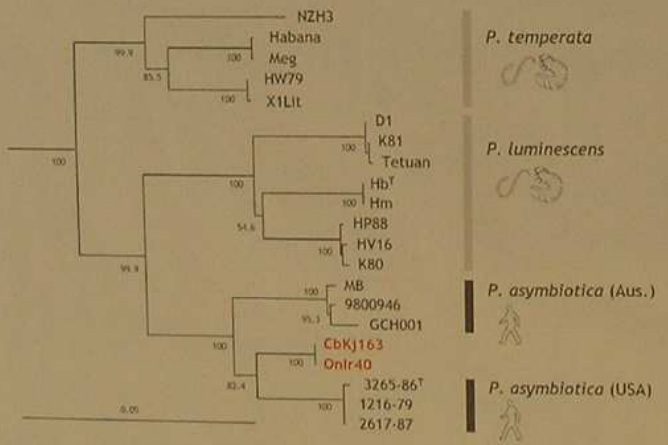

Phylogenetic relationships among *Photorhabdus* isolates based on the gyrase subunit B gene sequences

Growth and reproduction of *H. indica* on different *Photorhabdus* isolates.

	H. indica isolates		
	OnKn2	CbKj163	OnIr40
Bacteria isolates			
P. temperata			
HHL-A97	+	+	+
TyKb40	+	+	+
P. luminescens subsp. *laumondii*			
HB1.3	-	-	-
TT01	-	-	-
P. luminescens subsp. *luminescens*			
OnKn2	+	+	+
Photorhabdus sp.			
CbKj163	+	+	+
OnIr40	+	+	+
P. asymbiotica subsp. *asymbiotica*			
2617-87	-	+	+
P. asymbiotica subsp. *australis*			
9800946	+	+	+
9805888	-	+	+
9802892	-	+	+

+, Nematodes grew and reproduced; -, Nematodes did not grow
, IJs retained bacteria and showed insecticidal activity.
, Cadavers of *G. mellonella* larvae did not show reddish color.

Comparison of the color of *G. mellonella* larvae killed by freezing (control, left), *H. indica* harboring *P. luminescens* (middle) and *H. indca* harboring *Photorhabdus* sp. CbKj163 (right).

Comparison of phenotypic characters of *Photorhabdus* sp. CbKj163 and OnIr40 with those of known *Photorhabdus* species

Character	1	2	3	4	5	6
Insecticidal activity	+	+	+	+	+	+
Maximum growth °C	40	39	40	38	39	34
Bioluminescens	+	+	w	w	+	+
Protoplasmic inclusions	+	+	w	w	+	+
Dye adsorption	+	+	-		+	+
Indole production	+	-	+	-	d	[-]
Simon's citrate	+	+	d	+	d	d
Aesculin hydrolysis	-	-	-	+	+	d
Urease	-	+	-	+	d	[-]
DNase	-	-	[+]	-	-	+
Tryptophan deaminase	-	-	-	-	-	d
Acid production from:						
Mannitol	-	-	-	+	+	-
Inositol	+	+	+	d	[+]	[-]
Annular haemolysis:						
Sheep blood agar	+	+	d	+	+	+
Horse blood agar	+	+	-	+	d	+
Hydrolysis of:						
Tween 60	+	+	[-]	+	+	+
Tween 80	+	+	[-]	+	+	+

1, *Photorhabdus* sp. CbKj163; 2, *Photorhabdus* sp. OnIr40; 3, *P. asymbiotica* subsp. *australis* (Australian clinical isolates); 4, *P. asymbiotica* subsp. *asymbiotica* (American clinical isolates); 5, *P. luminescens* subsp. *akhurstii*; 6, *P. temperata* subsp. *temperata*.

Conclusion

¶ Based on the phylogenetic and phenotypic analyses, we conclude that the bacterial isolate CbKj163 and OnIr40 are a novel subspecies of *P. asymbiotica* that forms symbiotic association with *H. indica*.

¶ Symbiotic association of *P. asymbiotica* with entomopathogenic nematodes strongly indicates that the clinical isolates *P. aymbiotica* originated as a symbiont of *Heterorhabditis* nematodes and lost its symbiotic association with the nematodes.

Material and methods

Phylogenetic analyses of nematodes and bacteria used in this study

Phylogenetic relationship of heterorhabditid nematodes and their symbiotic bacteria were analyzed by using the sequences of the COI region of mitochondrial DNA and the nuclear 16S rRNA gene, respectively. These regions were amplified by PCR and DNA sequences were determined by direct sequencing.

Multiple-sequence alignments were created using CLUSTAL X version 1.81. The aligned sequence data were analyzed by the neighbor-joining method using a software package PHYLIP version 3.573c with Kimura 2-parameter model. The resulting NJ trees were evaluated by the bootstrap test with 1,000 replications. Trees were represented graphically with the software FreeView version 1. 6. 6.

Phenotypic characterization

API 20E kit (BIOMERIEUX) was used to test acid production and assimilation of carbon sources of bacteria according to the manufacturer's instructions. Bioluminescence was examined visually by observations in the dark. Maximum temperature for growth was determined in LB broth that had been incubated in a water bath with accuracy of ±0.2°C for 48h. Hemolysis was analyzed by using a hose and a sheep blood plates (NISSUI PHARMACEUTICAL Co., LTD). Lipase activity was analyzed by using LB plates containing Tween 60 or 80. Dye adsorption was assayed on MacConkey and NBTA plates.

Monoxenic culture of H. indica with Photorhabdus isolates in vitro

Three Japanese *H. indica* isolates and 11 *Photorhabdus* isolates were used in this study. Axenic 1st stage juveniles were obtained by surface sterilizing eggs and were monoxenically cultured with one of the *Photorhabdus* isolates on nutrient agar plates. Insecticidal activity of IJs obtained by the monoxenic culture was tested against the last instar larvae of *Galleria mellonella*. To detect retention of bacteria in the nematode intestine, IJs were surface-sterilized and crushed in a small amount of sterilized saline to release the bacteria from the nematode intestine. The bacterial suspension was spread on a MacConkey agar plate.

Monitoring of Insect-Hosts of Entomopathogenic Nematodes in Bulgaria

Denis Gradinarov*, Nikola Atanasov**
**Sofia University, Dragan Tzankov 8, 1164 Sofia, Bulgaria;*
***Plant Protection Institute, Panajot Volov, 2230 Kostinbrod, Bulgaria*

The entomopathogenic nematodes of the families Steinernematidae and Heterorhabditidae are intensively investigated because of their potential as biological control agents, but also because their specific biology. The cases of established naturally infected hosts are relatively rare. The aim of the following work is to systematize the knowledge of insects – hosts of entomopatogenic nematodes (EPN), discovered in Bulgaria.

The insects from 6 genera and 7 families were found in Bulgaria as natural hosts of entomophatogenic nematodes (Table 1). They belong to the orders Coleoptera, Hymenoptera and Diptera. Some of them are phytophagous another carnivores and the others are with mixed feeding.

The species *S. intermedium* is isolated from pupae of Cantharidae in town of Sofia (Fig.1).

Fig.1. Pupa of *Cantharis* with nematodes

Infected by *S. bicornutum* larvae or pupae of Curculionidae, Carabidae (Fig. 4), and Asilidae (Fig.3) were found in an riverside soil in the Zemen gorge (Fig. 2). This cases of invasion are of special interest. They shows that EPN parasitized not only phytophagous insects but also myxophagous and predators.

Fig.2. Zemen Gorge

Fig.3. Larva of *Asilidae* with nematodes

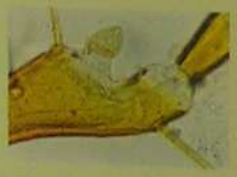

Fig.4. Antena and urogomphus of Harpalus with nematodes

Table 1. Detected natural host insects of the entomopathogenic nematodes in Bulgaria

Nematode	Host insect	Region	Habitat
S. kraussei	*Bibio* sp. (Bibionidae)	Vitosha Mts.	beech and pine forest, subalpine meadows
S. kraussei	Curculionidae g.sp.	Vitosha Mts.	subalpine meadow
S. carpocapsae	*Cydia pomonella* L. (Tortricidae)	Kjustendil	apple garden
S. carpocapsae	*Limonius* sp. (Elateridae)	Vitosha Mts.	mezophilic meadow
S. carpocapsae	*Formica cinerea* (Formicidae)	Hadjidimovo	swamp meadow
S. intermedium	*Cantharis* sp. (Cantharidae)	Sofia	garden
S. bicornutum	Curculionidae g.sp.	Zemen gorge	riverside meadow
S. bicornutum	*Harpalus* sp. (Carabidae)	Zemen gorge	riverside meadow
S. bicornutum	Asilidae g.sp.	Zemen gorge	riverside meadow
Steinernema sp.	*Bibio* sp. (Bibionidae)	Vitosha Mts.	pine forest
Steinernema sp.	Asilidae g.sp.	Osogovska Mts.	subalpine meadow
Steinernema sp. "*affine* group"	*Bibio* sp. (Bibionidae)	Vitosha Mts.	pine forest
H. bacteriophora	*Drasterius bimaculatus* Rossi (Elateridae)	Kostinbrod	strawberry fields

On Vitosha Mts. (Fig.5) several times we had found infected by EPN larvae of *Bibionidae* (*Bibio* sp.) (Fig.6). Almost in all cases the invasion density was 1 – 3 nematodes per a dipterian larva. The EPN appears to be one of the main factors, which control the density of the bibionid flies in forest habitats in Bulgaria.

Fig.5. Pine forest on Vithosha Mts.

Fig.6. Infected bibionid larvae

The species *S. carpocapsae* was isolated from a larva of Elateridae in soil from Vitosha Mt. and from female ant (Formicidae) in a riversides of Mesta. Infected with *S. carpocapsae* larvae of *Cydia pomonella* L. were found also near town of Kjustendil (Vega et al., 2000). The species *H. bacteriophora* was isolated from a larva and a pupa of *Drasterius bimaculatus* Rossi (Elateridae).

Laboratory tests for parasitized of some economically important insects were performed. We used insects, gathered from an alfalfa stand in experimental field near Sofia. These are imago of phytophagous *Subcoccinella*, *Phytodecta* and the beneficial species *Coccinella septempunctata* L. A experimental invasion was with nematode cultures of the species *H. bacteriophora* and *S. feltiae*, which were isolated from Bulgaria.

Even though the dosage of EPN was high, the results proved that these nematodes have relatively low efficiency against the insects of the genera *Subcoccinella* (Fig. 7) and *Phytodecta*. We determined via dissection that the mortality rate is *Coccinella septempunctata* does not account on EPN.

Fig.7. Infected imago of *Subcoccinella*

The results of the experiment can be generalized in the following statements:

1. The species *Subcoccinella* and *Phytodecta* are vulnerable to invasion with the nematode *H. bacteriophora*;
2. The imago of *Subcoccinella* sp. is most effectively invaded by the species *H. bacteriophora*;
3. The species *S. feltiae* is more pathogenic to *Phytodecta* then *H. bacteriophora*;
4. The beneficial species *Coccinella septempunctata* is not affected from the species *H. bacteriophora*.

Installation of a Swiss Zooparasitic Nematode Bank

S. Kuske, J. Grunder, E. Fischer
University of Applied Sciences Wädenswil HSW, Grüntal, PO Box 335, CH-8820 Wädenswil, Switzerland. Email: s.kuske@hsw.ch

HOCHSCHULE WÄDENSWIL

Background

Worldwide there are several nematode families known expressing bio-control potential, with a broad range of nematode products available for commercial use.
In recent years, more than 40 entomopathogenic nematode strains, belonging to more than 10 different species from more than100 monitoring sites, as well as about 100 isolates of the symbiotic bacteria have been collected and reared in Switzerland and are currently held in calibration at the Swiss Federal Research Station Agroscope ACW Wädenswil. These nematodes and their symbionts are available for further investigation concerning their bio-control potential.

Objectives

The goal of the Swiss zooparasitic nematode bank is to preserve the genetic resources of endemic nematodes and their symbiotic bacteria. It aims to ensure quick and reliable access to both nematodes and bacteria for research topics at the University of Applied Science in Wädenswil (HSW). It also aims to make sure that the biological activity of this living organisms can be maintained and stored using quality-ensured standard methods. The Swiss zooparasitic nematode bank will provide an universally available standard which can be used as a base for the development of new commercial products.

Species list

EPN's
Heterorhabditids
H. bacteriophora
H. megidis

Steinernematids
S. affine
S. arenarium
S. bicornutum
S. carpocapsae
S. feltiae
S. Swiss "glaseri" type
S. intermedium
S. kraussei
S. weiseri

Bacteria
P. luminescens
Xenorhabdus species isolated from the *Steinernema* species listed above.

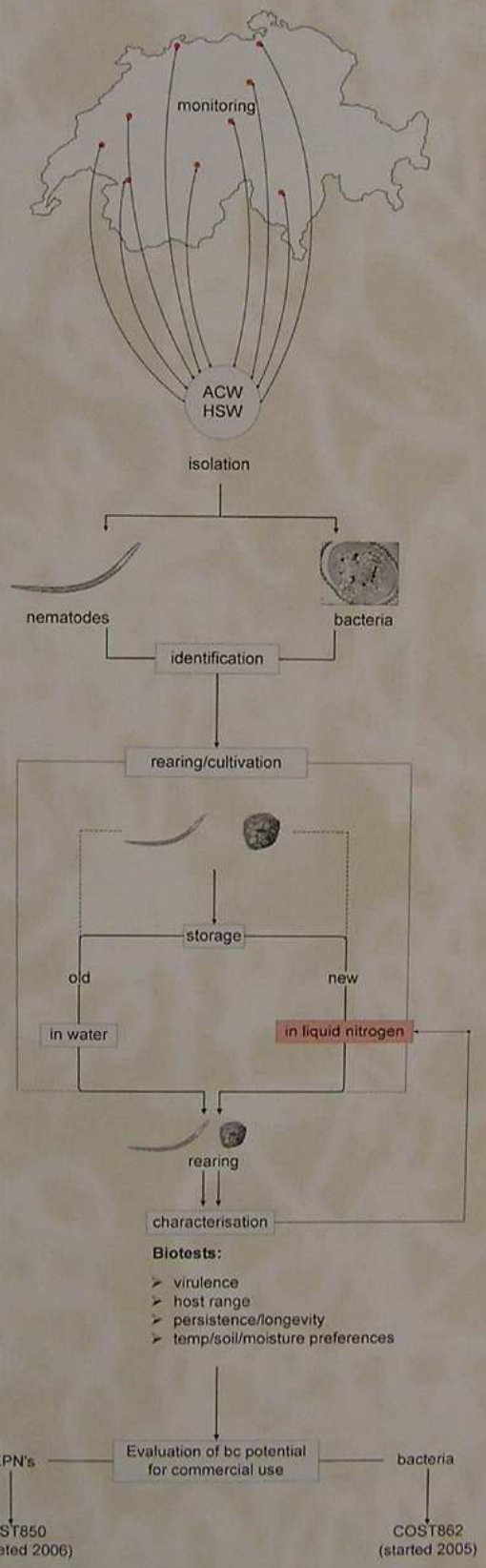

Methods

The general methods used for cryopreservation are based on the recommendations of Bai *et al.* (2004).

- Filtration of 100 ml IJ through a Whatman Nr. 1 Filter.
- Immersion of the IJ's in in glycerol (18% for *Steinernema spp.* and 13% for *Heterorhabditis spp.*) for a set time (48 hours for *Steinernema spp.*, 168 hours for *Heterorhabditis spp.*). The number of IJ's was adjusted to about 12'000 IJ's per 1 ml glycerol solution.
- Vacuum filtration onto a filter paper disk
- Immersion of the filter-paper in pre-chilled (10°C) Methanol (70%).
- Placement of the rolled filter-paper into pre-chilled (0°C) cryogenic vials and immediate immersion of the closed vial into liquid nitrogen.

The nematodes are thawed by pouring 1.5ml of Ringer's solution (24°C) into the cryogenic vial.

Virulence of selected strains was tested against the following pests:

- Black vine weevil *(Otiorhynchus sulcatus)*
- Hazelnut weevil *(Balaninus nucum)*
- Chestnut weevil *(Curculio elephas)*
- Chestnut tortrix *(Cydia splendana)*
- Cockchafer *(Melolontha melolontha)*
- European cherry fruit fly *(Rhagoletis cerasi)*
- Walnut husk-fly *(Rhagoletis completa)*

Perspectives

- live databank encompassing many species
- quick access
- good quality
- new species/strains
- ongoing characterisation
- new products

References

Bai C., Shapiro-Ilan D.I., Gaugler R. and Yi Shuxia, 2004. Effect of Entomopathogenic Nematode Concentration on Survival during Cryopreservation in Liquid Nitrogen. Journal of Nematology 36 (3): 291-294

Novel mitochondrial gene arrangement among some species of the Genus *Heterorhabditis*

Sassia O. Regeai and Ann M. Burnell
...of Bioengineering and Agroecology, National University of Ireland
Maynooth, Maynooth, Co. Kildare, Ireland

...studies of molecular evolution, phylogeny, phylogeography, population genetics, and as a species specific diagnostic marker. This study describes the mtDNA ...mtDNA sequence for a species within the genus *Heterorhabditis*. It also describes the size and mitochondrial gene arrangement of *Heterorhabditis* species. ...will be useful for the molecular characterization of this genus, and will be helpful in designing primers to conduct population genetic studies; and in improving ...

2. ...sitic nematode *Heterorhabditis bacteriophora*

...seven overlapping fragments (Fig 1) by long-PCR (Expand 20 Kb Kit, Roche) from total genomic DNA and its complete nucleotide sequence was determined. Figure 2 ...from its complete nucleotide sequence. The *H. bacteriophora* mtDNA genome contains 36 of the 37 genes typical of metazoan organisms (22 transfer RNAs, 2 ribosomal ...which is consistent with other nematode species mtDNA sequenced to date (except *Trichinella spiralis*). All genes are transcribed in the same direction and have a nucleotide ...contents are 47.02% (T), 28.81% (A), 16.10% (G), 8.08% [C], and 75.83% (AT).

Figure 1 PCR amplification of the seven mitochondrial fragments ...

Figure 2. ...

The total size of the mtDNA molecule from *H. bacteriophora* is 18,128 bp and is among the largest yet reported for a rhabditid nematode. It is ca. 4 Kb larger than typical. This large size is due to the presence of five regions of novel noncoding DNA: NC1 (114 bp), NC2 (159 bp), NC3 (498 bp) which is present in three dispersed copies, NC4 (1917 bp), and NC5 (2154 bp). The existence of noncoding DNA on such a large scale has not previously been observed in nematodes. *H. bacteriophora* is considered to be closely related to *C. elegans*, yet the mtDNA gene arrangement of *H. bacteriophora* is distinctly different from *C. elegans* and other nematode mtDNA genomes sequenced to date (Fig. 3).

The distinctive features of the mitochondrial gene order of *H. bacteriophora* include:

- a translocation of a block of seven genes: tRNA Q, tRNA F, Cytb, tRNA L (CUN), COIII, tRNA T, and ND4
- an inversion of the tRNA C and tRNA M genes, and
- a translocation of tRNA D and tRNA G genes.

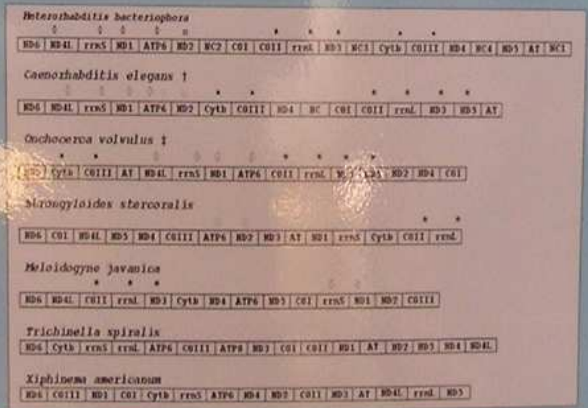

Figure 3. Comparison of mitochondrial gene arrangements among nematodes ...

3. Mitochondrial genome size of *Heterorhabditis* species

Field inversion gel electrophoresis (FIGE) was used to determine the approximate mtDNA genome size of other *Heterorhabditis* species. The approximate mtDNA genome size of *Heterorhabditis* species varied from ca. 17 to 22 Kb, with the exception of *H. mexicana* whose mtDNA genome (ca. 40 Kb) is exceptionally large (Fig. 4).

Figure 4. mtDNA genome size of *Heterorhabditis* species ...

4. Mitochondrial gene organization of *Heterorhabditis* species

The arrangement of protein coding genes and tRNA genes in all *Heterorhabditis* species was investigated by two assays: Southern blot analysis and PCR gene boundary analysis. Both of these assays confirm the presence of the gene block translocation (Cytb, COIII, and ND4) in two additional species of *Heterorhabditis*: *H. megidis* and *H. zealandica*. The other five *Heterorhabditis* species: *H. marelatus*, *H. downesi*, *H. taysearae*, *H. mexicana*, and *H. indica* appear to possess a mtDNA genome arrangement typical of *C. elegans* (Fig. 3). In the Southern blot analysis, AmaI and NsiI fragments (Fig. 5) were probed with two mtDNA probes: ND4 and COI. The ND4 probe detected the translocation in NsiI fragments from *H. bacteriophora*, *H. megidis*, and *H. zealandica*; this probe also hybridized to AmaI fragments from *H. marelatus*, *H. downesi*, *H. taysearae*, *H. mexicana*, and *H. indica*, indicating the absence of the translocation in these species (Fig. 6A). All the AmaI fragments hybridized to the COI probe, as expected (Fig. 6B).

Figure 5. AmaI and NsiI PCR amplification in all *Heterorhabditis* species ...

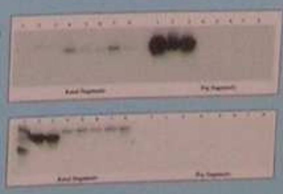

Figure 6. Southern blot of AmaI and NsiI PCR fragments probed with (A) ND4 probe (B) COI probe

5. The noncoding NC3 region

An assay for the presence of the NC3 region by PCR and DNA sequencing confirmed its existence in all *Heterorhabditis* species examined. All *Heterorhabditis* species amplified a single band of ca. 500 bp. Cloning and sequencing of this band showed almost 100% identity in all *Heterorhabditis* species. However, the copy number of NC3 region was not determined.

6. Conclusion

This study provides a resource for the comparative analyses of nematode mtDNA genomes and for studying the population genetics of *Heterorhabditis* species.

Acknowledgements
This research was funded by the Libyan Ministry of Higher Education and ...

Poster Presented at the EU COST 850 "Biocontrol Symbiosis" Workshop, Salzau, Germany, 1-6 June 2006.

Attempts to Develop an RNAi Protocol for *Steinernema carpocapsae*

I. Dix, T. Tyson and A.M. Burnell
Department of Biology, National University of Ireland Maynooth, Co. Kildare, Ireland.
Email: ilona.dix@may.ie

Introduction

RNAi has been shown to be a powerful technique by which individual genes can be inactivated so that their biological function may be examined. The RNAi gene knock-out effect was originally demonstrated in *C. elegans* by Fire *et al.* (1998) who reported that the microinjection of dsRNA for a portion of the *unc-22* gene into the nematode *C. elegans* resulted in a potent and specific inhibition of the *unc-22* gene.

Even with exhaustive experiments we have failed to demonstrate an RNAi effect in *Steinernema carpocapsae*.

Figure 1. Embryonic lethal phenotype of the F1 progeny of *C. elegans* injected with dsRNA of *his-60* gene of *S carpocapsae*.

Figure 2. F1 progeny of *C. elegans* injected with dsRNA of the translation factor of *S. carpocapsae*

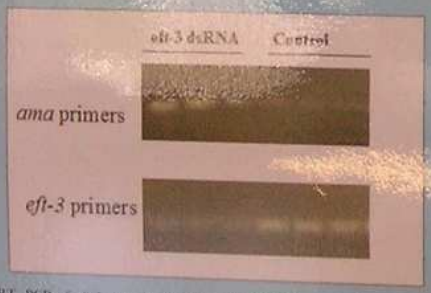

Figure 3. RT- PCR of *eft-3* gene. Single nematode RT-PCR was carried out on F1 progeny of *C elegans* injected with dsRNA of the *eft-3* gene from *S. carpocapsae*. RT-PCR of the *ama-1* gene (which encodes RNA polymerase II) was used as a control.

RNAi experiments

A. Microinjection of dsRNA

1. *C. elegans* embryonic lethal genes

We selected 7 *C. elegans* embryonic lethal RNAi clones from the Ahringer feeding library (Fraser *et al.*, 2000). These target genes were selected because they are highly conserved in *C. elegans*, *Drosophila melanogaster* and yeast. These constructs had a potent RNAi effect in *C. elegans* but did not have an RNAi phenotype in *S. carpocapsae*.

2. *S. carpocapsae* genes

Three housekeeping genes isolated from *S. carpocapsae* were tested for an RNAi effect in *S. carpocapsae* and *C. elegans*.

These genes did not have an RNAi phenotype in *S. carpocapsae*, but surprisingly all three had strong embryonic lethal phenotype in *C. elegans* (Table 1, Fig. 1). A reduction of *eft-3* mRNA levels was observed in *C. elegans* treated with dsRNA from the *S. carpocapsae eft-3* gene (Fig. 3).

3. Microinjection of dsRNA with TransIT-TKO

The TKO transfection reagent was used in attempts to enhance the uptake of the dsRNA of the *eft-3* and *inf-1* genes into *Steinernema carpocapsae*. Nematodes were injected into the haemocoel or gut, but no RNAi effect was found.

4. RNAi of other *S. carpocapsae* strains

No RNAi effect was observed when the *S. carpocapsae* C4A and DD136 strains were injected with dsRNA of *his-60* gene from the *S. carpocapsae* All strain.

B. Microinjection of siRNA

dsRNA prepared from the *his-60* gene of *S. carpocapsae* was digested with the Dicer endonuclease to yield 21mer siRNAs. These siRNAs were injected into the gut and haemocoel of *S. carpocapsae* females, but no RNAi effect was observed.

Table 1. Phenotypes of injected *S. carpocapsae* females and *C. elegans* adults after dsRNA of *C. elegans* genes

dsRNA construct	Injected nematode: Number of nematodes injected	Injected nematode: RNAi effect	*C. elegans*: Number of nematodes injected	*C. elegans*: RNAi effect
Histone gene *his-60*	9	None	17	Embryonic lethal 100%
Initiation factor *inf-1*	25	None	4	Embryonic lethal* 20-30%
Elongation factor *eft-3*	31	None	7	Embryonic lethal* 80%

* Those larvae which do hatch develop very slowly into dissected sterile adults (Figure 2).

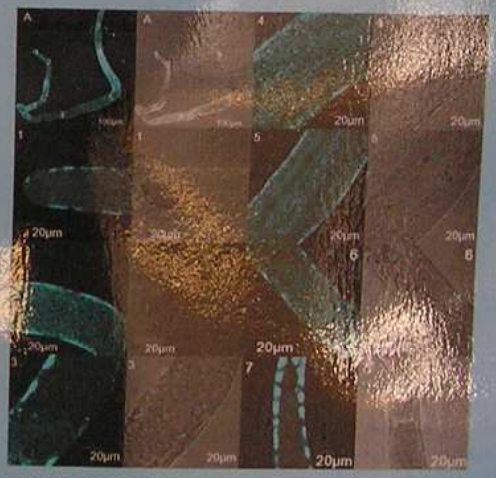

Figure 4. Confocal microscopic images of DAPI stained *S. carpocapsae* ovary.

Conclusions

We found it surprising that an RNAi effect could not be shown in *Steinernema carpocapsae* either by soaking worms in dsRNA (data not presented) or by injecting dsRNA or siRNA into the haemocoel, gut or ovary. The most likely reason for this is that *Steinernema carpocapsae* is missing some of the components necessary for the RNAi mechanism. Alternatively the lack of RNAi effect may be due to the *S. carpocapsae* ovary structure, which is very different from that of *C. elegans*, and appears to be cellular, unlike the syncytial structure of the *C. elegans* ovary (Fig. 3).

That our dsRNA constructs are able to evoke an RNAi effect is shown by the fact that they produce a very strong heterologous effect in *C. elegans*.

References

1. Fire, A *et al.* Potent and specific genetic interference by double-stranded RNA in *Caenorhabditis elegans*. *Nature* **391** 806-811 (1998)

2. Fraser, A.G et al. Functional genomic analysis of *C. elegans* chromosome I by systematic RNA interference *Nature* **408** 325-330 (2000)

Acknowledgements

This research was funded by Science Foundation Ireland

Poster Presented at the EU COST 850 "Biocontrol Symbiosis" Workshop, Salzau, Germany, 1-6 June 2006.

Testing the Male Colonisation Hypothesis in *Steinernema* Species

Mohamed Alsaiyah and Christine Griffin

Institute of Bioengineering and Agroecology, NUI Maynooth, Ireland.

NUI MAYNOOTH

Introduction:

According to the male colonisation hypothesis, infective juveniles that are destined to develop in to males invade insect earlier than females. This reported to be the case in several species of *Steinernema* by Grewal et al.(1993) but the hypothesis has been controversial. Stuart et al (1998) tested the hypothesis for *Steinernema glaseri*, one of the species reported by Grewal et al. , to show male colonisation. If males colonise first, the sex ratio is expected to male-biased following a short exposure to a host, but the bias should decrease with further exposure. Insect were exposed to *S. glaseri* infective juveniles in sand columns for various periods of time, but there was no evidence of earlier colonizing by males than females (Stuart et al 1998). In this study using the same approach as Stuart et al. we ask whether males or (females) colonise first, by looking for changes in the nematode sex ratio in hosts which are exposed to infective juveniles for different period of time. Since time of emergence from the host may also affect sex ratio in steinernematids (Lewis & Gaugler, 1994), infective juveniles were harvested at three times and harvests were tested separately.

Methods:

Culture and harvest of nematodes: *Steinernema feltiae* (4CFMO strain) and *Steinernema carpocapsae* (All strain) were reared in *Galleria mellonella*.Three harvests were collected, from early (Day 1), middle (Day 6) and late (Day 10) in the emergence period.

Assay: *G. mellonella* larvae were exposed to infective juveniles (100/insect) in sand for 4, 6, 8, 10, 20, 24 and 48 hours and washed. A 4 cm sand column was used for *S. feltiae* and 1 cm for *S. carpocapsae*. After about 5 days the Galleria were dissected and the number of male and female nematodes counted. There were 10 replicates per exposure period.

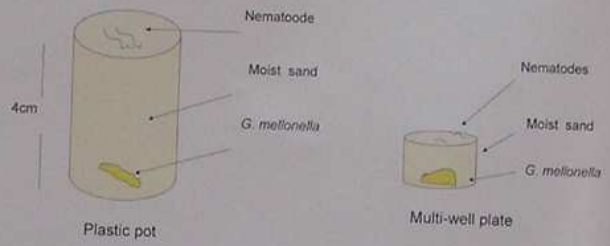

Results:

Fig. 1. The number of nematodes invading wax moth larvae increased with time of exposure. More female than males nematodes were found at each exposure period.

Fig. 2. There was no systematic change in sex ratio with time of exposure for any harvest of either *S. feltiae of S. carpocapsae*

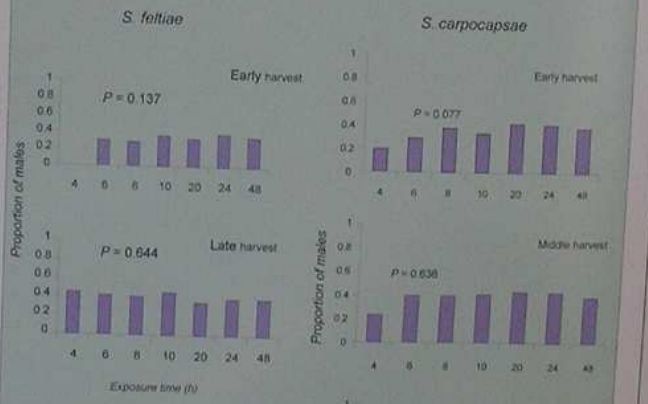

For *S. carpocapsae*, there was a trend for the proportion of males to increase over the 4-6-8 hours period , but there was no significant difference in sex ratio between these exposure times when the experiment was repeated (data not shown).

Fig. 3. The proportion of males was higher in later harvests for both species, the proportion of males in the population significantly influenced by harvest time, being higher in nematodes that emerged later from the natal cadaver.

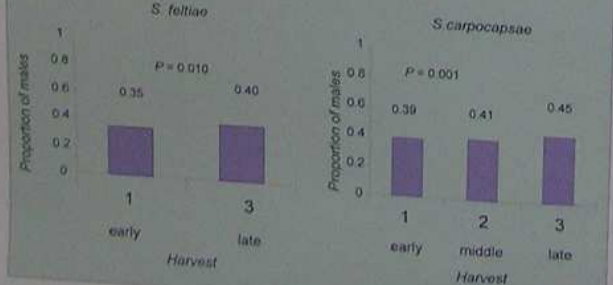

Conclusion:

1. There was no systematic change in sex ratio with exposure time for either *S. feltiae* (previously found not to be male first coloniser species) or *S. carpocapsae* (reported by Grewal et al. 1993) to be species with male-first coloniser).Therefore our data do not support the male colonisation hypothesis for S. carpocapsae.
2. *S.carpocapsae* and *S.feltiae* are female biased in the sex ratio .
3. Male tend to emerge from the hosts later than females in both *S.carpocapsae and S.feltiae*.

We are currently testing other species of *Steinernema* in a similar manner.

References:

1. Grewal, P. S., Selvan, S., Lewis, E. E., and Gaugler, R. 1993. Males insect-parasitic nematodes: a colonising sex. J. Experientia (49). 605-608.

2. Lewis, E. E., and Gaugler, R. 1994. Entomopathogenic nematodes (Rhabdita: Steinernematidae) sex ratio relates to foraging strategy. J. Invertebrate Pathology 64. 238-242.

3. Robin J. Stuart, Moeen Abu hatab, Gauglar, R. 1998. Sex ratio and the infection process in entomopathogenic nematodes: Are males the colonising sex. J. Invertebrate Pathology 72. 288-295.

A report on the occurrence of *Heterorhabditis indica* with two symbiotic bacterial species in Japan

M. Yoshida[1)], R. Kuwata[2)], T. Yoshiga[2)] and T. Mizukubo[1)]
1) National Agricultural Research Center, Tsukuba, Ibaraki 305-8666, Japan
2) Saga University, Saga 840-8502, Japan

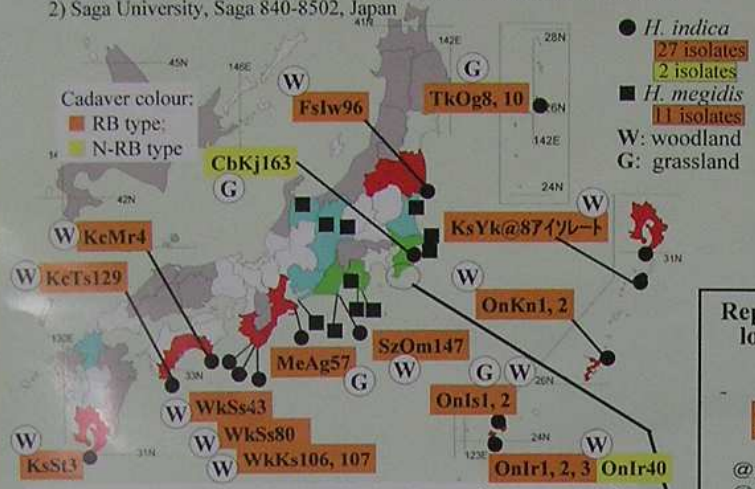

Distribution of heterorhabditids in Japan (1990～2000)

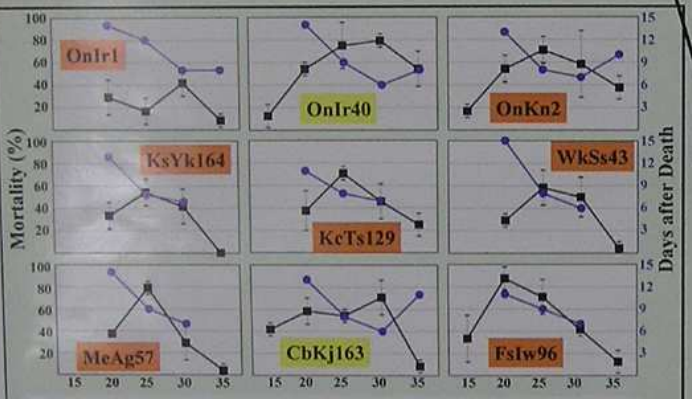

■: Mortality of *Galleria* larvae by *H. indica* infection at 5 days (20～35℃) and 10 days (15℃) after treatment;
●:First day emergence was observed; 1 Galleria / 10 IJs in 24 well plate, 8 wells / replicate, each isolate 3 replicate

Body colour of cadavers of *Galleria mellonella* infected by *Heterorhabditis indica*

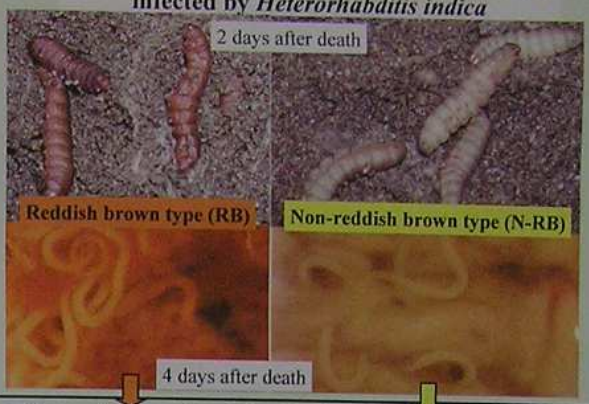

Reproduction activity ends with lost of reddish brown colour → symbiotic bacteria were examined → ***Photorhabdus luminescens***

Pathogenicity and reproductive activity is retained → symbiotic bacteria were examined → New subspecies of *P. asymbiotica*

@*P. asymbiotica* : clinical isolates / relationship with EPNs unknown
@about 5～10 years after isolation, the symbionts were studied

Questions:
1. Was *P. asymbiotica* a symbiont of the N-RB type?
2. Did replacements of symbionts occur during laboratory maintenance?

Symbionts of the isolates obtained from *Galleria* trap have to be examined.
A survey for *H. indica* in some regions, where the N-RB type has been isolated, is required.

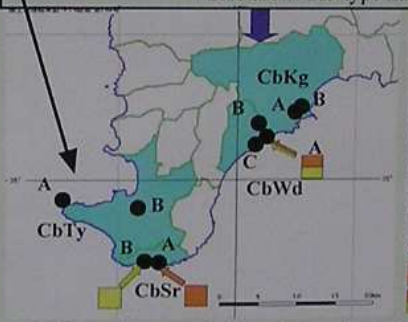

Survey for EPNs in southern Chiba Pref. (Cb), 2005. Sampling location (●) and positive sites (arrows) for *Heterorhabditis indica*. Arrow's colour indicates RB and/or N-RB types as follows.

: RB type; : N-RB type; : RB and N-RB type

Habitat characteristics of sampling sites in the southern Chiba Pref. (Cb) (9 locations, 21 sites, 120 samples)

Location	Site No.	No. Samples	Elevation (m)	Distance from sea (m)	Topography	Vegetation	No. positive samples: *Steinernema*	No. positive samples: *Heterorhabditis*
	A-1	5	<5	20-30	Beach	Sward	2	2
	A-2	5	<5	50-60	Coast	Pine (Windbreak)		
	A-3	5	<5	40-50	Coast	Tussock	1	
	A-4	5	<5	70-80	Coast	Evergreen+Pine (Park)	2	1
CbWd	B-1	4	65-75	Inland	Hill	Tussock		
	B-2	3	60-65	Inland	Hill	Cycad (Plantation)		
	B-3	3	55-60	Inland	Hill	Ume+Cycad (Plantation)		
	C-1	3	10-20	80-90	Beach	Tussock	1	
	C-2	7	10-20	90-100	Coast	Evergreen+Pine	1	
	C-3	5	10-20	100-120	Coast	Laurilignosa	4	
	A-1	5	<10	100-200	Coast	Laurilignosa		
	A-2	4	<10	80-90	Coast	Laurilignosa (Park)		
CbSr	A-3	3	<5	10-20	Beach	Sward		1
	A-4	3	<5	30-40	Coast	Pine (Windbreak)		
	B-1	19	3	40-50	Beach	Tussock		1
	B-2	6	3	30-40	Beach	Sward	2	2
	A-1	10	30-35	300-400	Coastal Hill	Laurilignosa	6	
CbTy	A-2	5	10	10-20	Beach	Sward		
	B	10	80-90	Inland	Hill	Evergreen+Cryptomeria		
CbKg	A/B	5/5	60-100	Inland	Hill	Laurilignosa	3/1	

Sites CbWd-A (2005)

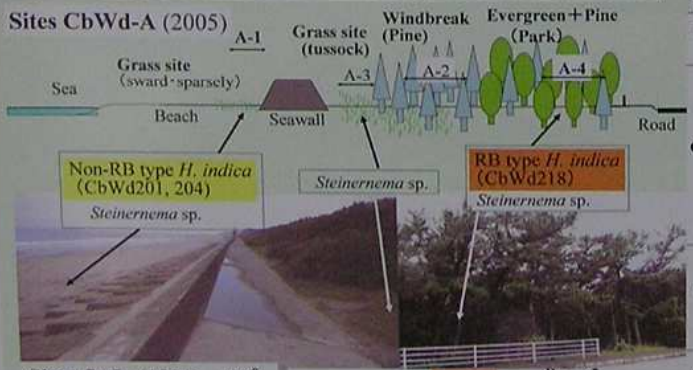

Sites OnIr (1991)

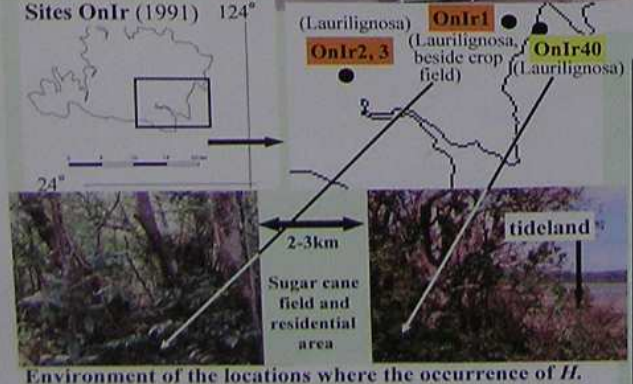

Environment of the locations where the occurrence of *H. indica* with two symbiotic bacterial species were observed.

Conclusion

@ The followings were proved by the field survey.
1. *H. indica* has a symbiotic relationship with *P. asymbiotica* too.
2. Insects infected by *H. indica* with *P. asymbitica* have a dark grey to pale yellow colour (not reddish colour).

@ Is there any environmental isolation (barrier) between the two symbiont types?
1. Habitat
Woodland: 19 sites – ***asymbiotica* type from 1 site** (OnIr40)
Grassland: 8 sites – ***asymbiotica* type from 4 sites**
(all 4 sites in the south part of Chiba Pref / Boso Peninsula)
2. Two cases on the adjacent occurrences
***asymbiotica* type: sea-side ⇔** *luminescens* type: inland-side
⇒ Did ***asymbiotica* type invade after** *luminescens* type colonized ?
Where did *asymbiotica* type come from? Did it come from sea?
3. Host preferences: further research required.

A review on entomopathogenic nematodes in Turkey

Alper Susurluk

Turkish Ministry of Agriculture and Rural Affairs,
Plant Quarantine Service, Department of Nematology, Liman Str. No: 11,
35230 Alsancak / Izmir-Turkey

In Turkey, entomopathogenic nematodes (EPNs) are considered as potential biological control agent against soil-borne insect pests. Thus, there are some studies on EPNs in Turkey as in all over the world. The aim of the presentation is to clarify the situation of EPNs in Turkey. The first scientific experiment in Turkey on EPNs carried out by Özer et al. in 1995. Many of these studies consist of survey experiments including extraction and identification techniques. Five steinernematid and one heterorhabditid species were isolated at the end of the surveys. In these surveys, the most common species was *Steinernema feltiae*. In addition to common species, a new species has been described as *S. anatoliense* by Hazir et al. (2003a). Many of the isolated species were described with molecular technique, PCR-RFLP. All described species were extracted by using of *Galleria mellonella* bait technique. Besides the survey experiments, nowadays some applied experiments of EPNs have been performed such as efficiency studies on *Ceratitis capitata* and *Rhagoletis cerasi* and some ecological studies such as host finding behavior, reproductive potential at different temperatures. But, there are no outdoor experiments, yet. Moreover, so far only two M.Sc. and one Ph.D. studies on EPNs have been conducted in Turkey, because of lacking of expert scientist on EPNs.

In conclusion, researches with the Turkish nematodes have only recently been initiated. Isolated species in Turkey provide opportunities for conducting fundamental studies for using them in biological control strategies against a lot of soil dwelling insect pests in cryptic habitats.

Distrubiton of Entomopathogenic Nematodes inTurkey

★ *S. feltiae*, ■ *S. carpocapsae*, ✦ *S. anatoliense*
● *S. affine*, ▲ *S. weiseri*, ◆ *H. bacteriophora*

At present, all described EPN species in Turkey

Nematode species	Isolation regions	Authors
Steinernema feltiae	Ankara, Kirsehir, Eskisehir (Center Anatolia), Rize and Sinop (North of Turkey), Burdur (South of Turkey), Van (East of Turkey), Canakkale (West of Turkey).	Özer et al. (1995), Susurluk et al. (2001), Hazir et al., (2003b)
S. anatoliense	Kars (East Anatolia)	Hazir et al., (2003a)
S. carpocapsae	Antalya and Icel (Soth of Turkey)	Kepenekçi (2002)
S. affine	Icel, Adana (South of Turkey), Mardin (Southeast Anatolia), Tokat (North of Turkey), Tekirdag, Kirklareli (Northwestern Turkey)	Hazir et al. (2003b)
S. weiseri	Ankara (Center Anatolia)	unpublished
Heterorhabditis bacteriophora	Ankara, Aksaray (Center Anatolia), Istanbul, Kirklareli, Tekirdag (Northwestern Turkey), Kayseri (Center Anatolia)	Susurluk et al. (2001), Hazir et al. (2003b)

REFRENCES:

Hazir, S., N. Keskin, S.P. Stock, et al., 2003a. A new entomopathogenic nematode, *Steinernema anatoliense* n. sp. (Rhabditida: Steinernematidae) from Turkey. Systematic Parasitol. 55: 211-220.

Hazir, S., S. P. Stock and N. Keskin, 2003b. Diversity and distribution of entomopathogenic nematodes (Rhabditida: Steinernematidae and Heterorhabditidae) in Turkey. Biodiversity Conserv. 12: 375-386.

Kepenekçi, I., 2002. Entomopathogenic nematodes (Rhabditida) in the Mediterranean Region of Turkey. Nematologia Mediterranea, 30: 13-16.

Özer N., Keskin N. and Kirbas Z., 1995. Occurrence of entomopathogenic nematodes (Steinernematidae, Heterorhabditidae) in Turkey. Nematologica, 41: 639-640.

Susurluk A., Ehlers R.U., Strauch O., Wyss U. and Ehlers R.U., 2001. Identification and ecological characterization of three entomopathogenic nematode-bacterium complexes from Turkey. Nematol., 3: 833-841.

POSTER 13

C | A | U
Christian-Albrechts-University Kiel
Faculty of Agriculture and Food Science
Institute for Phytopathology
Dept. Biotechnology & Biol. Control

Checking for synergistic effects between *Bacillus thuringienis* and *Steinernema carpocapsae* against *Plutella xylostella*

Introduction:

The Diamondback Moth (DBM) *Plutella xylostella* is a major pest of crucifers. Due to the intensive use of broad-spectrum chemical insecticides the potential of invertebrate natural enemies is limited and the pest has develeped resistance against all chemical insecticide, even against the biological insecticide *Bacillus thuringiensis* (Bt). In order to reduce the resistance level alternative biocontrol agents are needed for DBM control. Entomopathogenic nematodes (EPN) were successfully used against DBM and alternating applications with *Bacillus thuringiensis* resulted in good control during field experiemnts on Java, Indonesia. The objective of this study was to investigate whether synergistic effects occur if both agents are used together.

Material and Methods:

EPN: *S. carpocapsae* (EN03) e-nema GmbH, Germany
Bt: Dipel ES® (Bt var. kurstaki) Stähler Agrochemie GmbH & Co. KG, Germany
XenTari® (Bt. var. *aizawai*) Valent BioSciences Corporation, USA
Biomük (Bt var. israelensis) Biofa, Germany
Surfactant-polymer-formulation (SPF): 0.3% Rimulgan and 0.3% Xanthan

Application of EPN and Bt on cabbage leaf disks:

EPN: 40ml with flat-fan nozzle
Bt: 1ml with airbrush nozzle

Fig. 1. Bt-Application

One leaf disk with one 3rd larva in each well was incubated 48h at 25°C and 80% RH.

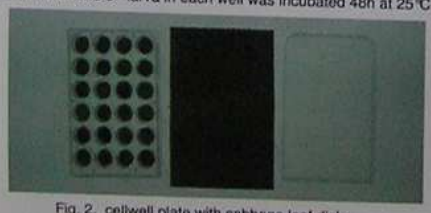
Fig. 2. cellwell plate with cabbage leaf disks

Statistic analysis:

$P_e = 1 - (1 - P_1)(1 - P_2)(1 - P_3)$
P_e: expected mortality for additive effects
P_1, P_2, P_3: mortality of single component
Statistic analysis of differences to additive effects were carried out with Fisher's exact test.

Tab. 1: Criteria for the interaction (according to Finney, 1971)

significant	$D_e > D_o$	antagonism
significant	$D_e < D_o$	synergism
not significant	$D_e = D_o$	additive effect

D_e: expected number of dead larvae ($D_e = P_e$ x total number of larvae)
D_o: observed number of dead larvae

Result:

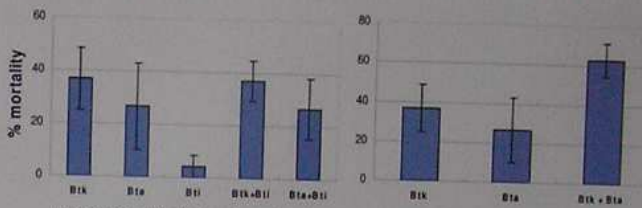

Fig. 3. Effect of single and combination use against *P. xylostella* 3rd instar larvae
Btk: Dipel, Bta: XenTari, Bti: Biomük, concentration: 20 ng cm^{-2}, n = 3 x 24

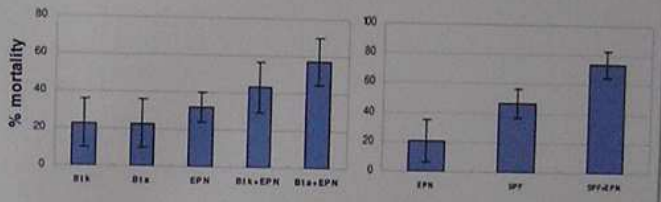

Fig. 4. Effect of single and combination use against *P. xylostella* 3rd instar larvae
Btk: Dipel, Bta: XenTari, EPN: *S. carpocapsae* EN03, SPF: 0.3% Rimulgan + 0.3% Xanthan, concentration: 20 ng cm^{-2} or 3-5 IJs/larva, n = 3 x 24

Tab. 2: Interaction of combined agents against 3rd instar *P. xylostella*

combination	replicates	interaction: additive	interaction: synergistic	interaction: antagonistic	spray method
Dipel (20ng/cm²) + Biomük (20ng/cm²)	5	5			mixed
XenTari (20ng/cm²) + Biomük(20ng/cm²)	5	5			mixed
Dipel (20ng/cm²) + XenTari (20ng/cm²)	5	4	1		mixed
Dipel (20ng/cm²) + XenTari (20ng/cm²) + Biomük (20ng/cm²)	4	3		1	mixed
Dipel (20ng/cm²) + EN03 (5/larva)	4	3		1	one after another
XenTari (20ng/cm²) + EN03 (5/larva)	4	4			one after another
SPF + EN03 (3/larva)	4	3	1		mixed
SPF + XenTari (10mg/l)	4	3	1		mixed
XenTari (10mg/l) + EN03 (3/larva)	4	3	1		mixed
SPF + EN03 (3/larva) + XenTari (10mg/l)	4	3	1		mixed

Conclusion and Discussion:

- Bti has no toxic effect against DBM
- mostly additive effects recorded with combinations of Bt (Btk, Bta) and EPN or Btk, Bta and Bti
- mixed application of Bt and EPN is economically not feasible
- alternating applications of Bt and EPN are a powerful and reliable tool to avoid or retard development of Bt resistance in *P. xylostella*
- Btk and Bta should also be used in alternating applications

Xiaoli Yi and Ralf-Udo Ehlers
Institute for Phytopathology
Dept. Biotechnol. + Biol. Control
Hermann-Rodewald-Str. 9
24118 Kiel
Tel. +49 431 880-4864
ehlers@biotec.uni-kiel.de
xiaoli.yi@biotec.uni-kiel.de
www.uni-kiel.de

Acknowledgments

Project: EU-ICA4-CT-2001-10003 **DIABOLO**
An integrative strategy for the sustainable control of diamondback moth (*Plutella xylostella*) by conservation of natural enemies and application of biocontrol agents

An experience on biocontrol of *Caliroa varipes* (Klug) (Hymenoptera, Tenthredinidae) by means of EPNs, in an urban park of Bologna suburbs (Emilia-Romagna, Northern Italy)

Giovanna Curto, Nicoletta Vai

Plant Protection Service, Regione Emilia-Romagna, via Saliceto 81, 40128 Bologna, Italy

gcurto@regione.emilia-romagna.it

Caliroa varipes (Klug) Hymenoptera Tenthredinidae at Italian latitudes completes two generations per year and overwinters as mature larva cocooned in the soil.

The adults, coming from overwintering larvae, fly from April to May. The females insert more than ten eggs under the lower leaf epidermis. The larvae hatch at mid May and develop until the end of the same month; when they are mature drop and bury themselves into the soil, where they cocoon and pupate, giving a second generation at the end of June. The larvae live gregarious on the leaf lower epidermis, eating the parenchyma as long as they skeletonise the leaf, leaving one cuticle intact.

The *C. varipes* control is based on cutting and removing the infested leaves, but in case of heavy infestations the cutting could be very drastic, and only biocontrol methods can be accepted by the frequenters of an urban park.

The Plant Protection Service experts were asked for controlling a very heavy *C. varipes* infestation in a small oak wood in the centre of Budrio, a small town in province of Bologna, Northern Italy.

OBJECTIVES

To check the effectiveness of:

- A soil application of *Heterorhabditis bacteriophora*, in the control of cocooned larvae before their pupation.
- *Steinernema feltiae*, formulated for foliar application, sprayed on the gregarious larvae on infested leaves.

MATERIAL AND METHODS

S. feltiae application to the leaves

On May 24th, 2005, 100 oak leaves, heavily infested by 104 larvae of *C. varipes*, were collected from the oak wood; 50 leaves with 54 larvae on top, were sprayed with *S. feltiae*, the other ones with 50 larvae on top, were hold as untreated control (table 1).

Assessments The leaves were maintained wet at 23 °C; a week later, the larval mortality was assessed, the larvae were scored as dead/live and a sample of the dead ones was dissected and examined under a stereomicroscope for checking nematodes inside.

Table 1 – Foliar application.

	Active ingredient	Comm. product	Dose (I.J. ha^{-1})	Application time
1	*Steinernema feltiae*	Nemasys F	5×10^9	May 24th, 2005
2	Untreated control			

H. bacteriophora application to the soil

Beneath the most damaged oak trees 100 m^2 were bounded and irrigated; *H. bacteriophora* was applied by means of a watering can, during the drop of the most mature larvae (table 2); then both the treated soil and 50 m^2 of an untreated area were covered with a net.

Table 2 – Soil application.

	Active ingredient	Comm. product	Dose (I.J. ha^{-1})	Application time
1	*Heterorhabditis bacteriophora*	Nematop	5×10^9	May 31st, 2005
2	Untreated control			

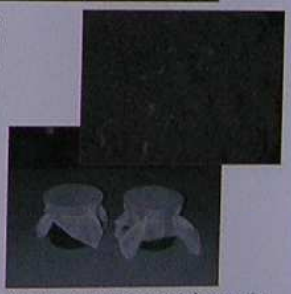

At the same time, 40 mature larvae were collected and transferred to the nematology laboratory, where they dug and buried themselves into the soil of two pots, each 16 cm diameter, before applying *H. bacteriophora* in the first one; the pots were covered with a net and stored in the lab at 23 °C, wetting the soil every two days.

Assessments 10 days after the treatment, the covering nets were removed and the emerged *C. varipes* adults were counted

RESULTS AND DISCUSSION

S. feltiae application to the leaves

S. feltiae suspension formulated with an adjuvant, showed some effects in controlling *C. varipes* infestation: 78% larval mortality was achieved, but the dissection of 36 dead larvae as sample, showed that only 57% larvae died of nematodes, probably because the oak leaves appeared quite waterproof and the experimental conditions were rather different from the natural environment.

Table 3 – Results of foliar application.

Assessment	Treatment (I.J. ha^{-1})	Larval mortality (%) (mts.d.)	Mortality due to EPNs (%)
May, 31st	*S. feltiae* (5×10^9)	78.0 ± 2.7	57.0
	Untreated control	14.0 ± 11.4	0.0

H. bacteriophora application to the soil

The EPN application to the soil at the most suitable time, succeeded in controlling the *C. varipes* first generation. In the urban oak wood, only 6 adults were collected under the net in the treated surface, while in the untreated control more than 170 specimens were counted.

The laboratory experiment confirmed as observed in the park: no adults emerged from the treated pot, while 17 specimens flew from the untreated one.

Overlooked important characters in females and infective juveniles of the entomopathogenic family Steinernematidae (Nematoda)

Zdeněk Mráček[1], Vladimír Půža[1,2] and Alice Hypšová[1,2]

1- Institute of Entomology, Biological Center, Czech Academy of Sciences, Branišovská 31, 370 05 České Budějovice, Czech Republic
2- Faculty of Biological Sciences, University of South Bohemia, Branišovská 31, 37005 České Budějovice, Czech Republic

Introduction

The family Steinernematidae includes more than 40 described species which morphological identification is based on several male and larval characters, such as shape of spicules and guberbaculum in males, position of excretory pore, lateral fields, length of tail and hyaline layer in infective juveniles (IJs) etc. Till present, a lack of taxonomically important characters was found for steinernematid females (Hominick et al. 1997). Such analysis of characters is fundamental for species distinguishing and essential for taxonomic purposes. Therefore, we focused our effort to study steinernematid females to clarify if there are any valuable differences in the external body morphology (tail protuberances, postanal swelling, vulval protruding) among species which could add new important characters to simplify the identification of species and the taxonomy of this family. Similarly, the IJ tail of different steinernematid species was studied because it belongs as well to the taxonomically important characters. Ratio c´ (tail length/width) and %Hy (length of hyaline layer/tail length x100) are used in diagnosis and relationship of species. Both, the methods of scanning electron microscopy and light microscopy were used for our study.

Females

Tail of the first and second generation

Tail shape in the first generation varies among species and partly depends on the age of studied female. In majority of species the tail is conical, but blunt in its tip. There is a big difference between females in the first and second generation (Tables 1 and 2). Conical tail tapering to a pointy end in the second generation females is uniform in most species.

Table 1. First generation female, morphology of tail

Table 2. Second generation female, morphology of tail

Tail protuberances

Some species possess the blunt tail with conical terminal projection (*S. kraussei, S. feltiae*). The finely rounded, blunt tail, in another species lacks this terminal projection (*S. glaseri* group, *S. diaprepesi*), however, bears several (2-5) minute papilla-like cuticular projections (mucrones) (Table 1 and 2, Figures). Such projections were mostly found in the first and rarely in the second generation. They were mentioned in recently published species, however, they were overlooked in older descriptions.

Postanal swelling

Postanal swelling varies from distinct to slight and missing among first generation female species (Table 1, Figures). This character seems to be stable in many species. E.g. *S. kraussei, S. silvaticum, S. weiseri* has no or slight postanal swelling whereas most species of *S. glaseri* group are characterized by the distinct swelling. The postanal swelling is reduced in the second generation.

Vulval region

Generally, the first generation females possess more protruding vulva than those in the second generation. The vulval morphology varies among steinernematid species from slightly to severely protruding (Table 3, Figures). Some species, such as *S. yirgalemense, S. diaprepesi* and *S. aciari* etc. have in the vulval aperture flapped or double flapped epiptygma. The origin of these species is mostly from subtropical and tropical regions.

Table 3. First generation female, vulval morphology

Infective juveniles

Tail of all infective juvenile species is conoid with pointed tip sometimes dorsally bent or depressed or even with drop-like extended in front of its tip (in some specimens of S. silvaticum). However, species significantly differ in their general tail shape (Figures) which depends on the length of hyaline layer and width at anus. Till present, ratios of tail morphometry were used in the family taxonomy. However, morphological tail character which appears as more or less slender and varies from attenuated to subdigitate among species has been also overlooked.

Conclusion:

Comparative study of females and IJs tail regions is needed to clarify real significance of above described morphological structures. Especially, female minute tail papilla-like protuberances and general tail character represents a good challenge for future studies.

References

Hominick W.M., Briscoe B.R., del Pino F.G., Heng J., Hunt D.J., Kozodoy E., Mráček Z., Nguyen K.B., Reid A.P., Spiridonov S., Stock P., Sturhan D., Waturu C. & Yoshida M. (1997): Biosystematics of entomopathogenic nematodes: current status, protocols, and definitions. J. Helminthol. 71: 271-298

Isolation and Characterization of New Populations of Entomopathogenic nematodes from Israel

N.Mikaia,[1] and I.Glazer [2], G. Chkhubianishvili[3]
[1-3] Biocontrol Department, Kanchaveli L., Research Institute of Plant Protection, 82, Chavchavadze Ave, 380062 Tbilisi, Georgia. E-mail: skarabidae@mail.ru
[2] Dept. of Nematology, ARO, the Volcani Center, Bet Dagan 50250, Israel E-mail: glazeri@int.gov.il

Introduction

Entomopathogenic nematodes (Steinernematidae and Heterorhabditidae) are known as effective biological agents against soil dwelling stages of insect pests. They inhabit diverse habitats world wide. In the present study were isolated nematodes from different locations in the Israel and than evaluated some beneficial traits in various bioassays: Reproduction potential; Desiccation & heat tolerance; Infectivity; Motility in sand colourns.

Survey sites

Reproduction potential: Average yield of 10 Galleria mellonella instars infected by 50 IJs/insect

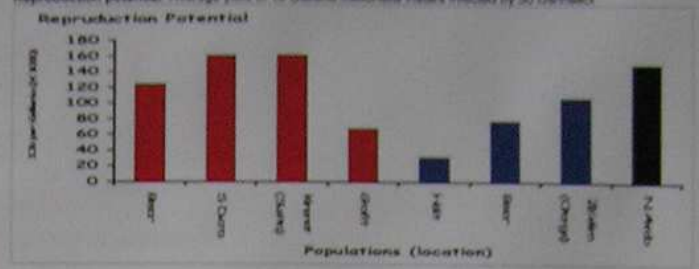

Desiccation tolerance: Exposure to 97% RH for 72 h followed by exposure to 85% RH

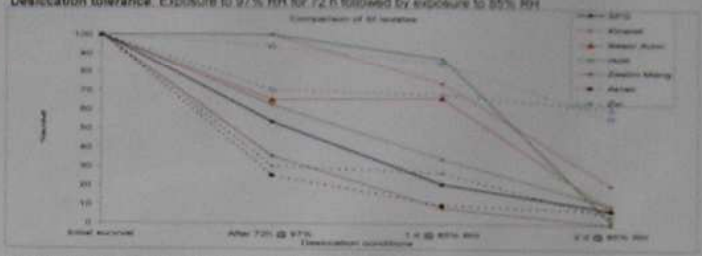

Infectivity: Exposure of *Tenebrio molitor* last instar to different conc. of nematodes in Petri dish

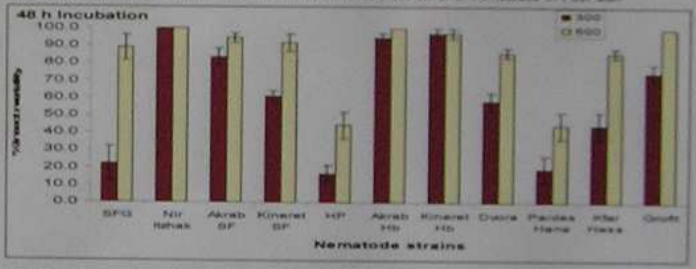

Movement in sand columns: 5000 IJs were added onto the top pf sand columns (5 cm diam., 15 cm height). No. of nematodes per layer was determined after 72 hr. Nematodes were extracted from soil by Bermann Funnel technique.

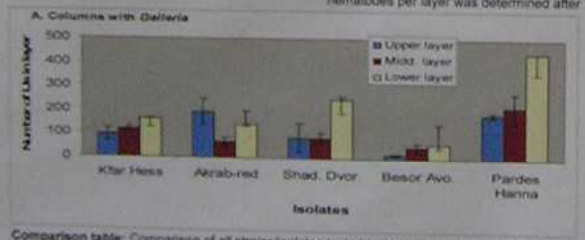

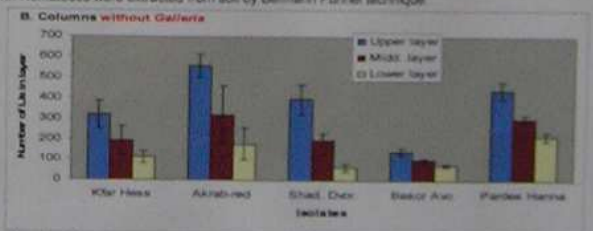

Comparison table: Comparison of all strains/isolates tested in the various assays. The performance of each strain was scored on a 1-10 scale (1= very poor; 10= excellent)

Genera	Strain/ Location	Location Characteristics	Basic Room	Desiccation	Heat Tolerance	Motility in Column	Invasion rate	Infec. Tenebrio	Reprod. Potential	Average
Steinernematids	SF G*	Lab reference	6	4	4	4	5	6	5	4.3
	Holit	Lemon orchard	4	5	6	4	4	7	2	4.0
	Besor	Avocado orchard	3	6	4	3	6	7	4	4.1
	Sulsa	Pasture	4	6	5	4	6	9	10	5.5
	Nir Itzhak	Medow	4	5	6	6	5	10	6	5.3
	Zeelim	Mango	4	5	5	5	3	7	5	4.3
	Zeelim	Citrus	3	5	5	4	8	7	5	4.6
	Nahal Akrab	Bushes	6	8	9	5	5	9	7	6.1
Heterorhabditids	HP*	Lab reference	2	2	4	4	2	3	5	2.8
	Besor Hb	Avocado	4	4	8	3	4	7	6	4.5
	Dvora	Olive trees	7	6	6	6	4	8	7	5.6
	Grofit	Palm trees	3	5	9	5	5	9	4	5.0
	Pardes Hana	Citrus	3	4	6	8	4	4	6	4.4
	Mishmeret	Citrus orchard	3	4	6	6	5	6	6	4.5
	Kfar Hess	Citrus orchard	3	4	6	5	7	7	6	4.8
	Nahal Akrab	Bushes	3	4	9	4	5	10	7	5.3

Conclusions and future work

Large variation was found among the new nematode populations in regard to their performance in the different bioassays. We will use this analysis as basis for selection of population for genetic improvement. The nematode populations with the highest desiccation tolerance will be evaluated against foliage pests.

A nematode symbiont for *Photorhabdus asymbiotica*

John Gerrard[1], Susan Joyce[2], David Clarke[2], Richard ffrench-Constant[2], Ed Feil[2] and Nick Waterfield[2]

1 Department of Medicine, Gold Coast Hospital, Queensland, Australia. 2 Biology and Biochemistry, University of Bath, Bath, UK.

The finding that *P. asymbiotica* exists in an entomopathogenic association similar to other members of the genus has implications for the role of invertebrates in the evolution of emerging human pathogens.

The story so far.....

- A new *P. asymbiotica* is recovered from a human wound at Kingscliff Australia, 2006.
- Soil baited at Kingsciff recovers a Heterorhabditid nematode.
- *P. asymbiotica* is recovered from the nematode.
- The clinical and worm isolates are shown to be identical using MLST.
- The worm forms a specific symbiosis with both the human and worm derived isolates .

(1) The Kingscliff patient has '*Photorhabditis*'

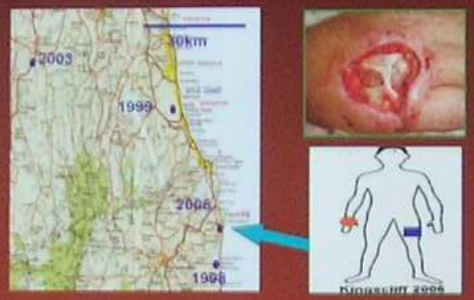

(2) A Kingscliff worm hunt

(3) An EPN complex is recovered

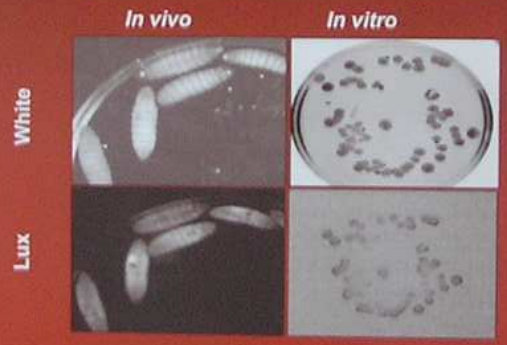

(4) Heterorhabditid taxonomy in progress

(5) Clinical and worm isolates 'primary phase'

(6) Clinical and worm strains identical

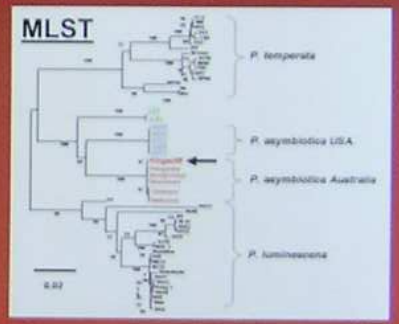

(7) The symbiosis is specific....

Clinical vigilance, a detailed and accurate case history and rapid response by our clinical team allowed us to confirm that *P. asymbiotica* is present in the environment in an entomopathogenic nematode complex. The presence of an previous small 'scabbed' wound on the hand of the patient suggests one possible route of entry for the *P. asymbiotica*, although the exact mechanism


Isolation of entomopathogens from South African soils using the Galleria mellonella-bait technique
PROJECT FLOW CHART
Introduction
Material & Methods
Results
TABLE 1. ENTOMOPATHOGENIC FUNGI ISOLATED FROM SOIL SAMPLES USING INSECT-BAIT TECHNIQUE
TABLE 2. ENTOMOPATHOGENIC NEMATODES ISOLATED FROM SOIL SAMPLES USING INSECT-BAIT TECHNIQUE
Discussion
References

SVALBARD REINDEER ANTLER CHARACTERISTICS REFLECTING THE LOCAL ENVIRONMENTAL CONDITIONS

VERONIKA KAVANOVÁ [1], JAN KAVAN [2]

(1) Department of Zoology, Faculty of Science, University of South Bohemia
(2) Department of Geography, Faculty of Science, Masaryk University

HYPOTHESIS

- Antler parameters as observed remotely could be used to estimate reindeer population fitness
- Populations in different localities have different fitness
- This depends on environmental conditions
- Locality with advantageous environmental conditions (climate, vegetation) will be inhabited by healthier reindeer population

METHODS

- We focused on parameters that could be estimated on distance with use of photography analysis
- Individuals were photographed from different angles if possible
- Shoulder height of an individual was estimated (S) and size/length of antler (A) from one single photography – from these parameters the relative size of antler was calculated (L) – see Figure 2
- Number of tines was calculated from different photos to ensure the correctness of such number

CASE STUDY

- Central part of Svalbard (Figure 1)
- Comparison of two distinct localities with independent populations
- Skansbukta X Petuniabukta
- Differences in climate, vegetation and terrain configuration
- Reindeers observed during August 2017
  Petuniabukta: 65 individuals
  Skansbukta: 94 individuals

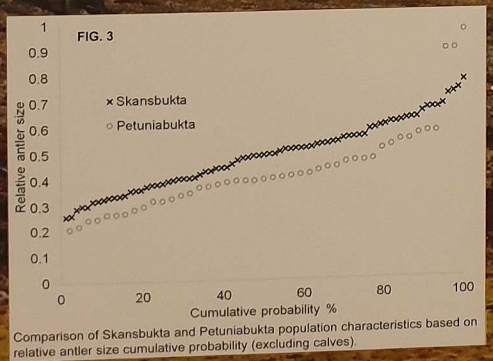

Comparison of Skansbukta and Petuniabukta population characteristics based on relative antler size cumulative probability (excluding calves).

Relative antler size significantly higher in Skanbukta population

Significant shift at around 70%

Larger proportion of individuals with larger antlers in Skansbukta

Missing group of 7-9 tines in Petuniabukta

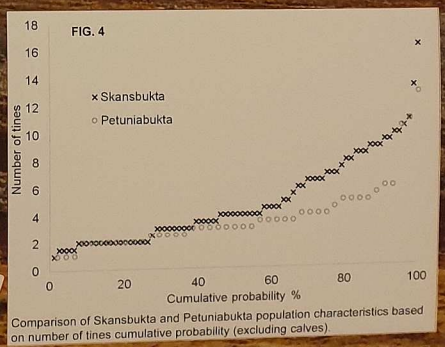

Comparison of Skansbukta and Petuniabukta population characteristics based on number of tines cumulative probability (excluding calves).

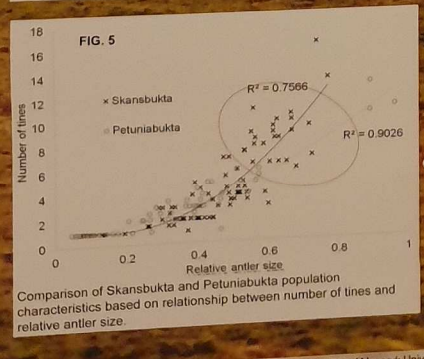

Comparison of Skansbukta and Petuniabukta population characteristics based on relationship between number of tines and relative antler size.

There is a missing group of reindeer with higher relative antler size and number of tines in Petuniabukta

CONCLUSIONS

- Reindeer population in Skansbukta is in better physical condition according to observed parameters – relative antler size and number of tines (Figures 3 and 4)
- This reflects well „better" environmental conditions – higher quality and density of vegetation cover, longer vegetation period and favourable terrain configuration
- Comparison of both populations suggests missing group of older/in better condition reindeers in Petuniabukta (highlighted in Figure 5)

SCAN ME

The research was financially supported by the project LM2015078 and project of Masaryk University MUNI/A/1251/2017 and Arctic Field Grant n. 282536. We also thank Nils Roar Saelthun for his support and UNIS logistics for support during the field work.

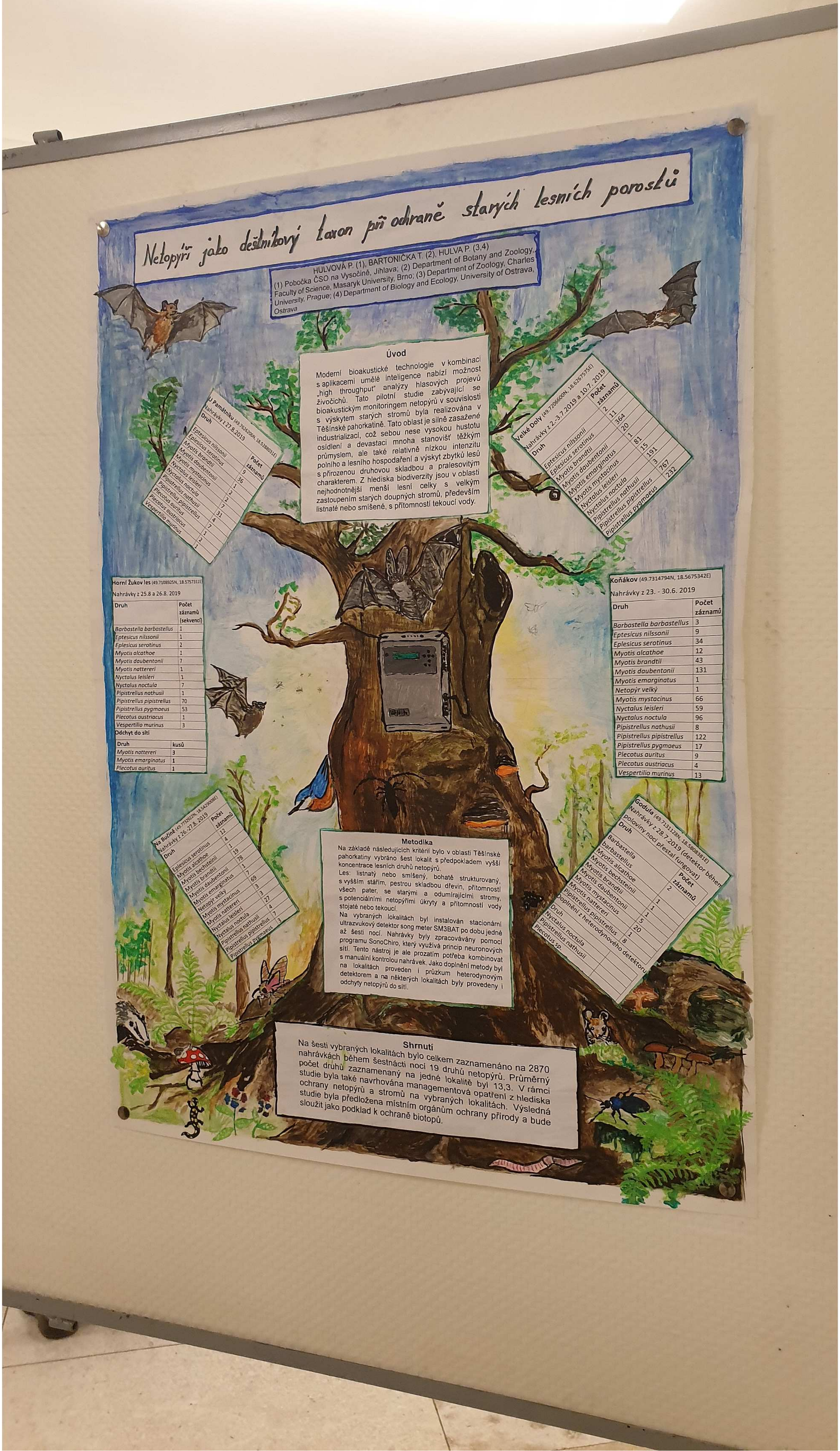
Netopýři jako deštníkový taxon při ochraně starých lesních porostů
HULVOVÁ P. (1), BARTONIČKA T. (2), HULVA P. (3,4)
(1) Pobočka ČSO na Vysočině, Jihlava; (2) Department of Botany and Zoology, Faculty of Science, Masaryk University, Brno; (3) Department of Zoology, Charles University, Prague; (4) Department of Biology and Ecology, University of Ostrava, Ostrava
Úvod
Moderní bioakustické technologie v kombinaci s aplikacemi umělé inteligence nabízí možnost „high throughput" analýzy hlasových projevů živočichů. Tato pilotní studie zabývající se bioakustickým monitoringem netopýrů v souvislosti s výskytem starých stromů byla realizována v Těšínské pahorkatině. Tato oblast je silně zasažené industrializaci, což sebou nese vysokou hustotu osídlení a devastaci mnoha stanovišť těžkým průmyslem, ale také relativně nízkou intenzitu polního a lesního hospodaření a výskyt zbytků lesů s přirozenou druhovou skladbou a pralesovitým charakterem. Z hlediska biodiverzity jsou v oblasti nejhodnotnější menší lesní celky s velkým zastoupením starých doupných stromů, především listnaté nebo smíšené, s přítomností tekoucí vody.
Horní Žukov les (49.7108925N, 18.5757311E)
Nahrávky z 25.8 a 26.8. 2019
Druh | Počet záznamů (sekvencí)
Barbastella barbastellus 1
Eptesicus nilssonii 1
Eplesicus serotinus 2
Myotis alcathoe 1
Myotis daubentonii 7
Myotis nattereri 1
Nyctalus leisleri 1
Nyctalus noctula 7
Pipistrellus nathusii 1
Pipistrellus pipistrellus 70
Pipistrellus pygmaeus 53
Plecotus austriacus 1
Vespertilio murinus 3
Odchyt do sítí
Druh | kusů
Myotis nattereri 3
Myotis emarginatus 1
Plecotus auritus 1
Koňákov (49.7314794N, 18.5675342E)
Nahrávky z 23. - 30.6. 2019
Druh | Počet záznamů
Barbastella barbastellus 3
Eptesicus nilssonii 9
Eplesicus serotinus 34
Myotis alcathoe 12
Myotis brandtii 43
Myotis daubentonii 131
Myotis emarginatus 1
Netopýr velký 1
Myotis mystacinus 66
Nyctalus leisleri 59
Nyctalus noctula 96
Pipistrellus nathusii 8
Pipistrellus pipistrellus 122
Pipistrellus pygmaeus 17
Plecotus auritus 9
Plecotus austriacus 4
Vespertilio murinus 13
Metodika
Na základě následujících kritérií bylo v oblasti Těšínské pahorkatiny vybráno šest lokalit s předpokladem vyšší koncentrace lesních druhů netopýrů.
Les: listnatý nebo smíšený, bohatě strukturovaný, s vyšším stářím, pestrou skladbou dřevin, přítomností všech pater, se starými a odumírajícími stromy, s potenciálními netopýřími úkryty a přítomností vody stojaté nebo tekoucí.
Na vybraných lokalitách byl instalován stacionární ultrazvukový detektor song meter SM3BAT po dobu jedné až šesti nocí. Nahrávky byly zpracovávány pomocí programu SonoChiro, který využívá princip neuronových sítí. Tento nástroj je ale prozatím potřeba kombinovat s manuální kontrolou nahrávek. Jako doplnění metody byl na lokalitách proveden i průzkum heterodynovým detektorem a na některých lokalitách byly provedeny i odchyty netopýrů do sítí.
Shrnutí
Na šesti vybraných lokalitách bylo celkem zaznamenáno na 2870 nahrávkách během šestnácti nocí 19 druhů netopýrů. Průměrný počet druhů zaznamenaný na jedné lokalitě byl 13,3. V rámci studie byla také navrhována managementová opatření z hlediska ochrany netopýrů a stromů na vybraných lokalitách. Výsledná studie byla předložena místním orgánům ochrany přírody a bude sloužit jako podklad k ochraně biotopů.

A secret weapon how to defeat a spider-(man)

aneb Testování vybraných rostlinných extraktů pro atraktanci/repelenci pavouků zápřednic (Araneae: *Cheiracanthium*)

Nela Gloríková, Helena Rothová, [illegible] Rostlinné výroby, v. v. i., tým: Funkce bezobratlých a rostlin v agrosystémech

PROBLÉM

- Expanze zápřednic (*Cheiracanthium* sp.) v České Republice
- Tyto druhy jsou medializovány kvůli riziku jejich kousnutí
- Zápřednice Mildeova osídluje lidská obydlí, kde ale není vítána

- Mapování areálu rozšíření zápřednice Mildeovi
- Informatizace veřejnosti o zcela zbytečném strachu z těchto neškodných druhů
- **Vyvinutí účinného repelentu proti těmto pavoukům**

ŘEŠENÍ

Za méně než 2.7 milionů korun :)

CÍL

Otestovat různé rostlinné extrakty za účelem nalezení potenciálního repelentního účinku na pavouky zápřednice.

METODY & MATERIÁL

Modelový organizmus

- Zápřednice Mildeova (*Cheiracanthium mildei*)
- juvenilní jedinci odchyceni v Praze v říjnu 2019

Statistika

- <1,0> binom.test (x, n, p)
- software R

Rostlinné extrakty

- použito bylo 15 přírodních rostlinných extraktů ze 14 rodů a 8 čeledí
- ředěny byly ethanolem v poměru 1:100

Průběh experimentu

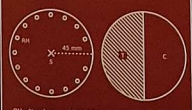

RH=větrací otvory, S=střed, T=testovací oblast (ošetřena roztokem), C=čistá oblast (ošetřena etanolem)

Hodnocení

- hodnocena byla přítomnost zámotku po 24 hodinách
- případy, kdy si pavouci úkryt nevybudovali, uhynuli, nebo byl zámotek na hranici ploch, byly z analýzy vyloučeny

KONTAKTUJTE NÁS

Adresa: VURV,v.v.i., Drnovská 507/73, Praha 6
Email: glorikova@vurv.cz
Ilustrace: www.landalomad.sk

PODPORA Grant od Ministerstva školství, mládeže a tělovýchovy ČR Inter-Excellence LTAUSA18171

VÝSLEDKY

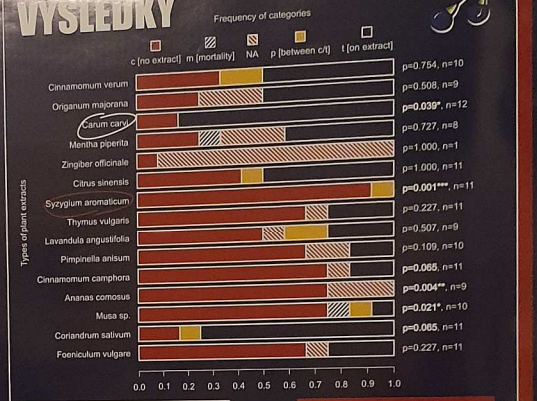

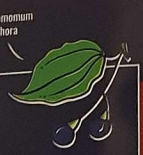

ATRAKTANCE

1. **Carum carvi**
   p=0.039*, n=12
2. **Coriandrum sativum**
   p=0.065, n=11

- pavouci preferovali stavbu zámotků na půlce misky ošetřené roztokem extraktu

REPELENCE

1. **Syzygium aromaticum**
   p=0.001***, n=11
2. **Ananas comosus**
   p=0.004**, n=9
3. **Musa sp.**
   p=0.021*, n=10
4. **Cinamomum camphora**
   p=0.065, n=11

THE SECRET WEAPON!

ZÁVĚREM

Nejvýraznější repelentní účinek jsme prokázali u hřebíčku

Z celkem otestovaných 15 extraktů jsme u 2 prokázali atraktantní účinky, u 4 repelentní účinky a v 1 případě látka zamezila stavbě zámotku pavouků.

Značení potravy pomocí lanthanoidů v koloniích čmeláka zemního (*Bombus terrestris*) a měření konzumace cukru a proteinu při standardních a stresových potravních podmínkách

Macháčková L.[1,5], Votavová A.[2], Mikát M.[1], Matějková S.[3], Řehoř I.[3,6], Gillarová S.[4], Straka J.[1]

1 - Katedra zoologie PřF UK v Praze, Viničná 7, 128 44 Praha
2 - Zemědělský výzkum, spol. s.r.o., Zahradní 1, 664 41 Troubsko
3 - Ústav organické chemie a biochemie AV ČR, Flemingovo náměstí 2, 166 10 Praha
4 - Ústav sacharidů a cereálií, Fakulta potravinářské a biochemické technologie VŠCHT, Technická 5, 166 28 Praha
5 - Entomologické oddělení, Národní muzeum, Cirkusová 1740, 193 00 Praha
6 - Ústav chemického inženýrství, Vysoká škola chemicko-technologická v Praze, Technická 3, 166 28, Praha

contact email: machackovalenka.jbc@seznam.cz, jakub.straka@aculeataresearch.com

Složitost nutričního toku a efektivita využívání pylu a cukru v kolonii eusociálních včel nejsou dosud plně pochopeny. Sledování pohybu potravy od zdroje až k larvám u včel postupně zásobujících své potomky (progressive provisioning bees) vyžaduje vhodný experimentální přístup. Pomocí lanthanoidových komplexů GdDTPA a DyDTPA (alternativně lanthanoid v komplexu s DOTA[5]) jsme označili cukr a pyl, jakožto jediné zdroje potravy v kolonii laboratorně chovaného čmeláka zemního (*Bombus terrestris*). Porovnali jsme kolonie krmené cukerným roztokem obsahujícím sacharózu s koloniemi krmenými roztokem fruktózy a glukózy (v poměru 1:1). Změřili jsme množství cukru a proteinu zkonzumovaných larvou během vývoje v dospělce a zjistili jsme, jak se mění příjem těchto zdrojů při standardních potravních podmínkách (krmení ad libitum) a při omezené dostupnosti jednoho ze zdrojů potravy.

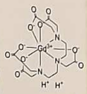

Gd-DTPA

Metodika

Larvy defekují až na konci larválního vývoje, což umožňuje sebrat veškeré exkrementy každé larvy z jejího kokonu[1,2,3]. Lanthanoidy nejsou v těle zvířat využívány a prochází trávicí soustavou ven z těla[4,5]. Množství zkonzumované potravy odpovídá množství lanthanoidu ve stolici, což je přesně kvantifikováno pomocí spektrometrické techniky ICP-OES či ICP-MS.

Pro experimenty jsme použili laboratorně chované čmeláky zemní (*Bombus terrestris*). Kolonie byla sestavena z 1 matky (alternativně je možné použít mikrokolonie složené ze 3 dělnic[5,6]).

Kolonie byly sestaveny do několika skupin: kolonie krmené disacharidem sacharózou (S) nebo monosacharidy fruktózou + glukózou v poměru 1:1 (FG), kolonie s potravou značenou lanthanoidy (Z), kontrolní kolonie bez lanthanoidů (K). Kolonie s odebíraným pylem na 6 hodin každý den (H). Celkem 5 typů kolonií: kontrolní (SK_{1-21} a FGK_{1-21}), značené (SZ_{1-23}, FGZ_{1-23}, FGH_{1-23}). x_2=počet kolonií

Všichni potomci (samice-dělnice a samci) byli zváženi a množství lanthanoidu (tedy zkonzumovaného pylu a cukru) bylo přiděleno ke každému jedinci.

oplach kokonu

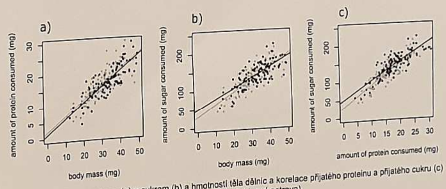

Obr. 2: Vztah mezi proteinem (a) a cukrem (b) a hmotností těla dělnic a korelace přijatého proteinu a přijatého cukru (c) (šedé tečky = sacharózová potrava, černé tečky = fruktózovo-glukózová potrava)

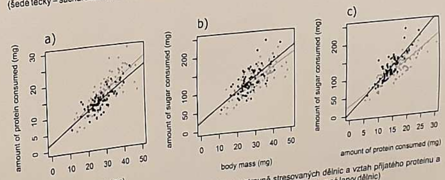

Obr. 3: Vliv přijatého proteinu a cukru na hmotnost jedince u potravně stresovaných dělnic a vztah přijatého proteinu a přijatého cukru (c) (šedé tečky = plně krmené larvy dělnic, černé tečky = potravně stresované larvy dělnic)

Výsledky

- Přítomnost lanthanoidů ani typ cukru (monosacharidy x disacharidy) nemělo signifikantní vliv na váhu dělnic a samců. (Obr. 1)
- Dělnice krmené neomezeně přijaly za svůj vývoj v průměru 0.54 mg proteinu a 4.26 mg cukru, samci pak 0.52 mg proteinu a 4.43 mg cukru na 1 mg suché tělesné váhy. Dělnice s omezenou dostupností potravy přijaly v průměru 0.51 mg proteinu a 4.65 mg cukru na 1 mg suché tělesné váhy.
- Ve všech experimentech byla silná pozitivní korelace mezi váhou jedinců, příjmem proteinu a příjmem cukru. (Obr. 2)
- Konzumace cukru však rostla strměji v porovnání s konzumací proteinu v koloniích, kterým byla omezena dodávka potravy (pylu) oproti neomezeně krmeným koloniím. (Obr. 3)

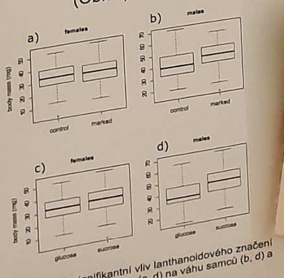

Obr. 1: Nesignifikantní vliv lanthanoidového značení (a, b) a cukerného typu (c, d) na váhu samců (b, d) a dělnic (a, c)

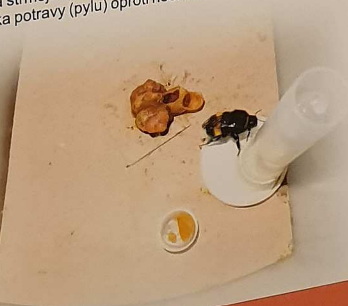

Závěr

Metoda sledování spotřeby potravy s použitím netoxického inertního lanthanoidového komplexu[4,5] dovoluje sledovat různé komponenty potravy uvnitř kolonie.

Při vhodném použití je metoda použitelná bez nutnosti zabití jedinců a současně může být použito až 15 různých prvků jako značících látek.

Monosacharidy (glukóza a fruktóza) a disacharidy (sacharóza) jsou rovnocenné zdroje potravy pro čmeláky.

Odlišný vzor příjmu proteinu a cukru mezi plně krmenými a potravně stresovanými koloniemi. (Velké dělnice konzumovaly menší množství proteinu a více cukru během vývoje v potravně stresovaných koloniích oproti plně krmeným koloniím)[7].

Financování

Studium bylo podpořeno Grantovou agenturou UK (projekt č. 338815/2015/B-Bio/PřF), SVV 260434/2019, Ministerstvem kultury České republiky (Národní muzeum, DKRVO 2019-2023/5.I.b.).

Zdroje

1. Alford DV (1975). Bumblebees. Davis-Poynter, London
2. Michener CD (2007). The bees of the world, 2nd edn. The Johns Hopkins University Press, Baltimore
3. Michener CD (1974). The social behavior of the bees: a comparative study. Harvard University Press, Cambridge
4. [illegible]
5. [illegible]
6. [illegible]
7. [illegible]

NDOP Downloader – stahování dat z Nálezové databáze ochrany přírody AOPK ČR v prostředí QGIS

Kaláb O.

Katedra biologie a ekologie PřF OU, Ostrava; OpenGeoLabs s.r.o., Praha

Úvod

NDOP – Nálezová databáze ochrany přírody AOPK ČR obsahuje záznamy o výskytu druhů od profesionálů i veřejnosti. Tato data jsou v drtivé většině volně dosupná a lze je prohlížet a stahovat přes webový filtr [1].

QGIS – Desktopový open-source GIS, který slouží ke správě, prohlížení, analýze a vizualizaci dat [2].

NDOP Downloader – Zásuvný modul do QGIS, který nabízí možnost jak pohodlně získat data z nálezové databáze a rovnou s nimi pracovat v prostedí QGIS [3].

Pro náročnější uživatele, lze využít samostatný **Python** modul, nebo nástroj příkazové řádky a tak si práci s databází plně automatizovat.

Instalace

Instaluje se stadardně jako ostatní zásuvné moduly.

Modul je v seznamu veden jako experimentální.

Spuštění

Po instalaci se v horní liště objeví ikonka zásuvného modulu.

Lze vyhledávat pomocí taxonu (druh, rod) a/ nebo pomocí předdefinovaného regionu.

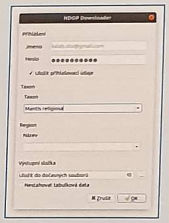

Stažená data

Po spuštění se stáhnou a zobrazí všechna dostupná data (vrstvy lokalit i tabulková data k nálezům).

Tabulková data se stáhnou ke všem záznamům naráz (narozdíl od webového filtru). U těchto dat se zobrazí souřadnice bodů nebo centroidů, které jsou v tabulce obsaženy.

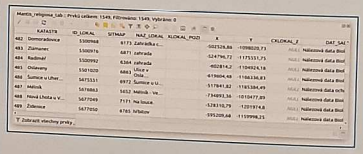

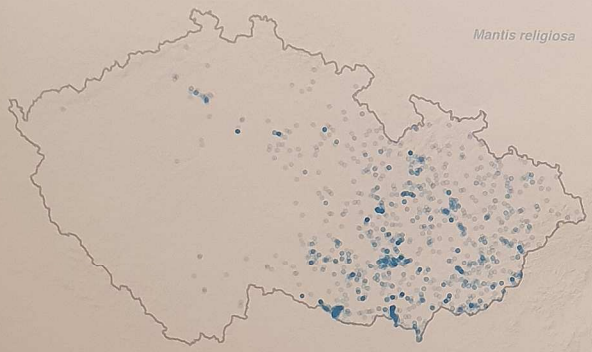

Práce s daty

Stažená data můžeme v QGIS rovnou analyzovat a vizualizovat.

Zjednodušený příklad rozšíření kudlanky nábožné *Mantis religiosa* v jednotlivých obdobích na základě všech dostupných dat z NDOP:

Python knihovna a příkazový řádek

Pro náročnější uživatele je dostupný Python modul s nástrojem příkazové řádky `ndop`, který můžeme použít přímo, nebo ho zařadit jako systémový příkaz do workflow v jiném jazyce (např. v R pomocí příkazu `system()`).

Python modul umožňuje zadat polygon jako vstupní parametr vymezení území, popř. lze navolit libovolný parametr pro request.

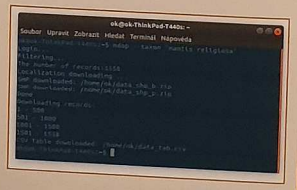

Zdroj a manuál

Zdrojový kód je volně dostupný na GitHub, kde je i seznam plánovaných funkcí a oprav:
https://github.com/OpenGeoLabs/qgis-ndop-downloader

Podrobný návod najdete na:
https://opengeolabs.github.io/qgis-ndop-downloader/

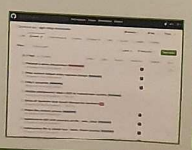

kalab.oto@gmail.com

[1] AOPK ČR (2020): Nálezová databáze ochrany přírody. *https://portal.nature.cz*
[2] QGIS Development Team (2020): QGIS Geographic Information System. Open Source Geospatial Foundation Project. *http://qgis.osgeo.org*
[3] Kaláb, O. (2019): NDOP Downloader - QGIS a Python modul. OpenGeoLabs. *https://github.com/OpenGeoLabs/qgis-ndop-downloader*

GitHub

Manuál


Deciphering regulatory mechanisms of distinct responses to nutrient balances between generalist and specialist species
Kaori Watanabe[1], Yukako Hattori[1], Yuuki Takahashi[1], Yuki Furumizo[1], Yasutetsu Kanaoka[1], Hironobu Uchiyama[2], Shunsuke Yajima[2], Masayoshi Watada[3], and Tadashi Uemura[1]
[1]Graduate School of Biostudies, Kyoto University, Japan, [2]NODAI Genome Research Center, Tokyo University of Agriculture, Japan,
[3]Graduate School of Science and Engineering, Ehime University, Japan
京都大学
KYOTO UNIVERSITY
Introduction
Nutrient balance is a critical environmental determinant for growth
How do developing animals cope with various nutritional changes?
Comparative multi-omics approaches to examine dietary responses of generalists and specialists
Drosophila species that have distinct feeding habitats
Generalists
Specialists
What are the underlying mechanisms of distinct adaptations to nutrient balances?
Nutrients
Macronutrients
1. Protein
2. Carbohydrates
3. Fat
Micronutrients
1. Minerals
2. Vitamins
Protein-to-carbohydrate ratio (P:C ratio) affects life-history traits
Lifespan
Reproduction
Obesity
Standard food
Cornmeal + Sucrose + Yeast
Carbohydrate (g/L)
Protein (g/L)
Isocaloric
Generalists
Adaptive systems
Dietary responses
Developmental rate
RNA-seq
Metabolomics
Specialists
Non-functional systems?
Results
Generalists developed on all of the diets, whereas specialists failed to develop on the carb-rich C diet
Developmental (pupation) rate
Generalist
Specialist
No pupa
Dietary responses in gene expression were distinct between the generalists and specialists
Whole-body RNA-seq
Are specialists D. sec and D. ele defective in Dawdle-dependent sugar sensing?
Dawdle (Daw): a Drosophila homolog of TGFβ/Activin
Midgut RNA-seq
Hypothesis
Generalist
Nutritious sugar
Dawdle (Daw)
Baboon (Babo)
p-Smox
Adaptation
Daw controls the expression of metabolic genes and metabolic homeostasis
KEGG metabolic pathways in Drosophila species
D. mel daw mutants failed to develop on our carb-rich diets
Developmental (pupation) rate
Control
daw mutant
Generalist D. mel daw mutant ≒ Specialist D. sec and D. ele
Daw target tissue responsible for larval growth: muscle
Muscle-specific babo KD
C diet
P diet
Developmental (pupation) rate
Control
KD in whole body
KD in muscle
The level of p-Smox in muscles: M diet > P diet only in the generalists?
Western blotting of p-Smox in muscles
Generalist
Specialist
Hypothesis
Adaptation
Discussion and future plans
Hypothesis
Generalist
Specialist
Carb-rich diet
Daw
Babo
p-Smox
Adaptation
Questions and ongoing analysis
Which step of Daw signaling is defective in the specialists?
Upstream TFs of daw?
Synthesis, processing, or secretion of Daw?
Downstream of Daw?
Regulation of metabolic genes in muscles
Muscle-specific RNA-seq
Lethality on carb-rich diets
Measurement of metabolites
Measurement of hemolymph pH
Acknowledgements
日本学術振興会

P053

Dissecting the Role of miRNAs in Muscular Dystrophy in *Drosophila melanogaster*

Shruti Chhetri and Halyna R Shcherbata
Max Planck Institute of Biophysical Chemistry
Gene Expression and Signaling
Am Fassberg 11, D-37077 Göttingen, Germany

1. Screening of miRNAs on MDs Model

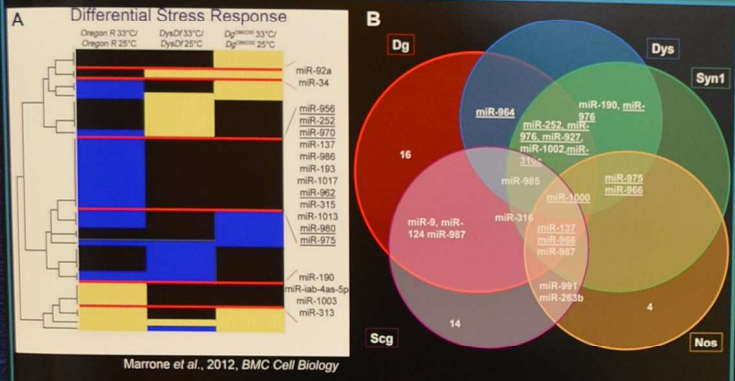

Marrone *et al.*, 2012, *BMC Cell Biology*

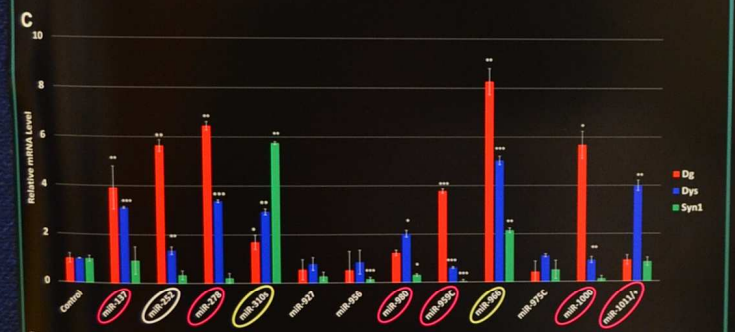

Fig.1 A) DGC dependent differential stress response miRNAs from microarray screen performed at normal (25˚C) and stressed (33˚C) conditions. Black indicates no change, yellow indicates upregulations, and blue indicates downregulations of the miRNAs listed. **B)** miRNAs that are predicted to target the DGC (Dystrophin Glycoprotein Complex); Source:- Target Scan Version 6.2. **C)** Loss of all the miRNAs tested affect mRNA level of Dg, Dys, and Syn1. Out of 12 miRNAs, 6 target either Dg, Dys, or both and are circled in magenta-; 2 target all Dg, Dys and Syn1 and are circled in yellow. In total, 9 of these miRNAs were considered for further screen. Data were analyzed using two-tailed Student's t-test: p-values; * ≤ 0.05, ** ≤ 0.01, *** ≤ 0.001.

2. miRNAs Mutants Exhibit Muscle Degeneration Phenotype

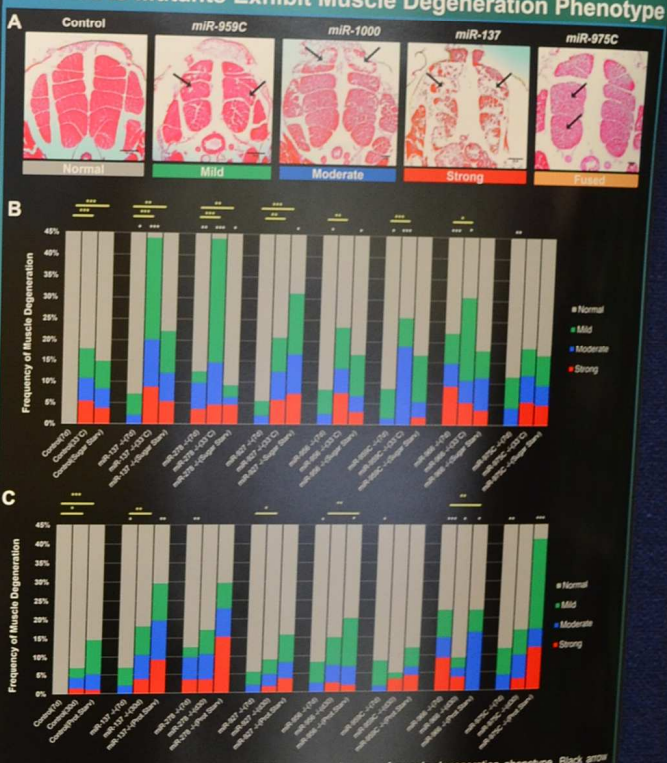

Fig.2 A) Quantification guidelines of miRNAs exhibiting various degrees of muscle degeneration phenotype. Black arrow indicates muscle degeneration. Scale bar 50 µm **B)** Quantification of muscle degeneration of miRNAs at young (7 days @ 25°C), temperature stressed (7 days @ 33°C), and sugar starved (7 days @ 25°C) **C)** Quantification of muscle degeneration of miRNAs at young (7 days), old (30 days), and protein starved (30 days) all at 25°C. Data were analyzed using χ²-distribution: p-values; * ≤ 0.05, ** ≤ 0.01, *** ≤ 0.001. White stars represents comparison within the genotype at the same condition while the yellow bars represent comparisons within the condition of the same genotype. Different miRNA mutants respond differently to different stresses. *miR-137* for example showed muscle degeneration in 3 tested condition.

3. Adult *Drosophila* Testis

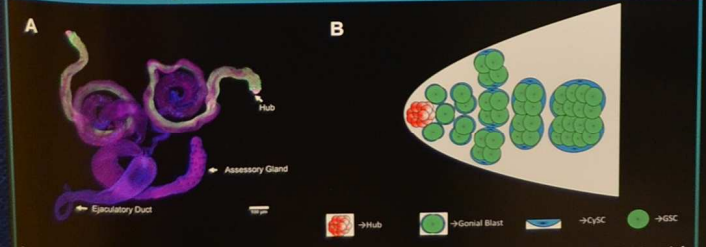

Fig.3 A) Male reproductive organ of adult male consist of 2 testes, 2 accessory glands, 2 seminal vesicles and 1 ejaculatory duct. Anterior end of testis, where GSCs (Germline Stem Cells) are located attached to somatic niche cells called the hub. Scale bar 10 µm. **B)** Illustration of *Drosophila* testicular GSC niche. The hub (peach) is a group of somatic niche cells. CySCs (Cyst Stem Cells) and GSCs divide asymmetrically to produce both self-renewing and differentiating daughter cells. The differentiating daughter cells exit the niche and are now called cyst cells (dark blue) and gonialblast (GB). When leaving the niche, two cyst cells envelop one GB. The GB inside a cyst undergoes four mitotic and two meiotic divisions, both with incomplete cytokinesis, resulting in a germline syncytium of 64 round haploid spermatids. The 64 spermatids elongate and later form the mature sperm.

4. *miRNA-137* is expressed in adult *Drosophila* testes

Fig.4 *In Situ* Hybridization of *miR-137* in adult fly testis using LNA (Lock Nucleic Acid) probe. *miR-137*^{ko} line was used as a negative control and shows no signal at the anterior part of the testis compared to the wildtype testis. This preliminary data suggest that *miR-137* is potentially expressed in a subset of cells in the anterior proliferative zone.

5. miR-137 mutants have increase in early somatic cyst cells

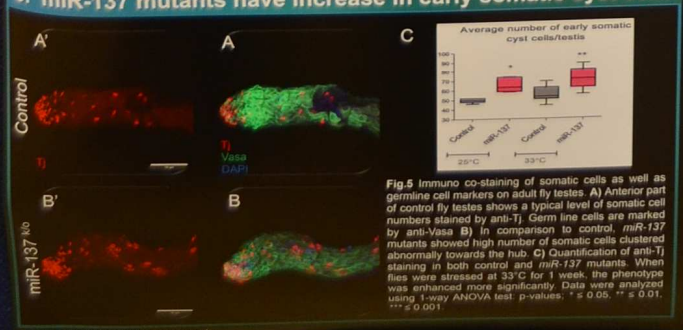

Fig.5 Immuno co-staining of somatic cells as well as germline cell markers on adult fly testes. **A)** Anterior part of control fly testes shows a typical level of somatic cell numbers stained by anti-Tj. Germ line cells are marked by anti-Vasa **B)** In comparison to control, *miR-137* mutants showed high number of somatic cells clustered abnormally towards the hub. **C)** Quantification of anti-Tj staining in both control and *miR-137* mutants. When flies were stressed at 33˚C for 1 week, the phenotype was enhanced more significantly. Data were analyzed using 1-way ANOVA test: p-values; * ≤ 0.05, ** ≤ 0.01, *** ≤ 0.001.

E-mail: Shruti.Chhetri@mpibpc.mpg.de

6. Future Direction & Outlook

- Staining for late-stage somatic cells
- Attempt to rescue testis phenotypes using somatic- or germline-specific gal4 driver
- Test the permeability barrier
- Attempt to rescue muscle phenotype
- Identify tissue specific *miR-137* target genes